Experimental Study of Sound Waves in Sandy Sediment

by Michael W. Yargus

Technical Report
APL-UW TR 0301
May 2003

Applied Physics Laboratory   University of Washington
1013 NE 40th Street   Seattle, Washington 98105-6698

Experimental Study of Sound Waves in Sandy Sediment

Michael W. Yargus

A dissertation submitted in partial fulfillment of the
requirements for the degree of

Doctor of Philosophy

University of Washington
2003

Program Authorized to Offer Degree: Electrical Engineering

University of Washington

Graduate School

This is to certify that I have examined this copy of a doctoral dissertation by

Michael W. Yargus

and have found that it is complete and satisfactory in all respects,
and that any and all revisions required by the final
examining committee have been made.

Chair of Supervisory Committee:

_____
Darrell R. Jackson

Reading Committee:

_____
Darrell R. Jackson

_____
Kevin L. Williams

_____
Terry E. Ewart

Date: _____

In presenting this dissertation in partial fulfillment of the requirements for the Doctoral degree at the University of Washington, I agree that the Library shall make its copies freely available for inspection. I further agree that extensive copying of the dissertation is allowable only for scholarly purposes, consistent with "fair use" as prescribed in the U.S. Copyright Law. Requests for copying or reproduction of this dissertation may be referred to Proquest Information and Learning, 300 North Zeeb Road, Ann Arbor, MI 48106-1346, to whom the author has granted "the right to reproduce and sell (a) copies of the manuscript in microform and/or (b) printed copies of the manuscript made from microform."

Signature _____

Date _____

University of Washington

Abstract

Experimental Study of Sound Waves in Sandy Sediment

Michael W. Yargus

Chair of the Supervisory Committee:
Professor Darrell R. Jackson
Electrical Engineering

This dissertation describes experiments intended to help understand the physics of sound (compressional waves) propagating through sandy sediments (unconsolidated porous media). The theory (using a lumped parameter model) and measurements (using a reflection ratio technique) includes derivations and measurements of acoustic impedances, effective densities, wave speeds (phase velocities), effective pressures, mode shapes, pressure reflection coefficients, and material moduli. The results show the acoustic impedance divided by the phase velocity, rendering an "effective density," is less than the total density of the sediment (effective density = 89% $\pm$ 3% of total). The results also show the fluid in the sediment oscillates back-and-forth 2.2 ± 0.4 times farther than the sand in the sediment (mode shape) during the passing of a sound wave. These facts suggest the existence of Biot waves (two compressional waves) in water-saturated sand.

TABLE OF CONTENTS

LIST OF FIGURES

LIST OF TABLES

ACKNOWLEDGMENTS

Chapter 1:
INTRODUCTION

This dissertation implements theory and procedures designed to measure physical parameters of acoustic waves (also called sound waves, compressional waves, bulk compressional waves, and dilatational waves) in sandy sediments. This experimental study was done to help understand the mechanics of sound propagating through water-saturated sand and in particular to look for effects only seen in porous media. These effects include different particle oscillation amplitudes of the sand and fluid (pore fluid in the sediment), a sound wave not "using" the total mass of the sediment, and the existence of two compressional waves with different speeds. These are characteristics of the two (fast and slow) Biot waves.

Sound wave measurements reported in this dissertation are obtained through a reflection ratio technique, a new technique that uses a reference surface and a pressure release surface to measure coherently averaged pressure reflection coefficients from a surface of interest. In the first of two parts, a signal of interest (reflected from the surface of interest) is divided by a reflected reference signal. The reference signal is a measure the sound wave being transmitted, and by dividing the reference signal into the signal of interest a transfer function is obtained. This has the advantage of setting a nearly perfect time reference so the reflections can be averaged coherently. In addition, the two signals from the transmitter do not have to be identical (the ringing of the transmitting hydrophone was actively canceled and the signal periodically needed to be "reshaped"). In the second part, the transfer function from the surface of interest is divided by a transfer function from a pressure release surface. The pressure release surface is set up so that the ratio of the two transfer functions leaves only the pressure reflection coefficient. This technique has the advantage of measuring a pressure reflection coefficient without needing to know the acoustic properties (dissipation, damping, spreading loss, etc.) of the media the sound travels through and without needing to calibrate the transducers (receiver and transmitter). With the reflection ratio technique, coherently averaged pressure reflection coefficients are measured without calibrating the transducers and without use of

geometric correction factors. By knowing pressure reflection coefficients, acoustic impedances of the sand can be obtained.

The mathematical theory is based on a lumped parameter model, a new model that visibly shows the physics of a Biot medium and facilitates use of free-body diagrams to find the distribution of pressures and the relative velocities between particles and acoustic waves, e.g., sand particle velocity to fast wave "effective" velocity. By knowing the fast and slow wave "effective" velocities, rigorous derivations of the fast and slow wave acoustic impedances are obtained for the first time.

1.1 OUTLINE OF DISSERTATION

This chapter includes: (1) A background of why knowledge of the physics of sound waves propagating through sand is of practical importance. (2) A short history of sound propagating through saturated porous materials. (3) Previous observations of Biot waves. (4) A look at two contemporary controversies. One is whether slow waves exist in unconsolidated porous materials, i.e., sediments, and another is whether the claimed compression waves in sediments at 1200 m/s are slow Biot waves or artifacts from scattering. (5) A list of key parameters and assumptions that play a role in the dynamic response of sediments. (6) A list of the new contributions published in this dissertation.

The second chapter of this dissertation goes through the mathematical theory and discusses a lumped parameter model. The third chapter discusses the acoustic measurements and the reflection ratio technique. The fourth chapter discusses the analysis and results; the last chapter gives a discussion with conclusions.

1.2 BACKGROUND

Understanding the physics of sound propagation into a sandy bottom of a shallow water environment is driven by a need to improve techniques for finding and classifying objects that are buried. Sonar, traditionally used to locate objects in water or map the water-sediment interface, can be used to locate objects such as mines, cables, pipelines and containers buried in sediment. The principle reason acoustic wave propagation and

scattering have been widely used to study processes and detect objects in the ocean is the limited range of optical and other electromagnetic wave propagation underwater. For a wide range of scientific and engineering problems dealing with the ocean environment, acoustic wave propagation and scattering is the only remote sensing technology available. A buried target can be illuminated with maximum intensity by a sonar signal normally incident on the sediment interface. However, the time taken to detect buried objects can become prohibitively large if only normal incidence is used. Using shallow incidence grazing angles can speed up detection operations considerably. For sand sediments, the compressional sound speed in the sediment is faster than in the water and the wave transmitted into the sediment is refracted at a smaller grazing angle than in the water. At the critical angle, typically at grazing angles of about 20 to 30 degrees, the refracted compressional wave is parallel to the interface and no longer propagates into the sediment. There is significant interest in mechanisms by which a compressional wave in the water can be coupled into the sediment at angles below the critical angle with energy sufficient enough for finding buried objects [24, 27, 34]. It has been proposed that the slow Biot wave may provide such a mechanism [34].

This dissertation explores normally incident waves in an attempt to understand the nature of sound propagating through sandy sediments. The results of this work are relevant to the general problem including incidence at angles smaller than the critical angle.

1.3 HISTORY

A complete theory for acoustic wave propagation in porous media was developed by Biot [3, 4, 5] and presented in a series of papers. Biot has developed a comprehensive theory for the static and dynamic response of linear, porous materials containing compressible fluid. This theory was derived by adding inertia terms into the equation of consolidation developed in earlier theories. Biot's theory predicts that in the absence of boundaries, three kinds of body waves, two dilatational and one shear, may exist in a fluid saturated porous medium [36].

Stoll and Kan [38] derived the complex reflection coefficient of plane acoustic waves from a poro-elastic sediment half-space. The boundary condition model is based on the classical work of Biot that, as previously stated, predicts three different body waves in the sediment. As a consequence, when plane waves in water are incident upon a water-sediment interface, as many as three waves can be generated in the sediment, depending on the angle of incidence.

Stoll and Kan used potentials in their derivation of the boundary conditions. Johnson and Plona rewrote Stoll and Kan's boundary conditions using displacements "as it is simpler than (although equivalent to)" the potential derivation [20]. Johnson and Plona's notation for the boundary conditions produces a symmetric determinant when solving for the eigenvalues and eigenvectors, which can be modeled into a physically realizable system. Also the density terms in Johnson and Plona's determinant add up to the density of the water-saturated sand. Neither of these are true for Stoll and Kan's notation and both are important for the lumped parameter model to be developed here.

1.4 OBSERVATIONS OF BIOT WAVES

Plona observed a second bulk compressional wave that propagated at speeds approximately 25% of the speed of the normal bulk compressional wave in a fluid-saturated porous medium [29]. This observation was made using an ultrasonic immersion technique and a fluid-saturated porous medium consisting of water and sintered glass spheres. The excitation of the slow wave in the solid was shown to be consistent with the principles of mode conversion and refraction at plane liquid/solid interfaces. To Plona's knowledge, this type of bulk wave had not been previously observed at ultrasonic frequencies.

Biot's theory has been used in several applications of acoustic wave propagation in porous media, such as superfluid/superleak systems [18], slow waves and the consolidation transition [19, 20], gels [21], bones [25], porous solids [15, 23, 30], marine sediments [17, 35, 41, 43, 45], pressure diffusion through porous media [8], and air-saturated consolidated porous media [16].

Johnson et al. [22] observed slow compression waves in consolidated fluid-saturated porous media, e.g., fused glass beads (called "Ridgefield Sandstone" even though it was man-made) and ceramic water filters (QF-20), and calculated for the first time all of the input parameters necessary for a complete description of the acoustic properties of all the modes over the entire frequency spectrum.

All observed slow Biot waves have been in consolidated porous media. There have been no uncontested observations of a slow Biot wave in an unconsolidated, e.g., sandy, medium. See Controversy-2 that follows.

1.5 CONTROVERSY-1 (Do slow Biot waves exist in sediments?)

Even though Biot theory predicts both fast and slow compressional waves, only the fast compressional wave, the wave of the first kind, and the shear wave have been observed in the vast majority of porous systems. Johnson and Plona, who observed slow Biot waves in water-saturated porous media where the solids are bonded together, have looked for slow Biot waves in unconsolidated water saturated glass beads where they conclude "both experimentally and theoretically there is only one compressional wave" [20].

Simpson et al., [34] did an experiment showing the wave fields in sand with smooth and rough interfaces at all angles of incidence. They concluded, "This data does not support the Biot medium model predictions of a second slower compressional wave in the unconsolidated water saturated porous medium."

Seifert et al., [33] did an experiment with sand saturated with fluids of different viscosities (water, two different silicon oils, and castor oil) to measure attenuation. They stated, "Biot's theory shows that acoustic waves create relative motion between the fluid and the solid matrix due to inertial effects, resulting in viscous dissipation of acoustic energy." But they concluded "The attenuation shows no correlation with the viscosity of the different pore fluids and thus theories that depend upon fluid flow cannot explain these data." They conclude Biot theory does not explain attenuations measured in fluid filled sand.

On the pro side, Stoll et al., [38] say Biot waves exists but, "Waves of the second kind are difficult to observe in sediments where water is the saturant because of their high attenuation and the way in which energy is partitioned at the interface."

1.6 CONTROVERSY-2 (Compressional waves at 1200 m/s are from slow Biot or scattering?)

Recent experimental results (Boyle and Chotiros 1992 [6], Chotiros 1995 [9]) reveal acoustic penetration from water into sandy sediments at grazing angles below the compressional critical angle in relation to the mean surface. These authors interpret their results to indicate the excitation of a Biot slow wave at 1200 m/s in the sediment.

But numerous authors disagree. Analytical derivations show that roughness of the water-sediment interface causes propagation of acoustical energy from water into the sediment at grazing angles below the compressional critical grazing angle, and simulations indicate that the experimental results can be explained in terms of diffraction of an ordinary longitudinal wave. By modeling sand as a fluid, and including a small amount of roughness, the simulation results match the acoustical penetration experimental results by Boyle and Chotiros (1992), both in magnitude and in arrival time [28, 40]. Mellema [27] demonstrated that significant energy is scattered across a rough fluid-solid interface at shallow grazing angles and that the received intensity can be accurately modeled using first order perturbation theory. For the roughened case, it is clear that the later time arrival is best described by an assumed ray path in the water to a point above the buried hydrophone, scattered from the roughened interface, and then propagation nearly vertically to the buried hydrophone at the speed of the ordinary compressional wave (1680 m/s). This can have the appearance of a wave traveling at 1200 m/s [34].

Recent field measurements [17, 26, 34] have strongly supported the conclusion that subcritical penetration in sands is due to scattering, not Biot slow waves.

To match the 1200 m/s slow compression wave using Biot theory, Chotiros [9] used structural and material moduli of sand different than previous authors. Stoll [39] and other authors used moduli that predict a slow wave having a speed of roughly 400

m/s. Stoll argues Chotiros "... is not justified in his claim that a Biot wave of the second kind, with a wave speed of 1200 m/s, had been detected in a near-bottom sand deposit. This opinion is based on the fact that the author (Chotiros) has used an unacceptable value for the bulk modulus of the skeletal frame and a questionable value for the bulk modulus of the individual grains."

Chotiros [11] replied that the approach advocated by Stoll to calculate bulk moduli works well for a porous materials with cemented frames, such as fused glass beads and sandstone, but it does not work for sand. Chotiros also contended that the measured reflection coefficient for normal incidence on a water-sand interface does not match elementary, Rayleigh, viscoelastic reflection theory but his parameters using Biot theory do produce a match with the measured coefficient.

1.7 PARAMETERS AND ASSUMPTIONS

A survey of the literature suggests that there are a number of parameters that play a principal role in controlling the dynamic response of saturated sediments. Of these, Stoll suggests the following may be important (not necessarily in the order listed) [37]:

a.   dynamic strain amplitude,

b.   porosity,

c.   static intergranular stress,

d.   gradation of sand size and grain shape,

e.   material properties of individual grains,

f.   degree and kind of lithification (bonding of particles),

g.   structure as determined by the mode of deposition.

In his classic development, Biot produced constitutive relationships for fluid-saturated granular media and followed these with an analysis of elastic wave propagation in such media by means of a Lagrangian formulation. The assumptions underlying this derivation are that [1]:

a.   The medium is isotropic, quasi-homogeneous and that the porosity is uniform throughout;

b.   The pore size is very much less than the wavelengths of interest;

c.   Scattering, in the sense of diffraction around individual grains or particles, can be ignored;

d.   Pore walls are impervious and the pore size is concentrated around an average value;

e.   Fluid is compressible;

f.   Fluid may flow relative to the solid.

1.8 NEW CONTRIBUTIONS OF THIS DISSERTATION

The contributions of this dissertation are both theoretical and experimental. On the theoretical side the primary contributions include: (1) Making a lumped parameter model from the continuous parameter Biot theory, fig. 2.1. (2) Deriving the fast and slow acoustic impedances, eqs. (2-35) and (2-37). (3) Deriving pressure reflection and transmission coefficients from impedances and effective pressures, tables 2.1 and 2.2. (4) Deriving mode shapes from effective pressures and effective densities, eqs. (4-27) and (4-28).

On the experimental side the primary contributions include: (5) A reflection ratio technique in which reflection amplitudes are divided leaving only information (pressure reflection coefficient) about the surface, e.g., eq. (4-1), without calibrating the transducers or using geometric corrections. (6) Measuring the fast and slow wave acoustic impedances, fig. 4.1. (7) Measuring the fast and slow effective densities, fig. 4.2. (8) Bounding the slow acoustic wave speed in an unconsolidated medium, fig. 4.3. (9) Measuring the fast and slow wave effective pressures from an open pore boundary condition, fig. 4.4. (10) Measuring the fast and slow wave mode shapes, fig. 4.6. (11) And last, measuring the generalized elastic coefficients (intermediate moduli), fig. 4.7.

Chapter 2:
MATHEMATICAL THEORY

This chapter reviews the continuous parameter equations of motion and boundary conditions, and then develops a lumped parameter model from which the fast and slow impedances, moment arms, effective densities, and effective pressures are derived. Then pressure coefficients are derived from impedances and effective pressures. Only normally incident pressure waves, waves propagating perpendicular to the sediment boundary, are considered in the following continuous parameter review and lumped parameter development. This consideration simplifies the equations by removing shear waves (and coupling between shear and pressure waves), and is sufficient for analysis of the experimental data discussed in the next chapter.

2.1 DIFFERENTIAL EQUATIONS OF MOTION AND BOUNDARY CONDITIONS

From Johnson and Plona [20], eq. (1a) and (1b), the homogeneous differential equations of motion with waves propagating in the z-direction with no shear displacements are:

$$P\frac{\partial^2 u_s}{\partial z^2}+Q\frac{\partial^2 u_f}{\partial z^2}-\rho_{11}\ddot{u}_s-\rho_{12}\ddot{u}_f+F\dot{u}_f-F\dot{u}_s=0 \tag{2-1}$$

$$R\frac{\partial^2 u_f}{\partial z^2}+Q\frac{\partial^2 u_s}{\partial z^2}-\rho_{12}\ddot{u}_s-\rho_{22}\ddot{u}_f-F\dot{u}_f+F\dot{u}_s=0 \; . \tag{2-2}$$

Eq. (2-1) is the equation of force on sand particles per unit area (area of sand plus area of fluid in sediment) and eq. (2-2) is the force equation on fluid particles per unit area. The unknowns, u_s and u_f, are displacements (in the z-direction) of the sand and fluid particles. P, Q, and R are the generalized elastic coefficients (intermediate moduli).

$$P=\frac{(1-\beta)\left(1-\beta-\dfrac{K_b}{K_s}\right)K_s+\beta\dfrac{K_s}{K_w}K_b}{1-\beta-\dfrac{K_b}{K_s}+\beta\dfrac{K_s}{K_w}}+\frac{4}{3}N \tag{2-3}$$

$$Q = \frac{\left(1 - \beta - \dfrac{K_b}{K_s}\right)\beta K_s}{1 - \beta - \dfrac{K_b}{K_s} + \beta \dfrac{K_s}{K_w}} \qquad (2\text{-}4)$$

$$R = \frac{\beta^2 K_s}{1 - \beta - \dfrac{K_b}{K_s} + \beta \dfrac{K_s}{K_w}} \qquad (2\text{-}5)$$

Where β is the porosity (volume of fluid per unit volume of sediment), K_b is the bulk modulus of the sand's skeletal frame, K_s is the bulk modulus of the sand, K_w is the bulk modulus of the water, and N is the shear modulus of the skeletal frame.

The density terms are:

$$\rho_{11} = (1 - \beta)\rho_s + (\alpha - 1)\beta\rho_f \qquad (2\text{-}6)$$

$$\rho_{22} = \alpha\beta\rho_f \qquad (2\text{-}7)$$

$$\rho_{12} = -(\alpha - 1)\beta\rho_f . \qquad (2\text{-}8)$$

Where ρ_s is the density of the sand grains, ρ_f is density of water, and α is a virtual mass constant, or tortuosity, expressing the apparent increase in the mass of the fluid. As a fluid particle oscillates in the z-direction it must translate slightly in the x- and y-directions to go around sand particles causing it to appear more massive.

The viscous term is:

$$F = \frac{\eta\beta^2\kappa^2}{4k} \frac{-i^{\frac{3}{2}} J_1\left(\kappa\exp\left(i3\dfrac{\pi}{4}\right)\right)}{\kappa J_0\left(\kappa\exp\left(i3\dfrac{\pi}{4}\right)\right) + 2\sqrt{i} J_1\left(\kappa\exp\left(i3\dfrac{\pi}{4}\right)\right)} \qquad (2\text{-}9)$$

$$\kappa = a\sqrt{\frac{\omega\rho_f}{\eta}} . \qquad (2\text{-}10)$$

The viscous term, F, is equivalent to bF, eq. (4.3) in [4], where b is defined by eq. (6.8) in [3]. In eqs. (2-9) and (2-10), η is the viscosity of water, k is the permeability of the medium, J_1 and J_0 are Bessel functions, and a is the average radius of the pore holes.

Solving eqs. (2-1) and (2-2) for plane waves, assume the solid displacements and fluid displacements are:

$$u_s = A \exp(i(\omega t - kz)) \tag{2-11}$$

$$u_f = B \exp(i(\omega t - kz)). \tag{2-12}$$

Here, k is wave number, t is time, A is the sand displacement amplitude and B is the fluid displacement amplitude. Put eqs. (2-11) and (2-12) into (2-1) and (2-2) and express the results in matrix form:

$$\begin{bmatrix} k^2 P - \omega^2 \rho_{11} + i\omega F & k^2 Q - \omega^2 \rho_{12} - i\omega F \\ k^2 Q - \omega^2 \rho_{12} - i\omega F & k^2 R - \omega^2 \rho_{22} + i\omega F \end{bmatrix} \begin{Bmatrix} A \\ B \end{Bmatrix} = \begin{Bmatrix} 0 \\ 0 \end{Bmatrix}, \tag{2-13}$$

$$k^2 \begin{bmatrix} P & Q \\ Q & R \end{bmatrix} \begin{Bmatrix} A \\ B \end{Bmatrix} = \omega^2 \begin{bmatrix} \rho_{11} - i\dfrac{F}{\omega} & \rho_{12} + i\dfrac{F}{\omega} \\ \rho_{12} + i\dfrac{F}{\omega} & \rho_{22} - i\dfrac{F}{\omega} \end{bmatrix} \begin{Bmatrix} A \\ B \end{Bmatrix}. \tag{2-14}$$

The square matrix on the right hand side of eq. (2-14) is the density matrix and will be referred to later. Solve for the eigenvalues (wave numbers squared) and eigenvectors (mode shapes). This will give displacements of the sand and fluid in terms of the wave numbers and the mode shapes.

$$u_s = A_1 \exp(i(\omega t - k_1 z)) + A_2 \exp(i(\omega t - k_2 z)) \tag{2-15}$$

$$u_f = B_1 \exp(i(\omega t - k_1 z)) + B_2 \exp(i(\omega t - k_2 z)) \tag{2-16}$$

Where the wave fast and slow numbers are:

$$k_1^2 = \frac{-b - \sqrt{b^2 - 4ac}}{2a}, \quad k_2^2 = \frac{-b + \sqrt{b^2 - 4ac}}{2a},$$

with
$$a = PR - Q^2 \tag{2-17}$$

$$b = \omega^2 \left(-P\rho_{22} - R\rho_{11} + 2Q\rho_{12} \right) + i\omega F (P + R + 2Q)$$

$$c = \omega^4 \left(\rho_{11}\rho_{22} - \rho_{12}^2 \right) + i\omega^3 F (\rho_{11} - \rho_{22} - 2\rho_{12}).$$

The mode shapes are (water particle displacement divided by sand particle displacement):

$$\frac{B_1}{A_1} = \frac{-k_1^2 P + \omega^2 \rho_{11} - i\omega F}{k_1^2 Q - \omega^2 \rho_{12} - i\omega F} = \frac{-k_1^2 Q + \omega^2 \rho_{12} + i\omega F}{k_1^2 R - \omega^2 \rho_{22} + i\omega F} \tag{2-18}$$

$$\frac{B_2}{A_2} = \frac{-k_2^2 P + \omega^2 \rho_{11} - i\omega F}{k_2^2 Q - \omega^2 \rho_{12} - i\omega F} = \frac{-k_2^2 Q + \omega^2 \rho_{12} + i\omega F}{k_2^2 R - \omega^2 \rho_{22} + i\omega F}. \tag{2-19}$$

The boundary conditions for the water-sediment (open pore) interface are taken from Johnson et al. [22] and specialized to normal incidence for which there is no excitation of shear waves. Combine equations (2.17), (2.18), (2.19), (2.20), (2.21), and (2.25) from ref. [22] and get:

$$P\frac{\partial u_s}{\partial z} + Q\frac{\partial u_f}{\partial z} + Q\frac{\partial u_s}{\partial z} + R\frac{\partial u_f}{\partial z} = K_w \frac{\partial u_i}{\partial z} + K_w \frac{\partial u_r}{\partial z}. \tag{2-20}$$

Eq. (2-20) says the force in the sand per unit area of interface (note: <u>not</u> the pressure in the sand because area is of sand and pore water) plus the force in the sediment fluid per unit area of interface is equal to the pressure in the water above the sediment. Johnson's W is the same as this dissertation's $u_i + u_r$. The variables u_i and u_r are the incident and reflected displacements, assumed to be of the form:

$$u_i = A_i \exp(i(\omega t - k_w z)) \tag{2-21}$$

$$u_r = A_r \exp(i(\omega t + k_w z)). \tag{2-22}$$

Combine equations (2.18), (2.20), and (2.23) from ref. [22] and get:

$$Q\frac{\partial u_s}{\partial z} + R\frac{\partial u_f}{\partial z} = \beta\left(K_w \frac{\partial u_i}{\partial z} + K_w \frac{\partial u_r}{\partial z}\right). \tag{2-23}$$

Eq. (2-23) says the force in the sediment fluid at the interface is equal to the force in the water above the sediment fluid per unit area of interface. From equations (2.22) and (2.25) from ref. [22]:

$$u_s(1-\beta) + u_f \beta = u_i + u_r. \tag{2-24}$$

Eq. (2-24) says the displacement of sand times the area of sand per unit area of interface plus the displacement of sediment fluid times the area of fluid per unit area of interface is equal to the displacements of the incident plus reflected waves in the water per unit area. This is the so-called open pore boundary condition. Eq. (2-24) can be rewritten:

$$u_{fast} + u_{slow} = u_i + u_r, \qquad (2\text{-}25)$$

where

$$u_{fast} = (A_1(1-\beta) + B_1\beta)\exp(i(\omega t - k_1 z)) \qquad (2\text{-}26)$$

$$u_{slow} = (A_2(1-\beta) + B_2\beta)\exp(i(\omega t - k_2 z)). \qquad (2\text{-}27)$$

Eq. (2-26) is the average of the sand and fluid particle displacements during the passing of a fast wave. Both previous equations will be used later to derive participation factors.

The closed pore boundary condition for displacements will be used later and is:

$$u = u_i + u_r, \qquad (2\text{-}27\text{a})$$

where at $z = 0$:

$$u = u_s = u_f = (A_1 + A_2)\exp(i\omega t) = (B_1 + B_2)\exp(i\omega t) \qquad (2\text{-}27\text{b})$$

This section (equations of motion and boundary conditions) has given the wave numbers, mode shapes, and the boundary conditions for a continuous, 2 degrees-of-freedom, Biot medium having a planar interface and normal incidence. The next section develops the lumped parameter model.

2.2 LUMPED PARAMETER MODEL

The lumped parameter method developed here was strongly influenced by the Dynamic Design Analysis Method (DDAM) introduced by Belsheim and O'Hara [2]. DDAM is used to analyze non-contact, bomb shock on Naval ships. See Appendix E. DDAM requires a physical system to be engineered into a lumped mass-spring model. Then the equations of motion are written in matrix form from the mass-spring model. The natural frequencies and mode shapes are calculated from the determinant of the eigenvalue problem, and the determinant is always symmetrical. Likewise, even though Biot's equations of motion are for continuous parameters, the determinant for the wave numbers is symmetrical using Johnson and Plona's notation. The inspiration for the lumped parameter model was the question "Can Biot's continuous parameter, symmetric determinate be reverse-engineered (through trial-and-error) into a lumped mass-spring

model?" A lumped parameter model has the advantage of allowing easy visualization of movements and drawing free body diagrams of the forces.

The continuous medium homogeneous differential equations of motion and boundary conditions eqs. (2-13), (2-20), (2-23), and (2-24) can be described by a lumped mass, linear spring, concentrated force, viscous damp-pot, rigid-bar mechanical system, see Fig. 2.1 and Appendix D.

Figure 2.1
Mass-Spring-Force Mechanical Model
of the Biot Medium
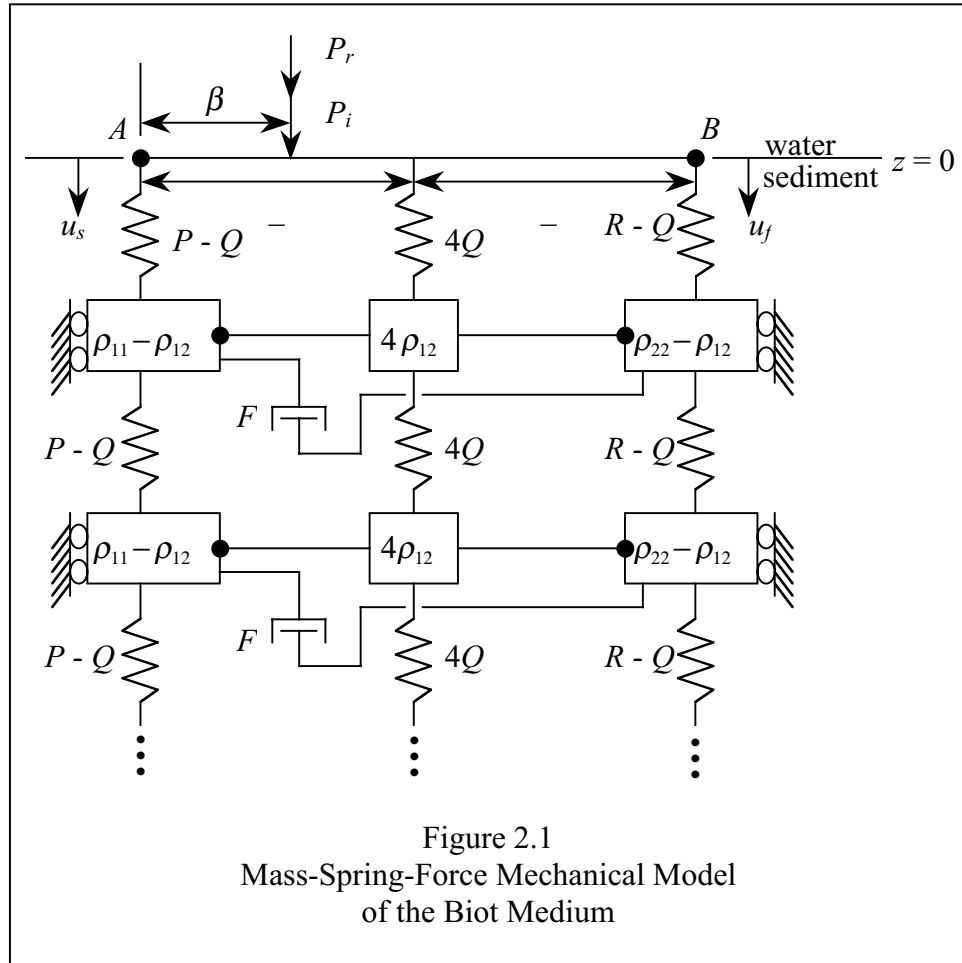
In going from the continuous model to the lumped model, stiffness (N/m) and modulus (Pa), mass (kg) and density (kg/m^3), force (N) and pressure (Pa), viscous damping (Ns/m) and body viscous damping (Ns/m^4), difference in displacement of two points (m) and strain (m/m), acoustic impedance (Pa $\cdot$ s/m) and mechanical impedance

(Ns/m) are used interchangeably. Hopefully this does not cause too much confusion. Point A in Fig. 2.1 is the "location" of the sand (displacement of point A equals the sand particle displacement) and point B is the "location" of the fluid in the sediment (also the displacement of point B equals the sediment fluid particle displacement). P_i and P_r are the incident and reflected forces.

To show that the boundary conditions of the mechanical system of Fig. 2.1 are equivalent to Johnson et al. [22] boundary conditions draw a free body diagram at $z = 0$, see Fig. 2.2. In Fig. 2.2 the positive direction is down. Eq. (2-20) is the sum of forces in the vertical direction. Eq. (2-23) is the sum of moments about point A. The incident and reflected displacements, u_i and u_r, are related to the solid and fluid displacements, u_s and u_f, by eq. (2-24). Fig. 2.3 is equivalent to Fig. 2.2 but in Rayleigh notation, i.e., $e^{i\omega t}$ suppressed (ref. [31], section 270, eq. (11)).

Figure 2.2
Free-Body Diagram of the Boundary

$iK_wk_wA_r$

β

$-iK_wk_wA_i$

A B —— $z = 0$

$i(P - Q)(k_1A_1 + k_2A_2)$

$i2Q(k_1A_1 + k_2A_2 ... + k_1B_1 + k_2B_2)$

1/2

1

$i(R - Q)(k_1B_1 + k_2B_2)$

Figure 2.3
Rayleigh Notation of Figure 2.2

F_1

δ_1

A B

A_1

B_1

u_s u_f

1/2   1/2

$i2Qk_1(A_1 + B_1)$

$i(R - Q)k_1B_1$

$i(P - Q)k_1A_1$

Figure 2.4
Free-Body Diagram of Fast Wave Mode Shape
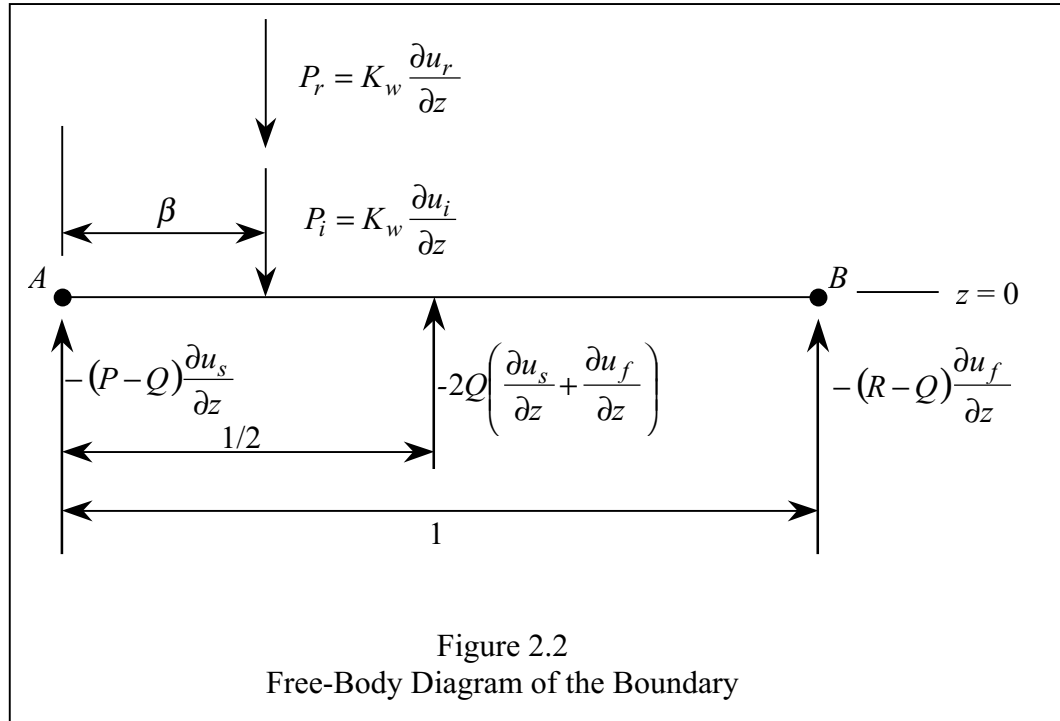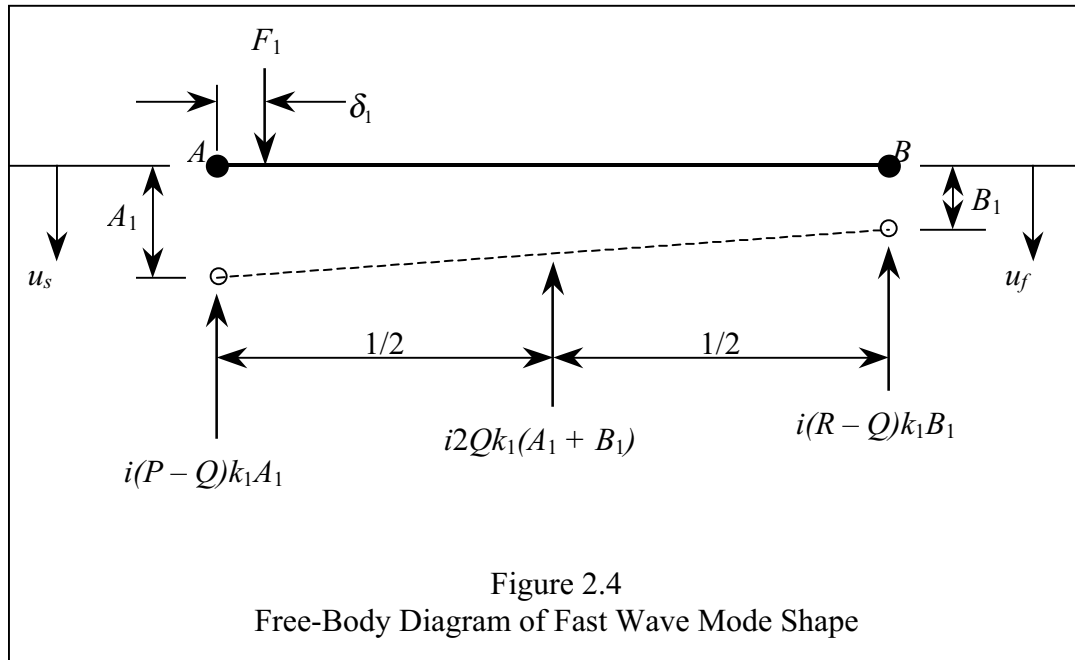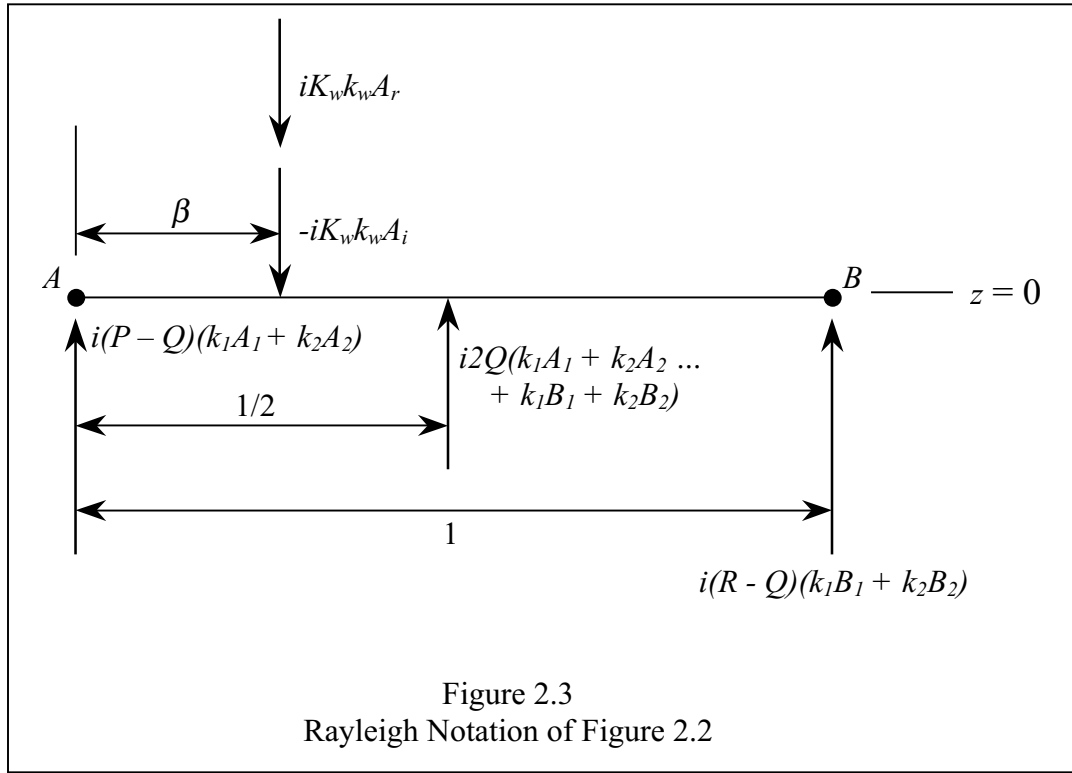
A force can be positioned that will only excite the fast wave. As will be seen, this is a consequence of mode orthogonality. See Fig. 2.4. From Fig. 2.4, sum forces in the vertical direction:

$$F_1 = i\left(Pk_1A_1 + Qk_1A_1 + Qk_1B_1 + Rk_1B_1\right). \tag{2-28}$$

The sum of the moments around point A in Fig. 2.4 is:

$$\delta_1 F_1 = i\left(Qk_1A_1 + Rk_1B_1\right). \tag{2-29}$$

From equations (2-28) and (2-29) the moment arm for a force to excite only mode 1 is:

$$\delta_1 = \frac{QA_1 + RB_1}{PA_1 + QA_1 + QB_1 + RB_1}. \tag{2-30}$$

Another way to find δ_1 is by knowing that a force applied at δ_2, the moment arm for mode 2 (slow wave), will cause no work at δ_1, i.e., the translation at δ_1 in the z-direction is zero. See Fig. 2.5.

$$\delta_1 = \frac{A_2}{A_2 - B_2} \tag{2-31}$$

Figure 2.5
Location of F_1 Using Orthogonality

These two relationships for δ_1, equations (2-30) and (2-31), are equivalent to the orthogonality relationship:

$$\left\{ \begin{matrix} A_1 \\ B_1 \end{matrix} \right\}^T \begin{bmatrix} P & Q \\ Q & R \end{bmatrix} \left\{ \begin{matrix} A_2 \\ B_2 \end{matrix} \right\} = 0 . \tag{2-32}$$

From Fig. 2.4 the velocity at point δ_1 is:

$$v_1 = i(1-\delta_1)\frac{\partial u_{s1}}{\partial t} + i\delta_1 \frac{\partial u_{f1}}{\partial t} = i[(1-\delta_1)\omega A_1 + \delta_1 \omega B_1]. \tag{2-33}$$

The impedance of first mode (fast wave) is:

$$Z_1 = \frac{F_1}{v_1} \tag{2-34}$$

$$Z_1 = \frac{k_1}{\omega}\frac{[(P+Q)A_1 + (R+Q)B_1]^2}{PA_1{}^2 + 2QA_1B_1 + RB_1{}^2} \quad \longleftarrow . \tag{2-35}$$

Similarly:

$$\delta_2 = \frac{QA_2 + RB_2}{PA_2 + QA_2 + QB_2 + RB_2} = \frac{A_1}{A_1 - B_1}, \tag{2-36}$$

$$Z_2 = \frac{k_2}{\omega}\frac{[(P+Q)A_2 + (R+Q)B_2]^2}{PA_2{}^2 + 2QA_2B_2 + RB_2{}^2} \quad \longleftarrow . \tag{2-37}$$

Because: $$K = Z\frac{\omega}{k} \tag{2-38}$$

$$\rho = \left(\frac{k}{\omega}\right)^2 K , \tag{2-39}$$

the modal stiffnesses (moduli) and masses (densities) of the first and second modes are:

$$K_1 = \frac{[(P+Q)A_1 + (R+Q)B_1]^2}{PA_1{}^2 + 2QA_1B_1 + RB_1{}^2} \tag{2-40}$$

$$K_2 = \frac{[(P+Q)A_2 + (R+Q)B_2]^2}{PA_2{}^2 + 2QA_2B_2 + RB_2{}^2} \tag{2-41}$$

$$\rho_1 = \left(\frac{k_1}{\omega}\right)^2 \frac{[(P+Q)A_1 + (R+Q)B_1]^2}{PA_1{}^2 + 2QA_1B_1 + RB_1{}^2} \tag{2-42}$$

$$\rho_2 = \left(\frac{k_2}{\omega}\right)^2 \frac{[(P+Q)A_2 + (R+Q)B_2]^2}{PA_2{}^2 + 2QA_2B_2 + RB_2{}^2}.$$ (2-43)

The following two equations are taken from the matrix equation of (2-14):

$$(PA + QB) = c^2 \left[\left(\rho_{11} - i\frac{F}{\omega}\right)A + \left(\rho_{12} + i\frac{F}{\omega}\right)B\right]$$ (2-44)

$$(QA + RB) = c^2 \left[\left(\rho_{12} + i\frac{F}{\omega}\right)A + \left(\rho_{22} - i\frac{F}{\omega}\right)B\right].$$ (2-45)

Add equations (2-44) and (2-45) and put in the numerators of (2-42) and (2-43). Also multiply equation (2-44) by A and (2-45) by B, add, and put in the denominators of (2-42) and (2-43). The results are the modal masses or the effective masses in terms of density (and viscous) parameters:

$$\rho_1 = \frac{[(\rho_{11} + \rho_{12})A_1 + (\rho_{12} + \rho_{22})B_1]^2}{\rho_{11}A_1{}^2 + 2\rho_{12}A_1B_1 + \rho_{22}B_1{}^2 - i\frac{F}{\omega}(A_1 - B_1)^2}$$ (2-46)

$$\rho_2 = \frac{[(\rho_{11} + \rho_{12})A_2 + (\rho_{12} + \rho_{22})B_2]^2}{\rho_{11}A_2{}^2 + 2\rho_{12}A_2B_2 + \rho_{22}B_2{}^2 - i\frac{F}{\omega}(A_2 - B_2)^2}.$$ (2-47)

These modal masses, eqs. (2-46) and (2-47), agree with the Dynamic Design Analysis Method (DDAM), see Appendix E. Also, Clough and Penzien [14] p. 559, show that the sum of the modal masses is equal to the sum of all the terms in the mass matrix, eq. (2-14), i.e., $\rho_1 + \rho_2 = \rho_{11} + \rho_{22} + 2\rho_{12} = (1-\beta)\rho_s + \beta\rho_f = \rho$. Where ρ is the total density of the water filled sand. With Johnson and Plona's form of the Biot equations, eqs. (2-1) and (2-2), the modal masses add up to the total mass, i.e., $\rho_1 + \rho_2 = \rho$.

The terms that link particle displacements to effective (or modal) displacements are called "participation factors" in this dissertation. For a single degree-of-freedom system, of course, particle displacements and effective displacements are equal. Transforming average particle displacement of the sand and fluid during the passing of a fast wave, eq. (2-26), into a lumped parameter model, Fig. 2.6, shows the average particle

displacement is located at a distance β from point A. In Fig. 2.6 points 1 and 2 are the locations of the first and second modes and points A and B are the locations of the sand and fluid particles. The symbols u_1 and u_2 are the effective or modal displacements. The fast wave participation factor is:

$$\widetilde{P}_1 = \frac{u_{fast}}{u_1}$$

$$= \frac{\delta_2 - \beta}{\delta_2 - \delta_1}. \qquad (2\text{-}48)$$

And likewise the slow wave participation factor is:

$$\widetilde{P}_2 = \frac{u_{slow}}{u_2}$$

$$= \frac{\beta - \delta_1}{\delta_2 - \delta_1}. \qquad (2\text{-}49)$$

Figure 2.6
Modal Displacement (u_1) and
Average Particle Displacement
(u_{fast}) for the Fast Wave
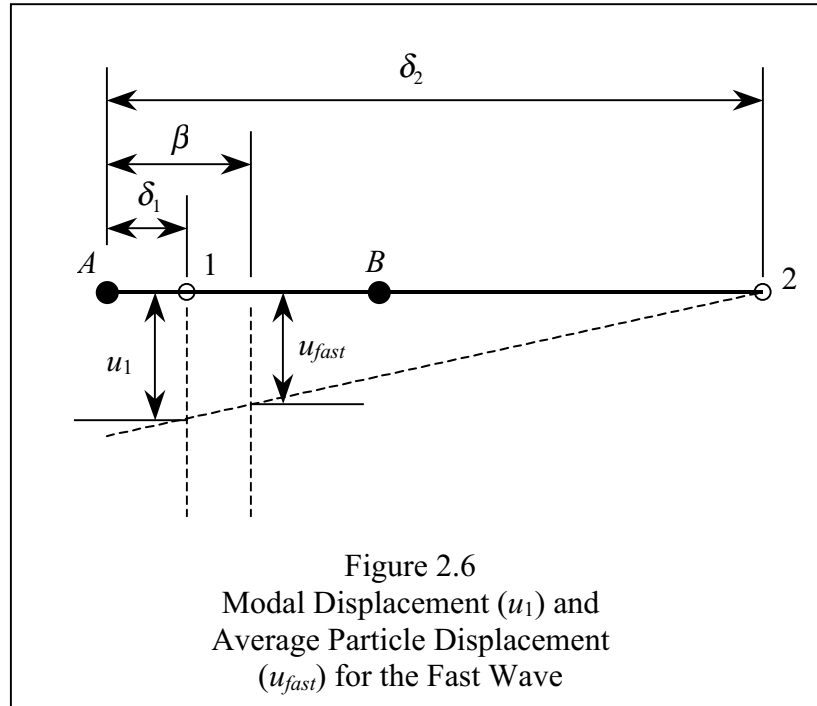
Fig. 2.7 is a mechanical system equivalent to Fig. 2.1 but in terms of modal parameters. The acoustic impedances for Biot waves are fully described by the impedances and the impedance moment arms, which are modal parameters independent of the loading of the mechanical system, i.e., they are homogeneous parameters (in a differential equation sense). The terms that link loading (boundary conditions) and modal parameters are the modal forces or effective forces.

Figure 2.7
Mechanical System Equivalent to Fig. 2.1
But In Terms of Modal Parameters
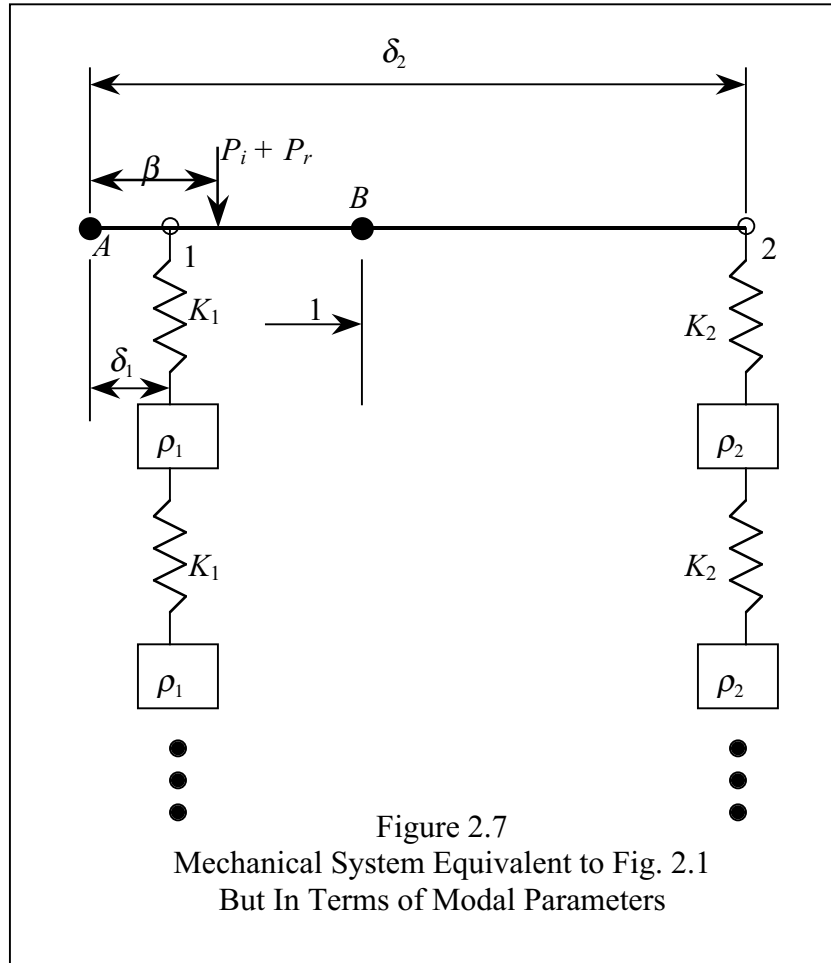
In the open pore boundary mentioned earlier, the water above the sediment and the fluid in the sediment are in direct contact. This is the most commonly used boundary condition for sediments. The terms that link external forces to forces on the first and second mode are called "effective forces." The incident and reflected forces act at a distance β from point A for an open pore interface, see Fig. 2.7. Let the incident and re-

flected forces equal one then from Fig. 2.8, P_1 is the "effective force" on mode 1 and P_2 is the "effective force" on mode 2.

$$P_1 = \frac{\delta_2 - \beta}{\delta_2 - \delta_1} \qquad (2\text{-}50)$$

$$P_2 = \frac{\beta - \delta_1}{\delta_2 - \delta_1} . \qquad (2\text{-}51)$$

Figure 2.8
Effective Forces P_1 and P_2
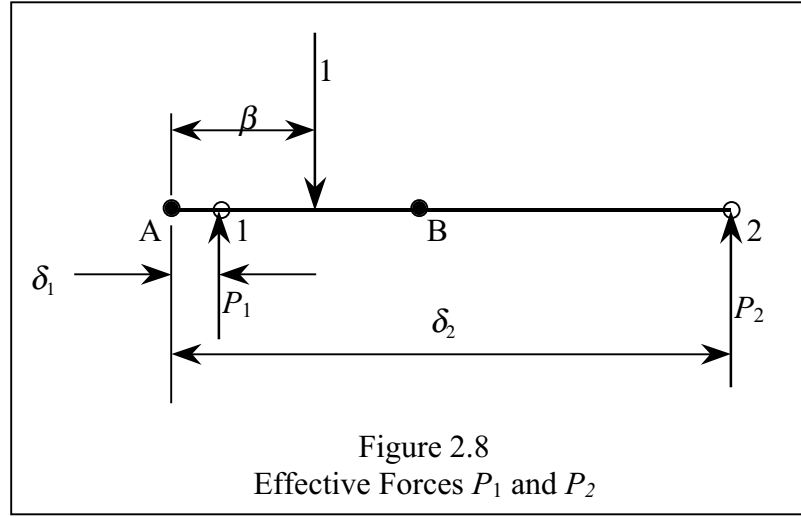
Note that, numerically, open pore effective forces are equal to participation factors even though their meanings are different.

For a closed pore boundary the sediment is in contact with a non-porous material, like acrylic. In a closed pore boundary the sand and fluid particles and the fast and slow modal displacements move with the same amplitude at the interface, and the modal points 1 and 2 move equally, see eq. (2-27b). The forces needed to move these points equally are the closed pore effective forces.

$$P_1^{(c)} = \frac{Z_1}{Z_1 + Z_2} \qquad (2\text{-}52)$$

$$P_2^{(c)} = \frac{Z_2}{Z_1 + Z_2} \qquad (2\text{-}53)$$

The next section calculates the pressure reflection and transmission coefficients using impedances and effective forces.

2.3 REFLECTION AND TRANSMISSION PRESSURE COEFFICIENTS FOR A SOUND WAVE IN WATER INCIDENT UPON A SAND INTERFACE (OPEN PORE)

This section finds the reflection and transmission coefficients for various boundary conditions of a medium that supports Biot waves. If the distance from the first to second modes, points 1 and 2, are normalized to one, the normalized distances from an applied unit force (the force is applied at a position to make the forces on Z_1 and Z_2 equal to P_1 and P_2) to the locations of the modes are numerically equal to the normalized effective forces, P_1 and P_2, see Fig. 2.9. These normalized forces and normalized distances will be assigned the same symbols, P_1 and P_2. The impedance of the Biot medium is found by applying a force of 1 at a distance P_2 from the left in Fig. 2.9. The springs in the figure are labeled as impedances, Z (units of Ns/m in lumped system). Technically, the spring constants should be $Z\omega$ (N/m), but the frequency terms are dropped. Velocities of the first and second modes are:

$$v_1 = \frac{P_1}{Z_1}, \quad v_2 = \frac{P_2}{Z_2}.$$

(2-54)

The velocity at the point of unit force is:

$$v = v_1 P_1 + v_2 P_2 = \frac{Z_2 P_1^2 + Z_1 P_2^2}{Z_1 Z_2}.$$

(2-55)

The impedance "seen" by an incident wave from water to a Biot medium is:

$$Z = \frac{1}{v}$$

$$Z = \frac{Z_1 Z_2}{Z_2 P_1^2 + Z_1 P_2^2}.$$

(2-56)

The pressure reflection coefficient of a sound wave off a Biot medium (water to sand) is (where Z_w is the impedance of water):

$$R_{ww} = \frac{Z - Z_w}{Z + Z_w}$$

$$R_{ww} = \frac{Z_1 Z_2 - Z_w Z_1 P_2^2 - Z_w Z_2 P_1^2}{Z_1 Z_2 + Z_w Z_1 P_2^2 + Z_w Z_2 P_1^2}.$$

(2-57)

Figure 2.9
Model Used to Find Acoustic Imped-
ance
of Biot Medium
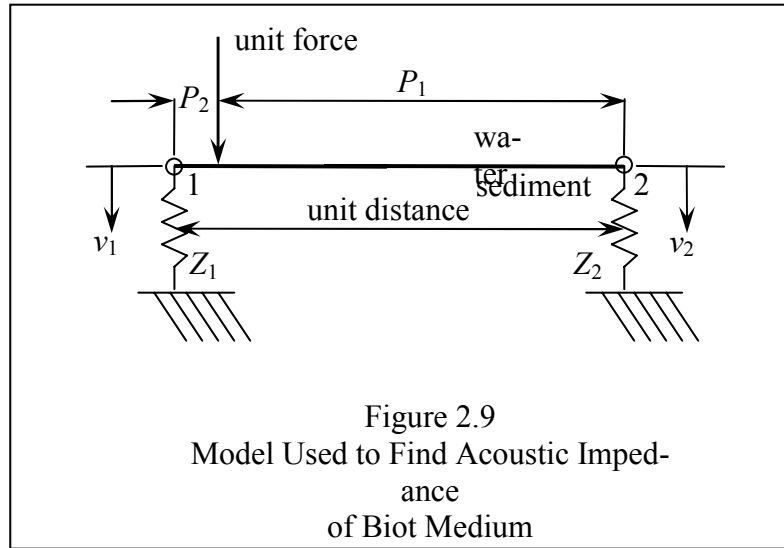
The pressure transmission coefficient for the fast and slow waves combined is:

$$T_{ws} = \frac{2Z}{Z + Z_w}$$

$$T_{ws} = \frac{2Z_1 Z_2}{Z_1 Z_2 + Z_w Z_1 P_2{}^2 + Z_w Z_2 P_1{}^2} . \qquad (2\text{-}58)$$

From the free-body diagram of Fig. 2.10 the fast wave transmission coefficient is:

Figure 2.10
Free Body Diagram of Incident,
Reflected, and Transmitted Waves
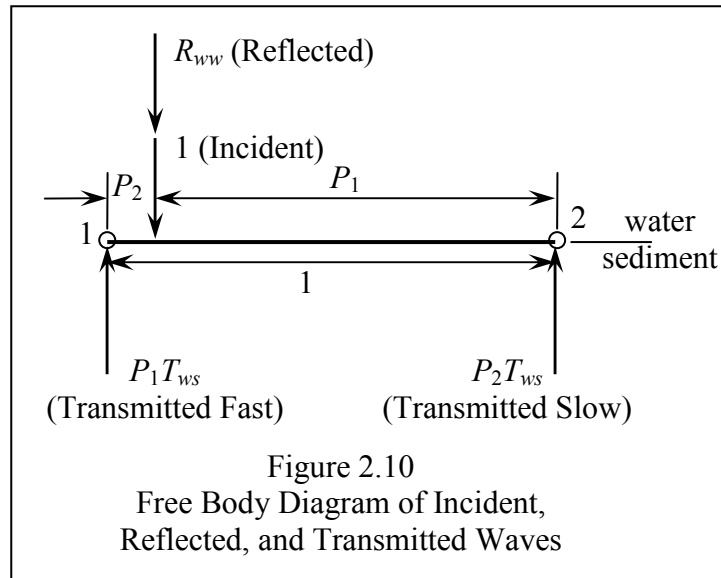
$$T_{w1} = P_1 T_{ws}$$

$$T_{w1} = \frac{2P_1 Z_1 Z_2}{Z_1 Z_2 + Z_w Z_1 P_2^2 + Z_w Z_2 P_1^2} .$$ (2-59)

And the slow wave transmission coefficient is:

$$T_{w2} = P_2 T_{ws}$$

$$T_{w2} = \frac{2P_2 Z_1 Z_2}{Z_1 Z_2 + Z_w Z_1 P_2^2 + Z_w Z_2 P_1^2} .$$ (2-60)

2.4 TRANSMISSION AND REFLECTION COEFFICIENTS OF A FAST WAVE FROM SAND TO WATER (OPEN PORE)

The impedance diagram for a fast wave in sand incident on a water interface is shown in Fig. 2.11. The water particle velocity at a point P_2 from the left from unit force at the left is:

$$v_w = \frac{1}{P_1} \frac{1}{Z_w} .$$ (2-61)

The slow wave particle velocity is:

$$v_2 = \frac{P_2}{P_1} \frac{1}{Z_2} .$$ (2-62)

Therefore the fast wave particle velocity from a unit force at the fast wave is:

$$v_1 = \frac{1}{P_1} v_w + \frac{P_2}{P_1} v_2 = \left(\frac{1}{P_1}\right)^2 \frac{1}{Z_w} + \left(\frac{P_2}{P_1}\right)^2 \frac{1}{Z_2} .$$ (2-63)

The impedance of a fast wave incident on a sand-water interface is:

$$Z_{1w} = \frac{1}{v_1} = \frac{P_1^2 Z_w Z_2}{Z_2 + P_2^2 Z_w} .$$ (2-64)

The transmitted pressure coefficient from a fast wave into the water and into the slow wave is:

$$T_{1-w\&2} = \frac{2Z_{1w}}{Z_{1w} + Z_1}$$

$$T_{1-w\&2} = \frac{2P_1^2 Z_w Z_2}{Z_1 Z_2 + P_1^2 Z_w Z_2 + P_2^2 Z_w Z_1} . \tag{2-65}$$

Figure 2.11
Fast Wave Incident
on Sand-Water Interface
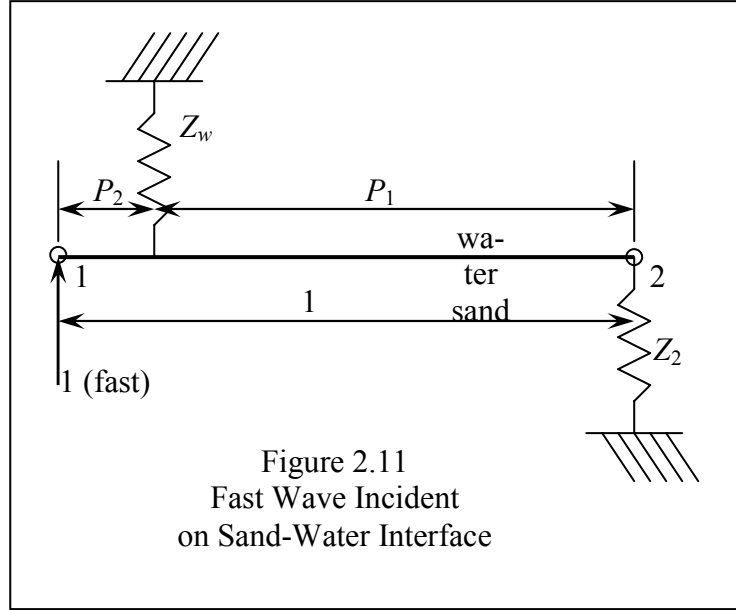
From Fig. 2.12 the transmitted wave into the water from an incident fast wave is:

$$T_{1w} = \frac{1}{P_1} T_{1-w\&2}$$

$$T_{1w} = \frac{2P_1 Z_w Z_2}{Z_1 Z_2 + P_1^2 Z_w Z_2 + P_2^2 Z_w Z_1} . \tag{2-66}$$

The reflected pressure coefficient (reflected fast wave from an incident fast wave, open pore, water interface) is:

$$R_{11}^{(w)} = \frac{Z_{1w} - Z_1}{Z_{1w} + Z_1}$$

$$R_{11}^{(w)} = \frac{P_1^2 Z_w Z_2 - Z_1 Z_2 - P_2^2 Z_w Z_1}{P_1^2 Z_w Z_2 + Z_1 Z_2 + P_2^2 Z_w Z_1} . \tag{2-67}$$

$$T_{1w} = \frac{1}{P_1} T_{1-w\&2} \quad \text{(Transmitted)}$$

P_2

P_1

water

sedi-
ment

1

1

1 (Incident, Fast)

$R_{11}^{(w)}$

(Reflected Fast)

$\frac{P_2}{P_1} T_{1-w\&2}$

(Reflected Slow)

Figure 2.12
Free-Body Diagram of Incident and Reflected
Forces on Sand-Water Interface
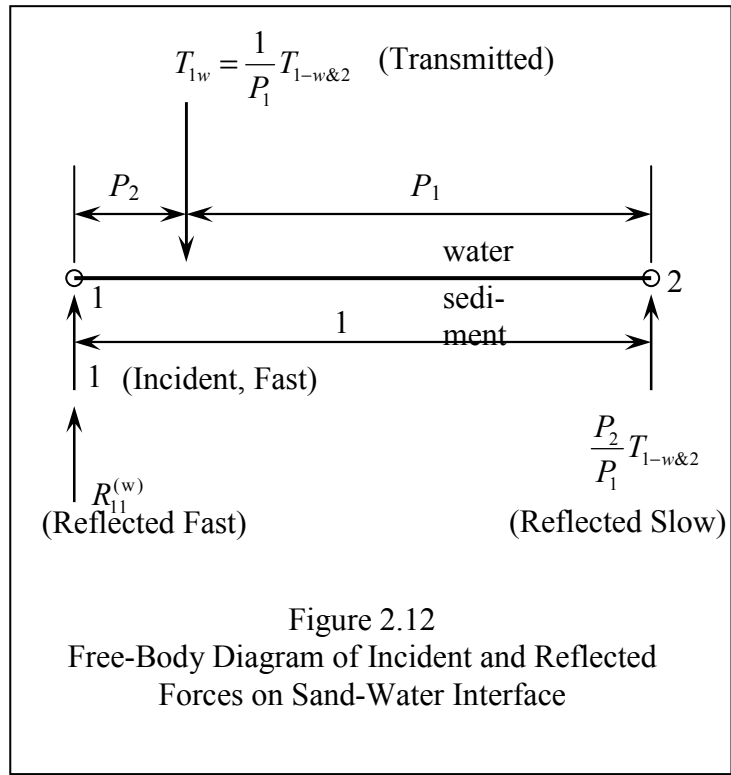
The reflected slow wave pressure coefficient is:

$$R_{12}^{(w)} = \frac{P_2}{P_1} T_{1-w\&2}$$

$$R_{12}^{(w)} = \frac{2P_1 P_2 Z_w Z_2}{Z_1 Z_2 + P_1^2 Z_w Z_2 + P_2^2 Z_w Z_1}. \qquad (2\text{-}68)$$

2.5 TRANSMISSION AND REFLECTION COEFFICIENTS OF A SLOW WAVE FROM SAND TO WATER (OPEN PORE)

The impedance of a slow wave incident on a sand-water interface is:

$$Z_{2w} = \frac{P_2^2 Z_w Z_1}{Z_1 + P_1^2 Z_w}. \qquad (2\text{-}69)$$

The transmitted pressure coefficient from a slow wave into the water and into the fast wave is:

$$T_{2-w\&1} = \frac{2Z_{2w}}{Z_{2w} + Z_2}$$

$$T_{2-w\&1} = \frac{2P_2^2 Z_w Z_1}{Z_1 Z_2 + P_1^2 Z_w Z_2 + P_2^2 Z_w Z_1}. \tag{2-70}$$

The transmitted wave into the water from an incident slow wave is:

$$T_{2w} = \frac{1}{P_2} T_{2-w\&1}$$

$$T_{2w} = \frac{2P_2 Z_w Z_1}{Z_1 Z_2 + P_1^2 Z_w Z_2 + P_2^2 Z_w Z_1}. \tag{2-71}$$

The reflected pressure coefficient is (reflected slow wave from an incident slow wave, open pore, water interface):

$$R_{22}^{(w)} = \frac{Z_{2w} - Z_2}{Z_{2w} + Z_2}$$

$$R_{22}^{(w)} = \frac{P_2^2 Z_w Z_1 - Z_1 Z_2 - P_1^2 Z_w Z_2}{P_1^2 Z_w Z_2 + Z_1 Z_2 + P_2^2 Z_w Z_1}. \tag{2-72}$$

The reflected fast wave pressure coefficient:

$$R_{21}^{(w)} = \frac{P_1}{P_2} T_{2-w\&1}$$

$$R_{21}^{(w)} = \frac{2P_1 P_2 Z_w Z_1}{Z_1 Z_2 + P_1^2 Z_w Z_2 + P_2^2 Z_w Z_1}. \tag{2-73}$$

2.6 REFLECTION AND TRANSMISSION COEFFICIENTS OF A FAST WAVE FROM SAND TO NON-POROUS (CLOSED PORE) INTERFACE

Figure 2.13 is the impedance diagram for a fast wave incident on a non-porous interface that has a closed pore surface (e.g., sand on acrylic, sand on Ethafoam, etc.). The sand particles, water particles, first mode, and second mode all have the same displacement on a closed pore surface; therefore the fast and slow wave particle velocities, v_1 and v_2, are the same at the interface. Impedance seen by fast wave (Z_c is impedance of a closed pore, non-porous medium):

$$Z = Z_2 + Z_c.$$ (2-74)

The fast, pressure reflection coefficient from a fast incident wave off a closed pore surface is:

$$R_{11}^{(c)} = \frac{Z - Z_1}{Z + Z_1}$$

$$R_{11}^{(c)} = \frac{Z_2 + Z_c - Z_1}{Z_2 + Z_c + Z_1}.$$ (2-75)

The transmitted coefficient from a fast incident wave on a closed pore surface is:

$$T_{1c} = \frac{2Z_c}{Z + Z_1}$$

$$T_{1c} = \frac{2Z_c}{Z_2 + Z_c + Z_1}.$$ (2-76)
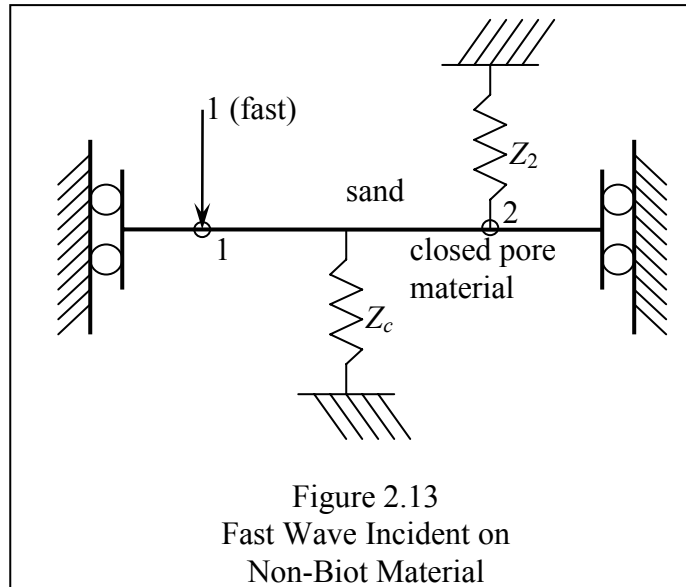
Figure 2.13
Fast Wave Incident on
Non-Biot Material

The slow, pressure reflection coefficient from a fast incident wave off a closed pore surface is:

$$R_{12}^{(c)} = \frac{-2Z_2}{Z + Z_1}$$

$$R_{12}^{(c)} = \frac{-2Z_2}{Z_2 + Z_c + Z_1} \qquad (2\text{-}77)$$

2.7 REFLECTION AND TRANSMISSION COEFFICIENTS OF A SLOW WAVE FROM SAND TO NON-POROUS (CLOSED PORE) INTERFACE

The impedance seen by slow wave is:

$$Z = Z_1 + Z_c. \qquad (2\text{-}78)$$

The slow, pressure reflection coefficient from a slow incident wave off a closed pore surface is:

$$R_{22}^{(c)} = \frac{Z - Z_2}{Z + Z_2}$$

$$R_{22}^{(c)} = \frac{Z_1 + Z_c - Z_2}{Z_2 + Z_c + Z_1}. \qquad (2\text{-}79)$$

The transmitted coefficient from a slow incident wave on a closed pore surface is:

$$T_{2c} = \frac{2Z_c}{Z + Z_2}$$

$$T_{2c} = \frac{2Z_c}{Z_2 + Z_c + Z_1}. \qquad (2\text{-}80)$$

The fast, pressure reflection coefficient from a slow incident wave off a closed pore surface is:

$$R_{21}^{(c)} = \frac{-2Z_1}{Z + Z_1}$$

$$R_{21}^{(c)} = \frac{-2Z_1}{Z_2 + Z_c + Z_1}. \qquad (2\text{-}81)$$

2.8   REFLECTION AND TRANSMISSION COEFFICIENTS OF AN INCIDENT
WAVE FROM A NON-POROUS MATERIAL TO SAND

Figure 2.14 is the impedance diagram for a fast wave incident on sand from a
closed pore surface. The impedance seen by the incident wave is:

$$Z = Z_1 + Z_2.$$

(2-82)

The transmission of the fast wave is:

$$T_{c1} = \frac{2Z_1}{Z_1 + Z_2 + Z_c}.$$

(2-83)

The transmission of the slow wave is:

$$T_{c2} = \frac{2Z_2}{Z_1 + Z_2 + Z_c}.$$

(2-84)

Reflection back into the closed pore material:

$$R_{cc} = \frac{Z_1 + Z_2 - Z_c}{Z_1 + Z_2 + Z_c}.$$

(2-85)
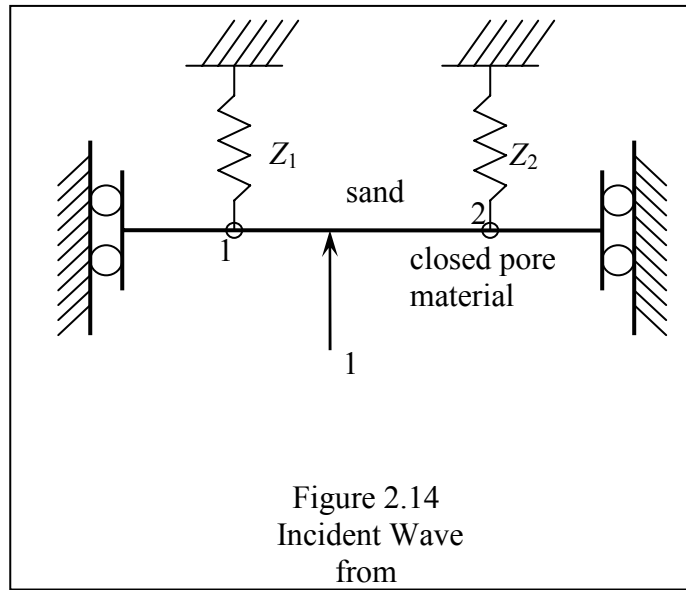
Figure 2.14
Incident Wave
from
Non-Biot Material

2.9 SUMMARY OF PRESSURE COEFFICIENTS

The Tables 2.1 and 2.2 summarize the pressure coefficients. The energy balances for these coefficients, i.e., pressure times velocity of the incident wave equals pressure times velocity of the response waves, e.g., $\dfrac{1}{Z_1} = \dfrac{\left(R_{11}^{(w)}\right)^2}{Z_1} + \dfrac{\left(R_{12}^{(w)}\right)^2}{Z_2} + \dfrac{T_{1w}^2}{Z_w}$. Also the pressures on each side of the interface are equal, i.e., one plus reflected equals transmitted, e.g., $1 + R_{11}^{(w)} + R_{12}^{(w)} = T_{1w}$ (given $P_1 + P_2 = 1$). Appendix B numerically checks parts of Table 2.1. The closed pore table (Table 2.2) can also be calculated from the open pore table by using the effective pressures for closed pore, eqs. (2-52) and (2-53).

Pressure coefficients are used in the next chapters where different combinations of acoustic measurements are taken to extract impedances, effective densities, wave speeds, effective pressures, mode shapes, and intermediate moduli. Only four of the 18 pressure coefficients (R_{cc}, T_{1c}, T_{c1}, and R_{11}) derived are used in this experiment. The other 14 coefficients are included only for completeness.

33

Table 2.1 – Pressure Coefficients, Open Pore, Sand-Water Interface

	Response Wave		
Incident Wave	Fast	Slow	Water
Fast	$R_{11}^{(w)} = \dfrac{P_1^2 Z_w Z_2 - Z_1 Z_2 - P_2^2 Z_w Z_1}{P_1^2 Z_w Z_2 + Z_1 Z_2 + P_2^2 Z_w Z_1}$	$R_{12}^{(w)} = \dfrac{2 P_1 P_2 Z_w Z_2}{Z_1 Z_2 + Z_w Z_1 P_2^2 + Z_w Z_2 P_1^2}$	$T_{1w} = \dfrac{2 P_1 Z_w Z_2}{Z_1 Z_2 + P_1^2 Z_w Z_2 + P_2^2 Z_w Z_1}$
Slow	$R_{21}^{(w)} = \dfrac{2 P_1 P_2 Z_w Z_1}{Z_1 Z_2 + Z_w Z_1 P_2^2 + Z_w Z_2 P_1^2}$	$R_{22}^{(w)} = \dfrac{P_2^2 Z_w Z_1 - Z_1 Z_2 - P_1^2 Z_w Z_2}{P_1^2 Z_w Z_2 + Z_1 Z_2 + P_2^2 Z_w Z_1}$	$T_{2w} = \dfrac{2 P_2 Z_w Z_1}{Z_1 Z_2 + P_1^2 Z_w Z_2 + P_2^2 Z_w Z_1}$
Water	$T_{w1} = \dfrac{2 P_1 Z_1 Z_2}{Z_1 Z_2 + Z_w Z_1 P_2^2 + Z_w Z_2 P_1^2}$	$T_{w2} = \dfrac{2 P_2 Z_1 Z_2}{Z_1 Z_2 + Z_w Z_1 P_2^2 + Z_w Z_2 P_1^2}$	$R_{ww} = \dfrac{Z_1 Z_2 - Z_w Z_1 P_2^2 - Z_w Z_2 P_1^2}{Z_1 Z_2 + Z_w Z_1 P_2^2 + Z_w Z_2 P_1^2}$

Table 2.2 – Pressure Coefficients, Closed Pore, Sand-NonBiot Interface

Incident Wave	Response Wave		
	Fast	Slow	Closed Pore
Fast	$R_{11}^{(c)} = \dfrac{Z_2 + Z_c - Z_1}{Z_2 + Z_c + Z_1}$	$R_{12}^{(c)} = \dfrac{-2Z_2}{Z_2 + Z_c + Z_1}$	$T_{1c} = \dfrac{2Z_c}{Z_2 + Z_c + Z_1}$
Slow	$R_{21}^{(c)} = \dfrac{-2Z_1}{Z_2 + Z_c + Z_1}$	$R_{22}^{(c)} = \dfrac{Z_1 + Z_c - Z_2}{Z_2 + Z_c + Z_1}$	$T_{2c} = \dfrac{2Z_c}{Z_2 + Z_c + Z_1}$
Closed Pore	$T_{c1} = \dfrac{2Z_1}{Z_1 + Z_2 + Z_c}$	$T_{c2} = \dfrac{2Z_2}{Z_1 + Z_2 + Z_c}$	$R_{cc} = \dfrac{Z_1 + Z_2 - Z_c}{Z_1 + Z_2 + Z_c}$

Chapter 3:
ACOUSTIC MEASUREMENTS

The Applied Physics Laboratory has an acoustic water tank system suitable for measuring pressure amplitudes of waves transmitted and reflected through various media. In this chapter, specifications are reviewed, reflection equations are derived, and frequency measurements are discussed.

3.1 SPECIFICATIONS

The water tank is 1.6 m deep, 2.3 m diameter, and holds 5000 liters of water. The tank has a lid that can be sealed and a vacuum pump can be used to de-gas the contents in the tank. The tank has a piping and filter system that can recirculate and purify the water. A resistivity probe monitors purity and indicates when the filters need to be changed. With the de-gassing and purifying systems the water is "pure" and the sand is bubble free. The tank has a positioning system for the transmitter and receiver with an accuracy of about 25 μm and a computer based measuring system including a data acquisition system and waveform generator. The data acquisition employs a 12 bit analog-to-digital converter and samples at 10 MHz. An overhead electric crane handles all heavy items going in and coming out of the tank.

The pulses were shaped so that the residual ringing of the transducer was actively canceled (see Appendix G). Return pulses were windowed with a Gaussian window 30 μs wide. Measurements of each surface were taken at 100 different locations with 100 samples at each location. The raw data shown in Figs. 3.2, 3.4, 3.6, and 3.8 are the coherent time averages of 100 samples at 100 locations (10,000 total samples).

The sand used was Ottawa sand, with an average size of 279 μm and a standard deviation of about 100 μm. Appendix H has a more detailed analysis of sand size and composition.

3.2 REFLECTION EQUATIONS

A reflection ratio technique was used to extract desired information. The strategy behind the reflection ratio method is to form a ratio that removes most unknowns from measured reflections. Measurements were taken so that two different acoustic pulses had exactly the same propagation path but different reflection surfaces so that dividing the two acoustic pulses factored out all unknowns in the transmitter's signal, the acoustic path, and the hydrophone's reception, leaving only information about the surfaces. Jumping ahead a little, if the reflection from the second surface of acrylic-sand, r_{2s}, in Fig. 3.1 is divided by the reflection of the second surface of acrylic-air, r_{2air}, in Fig. 3.3 what remains is only information about the second surface. Mathematically eq. (3-3) is divided by eq. (3-2) and what is left is eq. (4-1), which is greatly simplified and has only two unknowns. These reflection ratios were then used to find selected acoustic parameters in Chapter 4. To this end, sand was held in a tray where the transmitter and receiver could be positioned below the tray. Then the top surface, of the sand or the tray, could be changed without disturbing the path. Plans of the tray and lid are shown in Appendix F.

The analysis in Chapter 4 shows there are 14 unknowns with 4 equations from reflection ratios and 10 other supporting equations. The 4 equations from reflection ratios were taken from 6 different interfaces, which are: (1) water-acrylic, (2) acrylic-air, (3) acrylic-sand, (4) sand-air, (5) sand-Ethafoam, and (6) sand-water.

The complex reflection amplitude from the first surface of acrylic (water-acrylic) is (e.g., Fig. 3.1):

$$R_{1a} = \frac{A_t}{d_{1a}} \frac{Z_a - Z_w}{Z_a + Z_w} \exp\left(-ik_w d_w^{(a)}\right). \tag{3-1}$$

R_{1a} is the Fourier Transform of r_{1a} (Fig. 3.2), A_t is the pressure amplitude a unit distance from the acoustic center, whose distance from the interface is $d_{1a}/2$. Z_a is the impedance of the 4-inch acrylic, Z_w is the impedance of water, k_w is the wave number of water, and $d_w^{(a)}$ is the distance the sound travels through water to the acrylic surface and back. Due to the mechanics of the transducers d_{1a} may not equal $d_w^{(a)}$. Thorsos et al [40] shows eq.

(3-1) is a good approximation when $d_w^{(a)}/2$ is much larger than the wavelength ($d_w^{(a)}/2$ approximately 0.127 m, wavelength approximately 0.006m).

Assuming the impedance of air is very small compared with acrylic, the reflection from the second surface with air (acrylic-air) is (Fig. 3.3):

$$R_{2air} = \frac{A_t}{d_2} \frac{2Z_a}{Z_a + Z_w} (-1) \frac{2Z_w}{Z_a + Z_w} \exp\left(-ik_w d_w^{(a)}\right) \exp\left(-i2k_a t_a\right) \qquad (3\text{-}2)$$

Where d_2 is a transmission loss factor and can be considered as twice the distance from the "virtual" acoustic center to the second acrylic surface. This is not equal to the distance from the transducer to the second acrylic surface because the propagation through two media forms a different focusing point. The wave number of the acrylic is k_a, and the thickness of the acrylic is t_a.

The reflection from the second surface with sand (acrylic-sand) is (Fig. 3.5):

$$R_{2s} = \frac{A_t}{d_2} \frac{2Z_a}{Z_a + Z_w} (R_{cc})_a \frac{2Z_w}{Z_a + Z_w} \exp\left(-ik_w d_w^{(a)}\right) \exp\left(-ik_a t_a\right) \qquad (3\text{-}3)$$

Where $(R_{cc})_a$ is the reflection of a wave from a closed pore material back to the closed pore material from a closed pore-sand interface where acrylic is the closed pore material. R_{cc} is taken from Table 2.2.

The reflection of the third surface with water (sand-water) is (Fig. 3.1):

$$R_{3w} = \frac{A_t}{d_3} \frac{2Z_a}{Z_a + Z_w} (T_{c1})_a R_{11}^{(w)} (T_{1c})_a \frac{2Z_w}{Z_a + Z_w} \cdots$$
$$\cdot \exp\left(-ik_w d_w^{(a)}\right) \exp\left(-i2k_a t_a\right) \exp\left(-i2k_1 t_s\right) \qquad (3\text{-}4)$$

Where d_3 is a transmission loss factor, $(T_{c1})_a$ is the transmission coefficient of a wave from a closed pore material to a fast wave in sand where the closed pore material is acrylic, $(T_{1c})_a$ is the transmission coefficient of a fast wave from sand to a closed pore material where the closed pore material is acrylic, $R_{11}^{(w)}$ is the reflection of a fast wave back to a fast wave from a sand-water interface. T_{c1} and T_{1c} are taken from Table 2.2. $R_{11}^{(w)}$ is taken from Table 2.1.

The third surface with Ethafoam (sand-Ethafoam) is (Fig. 3.5):

$$R_{3E} = \frac{A_t}{d_3} \frac{2Z_a}{Z_a + Z_w} (T_{c1})_a \left(R_{11}^{(c)}\right)_E (T_{1c})_a \frac{2Z_w}{Z_a + Z_w} \cdots$$
$$\cdot \exp\left(-ik_w d_w^{(a)}\right) \exp\left(-i2k_a t_a\right) \exp\left(-i2k_1 t_s\right)$$

(3-5)

Where $(R_{11}^{(c)})_E$ is the reflection of a fast wave to a fast wave from a sand-closed pore interface where Ethafoam is the closed pore material. $R_{11}^{(c)}$ is taken from Table 2.2.

The third surface with air (sand-air) is (Fig. 3.7):

$$R_{3air} = \frac{A_t}{d_3} \frac{2Z_a}{Z_a + Z_w} (T_{c1})_a (-1)(T_{1c})_a \frac{2Z_w}{Z_a + Z_w} \cdots$$
$$\cdot \exp\left(-ik_w d_w^{(a)}\right) \exp\left(-i2k_a t_a\right) \exp\left(-i2k_1 t_s\right)$$

(3-6)

Where t_s is the thickness of the sand.

Reflection ratios are obtained with the lid (2 inch acrylic and Ethafoam) on and off. The weight of the lid underwater with Ethafoam attached is 2.641 kg. The contact area of the lid is 0.4560 m^2. This gives an overburden pressure equivalent to a depth of 5 mm of water saturated, buoyant sand. The resulting small stress should not influence the reflection ratios.

3.3 FREQUENCY MEASUREMENTS

In the following chapters the frequency domain reflections, R, are the Fourier transforms of the time domain reflections, r. The reflection data for each location were averaged coherently in the frequency domain of 100 transmissions.

Figure 3.1
Schematic for Sand-Water Reflection (r_{3w}),
and Acrylic-Sand Reflection (r_{2s})

Figure 3.2
Sand – Water Interface (r_{3w})
Acrylic – Sand Interface (r_{2s})

Figure 3.3
Schematic for Acrylic-Air Reflection (r_{2air})

Figure 3.4
4" Acrylic – Air Interface (r_{2air})

Figure 3.5
Schematic for Sand-Ethafoam Reflection (r_{3E})
and Water-Acrylic Reflection (r_{1a})

Figure 3.6
Sand - Ethafoam Interface (r_{3E})

Figure 3.7
Schematic for Sand-Air Reflection (r_{3air})

Figure 3.8
Sand – Air Interface (r_{3air})

Chapter 4:
ANALYSIS

This chapter uses the theory in Ch. 2 and the measurements in Ch. 3 and solves for various physical parameters and acoustical properties, which include: fast and slow impedances, fast and slow wave speeds, fast and slow effective densities, fast and slow effective pressures, fast and slow mode shapes, the three intermediate moduli, and a term that will be called the mass factor, which is a combination of viscosity and tortuosity terms. But the measurements for three other parameters, the sand frame modulus, sand particle modulus, and shear modulus, were not made successfully and the reasons are discussed. Other parameters that were measured for this chapter's analysis include: the density of the water saturated sand, the density of the sand particles, the impedance of the acrylic, the impedance of the Ethafoam, the thickness of the sand, the porosity of the sand, and the volume of the water saturated sand.

4.1 FAST AND SLOW WAVE IMPEDANCES

Reflection ratios are used to calculate the fast and slow wave impedances. The use of reflection ratios uses relative measurements and removes the need for measuring absolute phases and amplitudes (calibrating the transducers and compensating for propagation effects). From the reflections, the fast and slow wave impedances are calculated by the following formulas. The pressure reflection coefficient ratio of the second surface is (combine eqs. (3-3), (3-1), and (3-2)):

$$R_{2s\_2air} = \frac{\left| \dfrac{(R_{2s})_{II}}{(R_{1a})_{II}} \right|}{\left| \dfrac{(R_{2air})_I}{(R_{1a})_I} \right|} = -\left(\frac{Z_1 + Z_2 - Z_a}{Z_1 + Z_2 + Z_a} \right). \tag{4-1}$$

The subscripts *I* and *II* represent acoustic pulses in which the transducer generated amplitude, A_t, may be slightly different. R_{2air} and R_{2s} are divided by R_{1a} to normalize the amplitudes. The acoustic centers and distance traveled through water were held the same. Unfortunately phase measurements were not accurate. That is why the absolutes of the

reflections and the negative in front of the right hand side are used in eq. (4-1). It is felt the phases were not accurate because of possible disturbances of the top sand surface (Ethafoam on and off). The wavelength of sound in sand was 6.6 mm so a 0.55 mm change in sand thickness (travel distance of 1.1 mm) would make a 60° difference in phase. The error from taking absolute reflections is estimated in Appendix C. Also the pressure reflection coefficient of the third surface is (combine eqs. (3-5), (3-1), and (3-6)):

$$R_{3E\_3air} = \frac{\frac{\left|(R_{3E})_{II}\right|}{\left|(R_{1a})_{II}\right|}}{\frac{\left|(R_{3air})_{I}\right|}{\left|(R_{1a})_{I}\right|}} = -\left(\frac{Z_E + Z_2 - Z_1}{Z_E + Z_2 + Z_1}\right), \qquad (4\text{-}2)$$

where Z_E and Z_a are measured in Appendix A. From eqs. (4-1) and (4-2), the imped-ances of the fast and slow waves are:

$$Z_1 = \frac{Z_E\left(1 + R_{3E\_3air}\right)\left(1 + R_{2s\_2air}\right) + Z_a\left(1 - R_{2s\_2air}\right)\left(1 + R_{3E\_3air}\right)}{2\left(1 + R_{2s\_2air}\right)} \qquad (4\text{-}3)$$

$$Z_2 = \frac{Z_a\left(1 - R_{2s\_2air}\right)}{1 + R_{2s\_2air}} - Z_1. \qquad (4\text{-}4)$$

The fast and slow impedances were measured in 100 different locations. The av-erage fast and slow impedances and their standard deviations are shown in Fig. 4.1.

The bands or tolerances on the following plots are all sample standard deviations and not expected error. At band center (250 kHz) the measurement errors (Appendix C) are about one-third as large as the observed fluctuations in measurements; therefore this fluctuation must be ascribed to spatial variability of the sand sample. At the band edges (150 kHz and 350 kHz, the pulse has a bandwidth of 200 kHz), however, the fluctuations become larger and in some cases even erratic. This is from system noise because of the low signal-to-noise ratio at the edges.

Figure 4.1
Impedances of Fast and Slow Waves
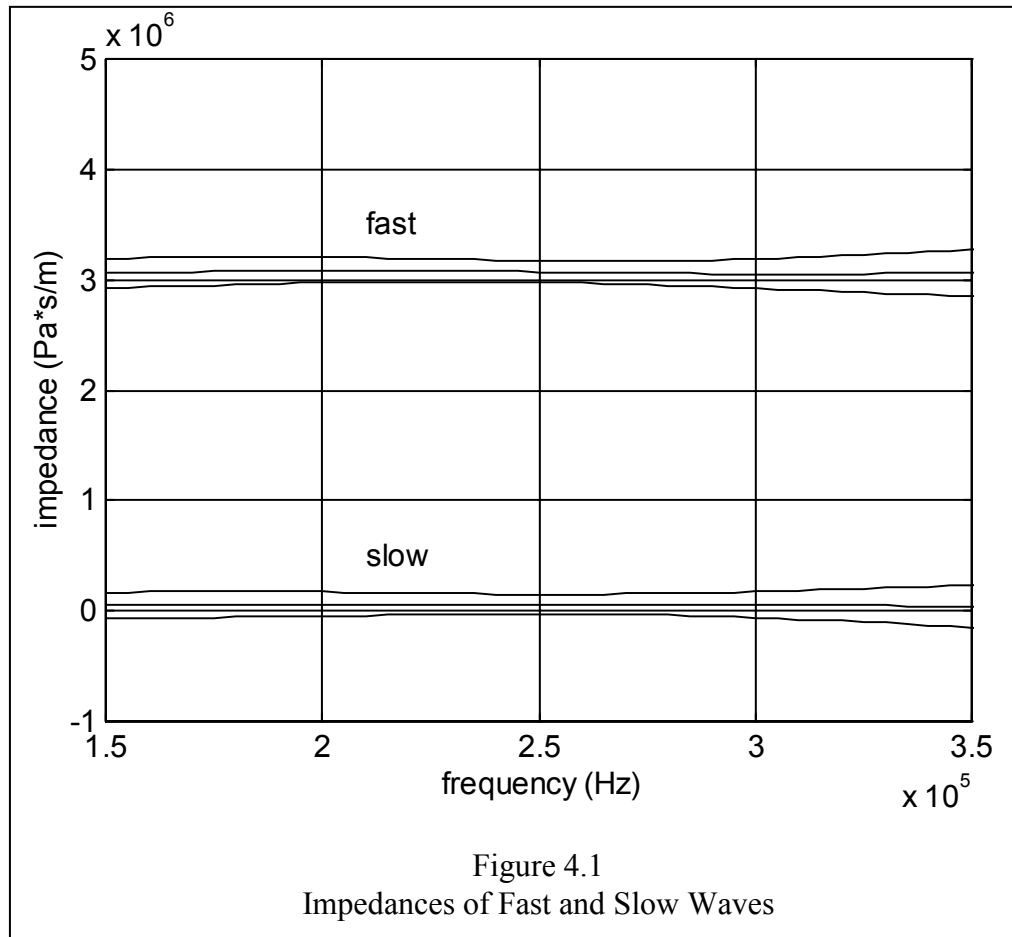
At 250 kHz, the fast and slow wave impedances are:

$$Z_1 = (3.072 \pm 0.097) \cdot 10^6 \quad \text{Pa} \cdot \text{s} \Big/ \text{m}$$
$$Z_2 = (6.2 \pm 8.8) \cdot 10^4 \quad \text{Pa} \cdot \text{s} \Big/ \text{m}$$

(4-5)

As can be seen, the impedance of the slow wave is consistent with zero. This plot does not support the existence of the Biot waves.

4.2 WAVE SPEEDS AND MODAL MASSES

The fast wave number is calculated from eqs. (3-2) and (3-6):

$$R_{3air\_2air} = \frac{\left(\dfrac{(R_{3air})_{II}}{(R_{1a})_{II}} \right)}{\left(\dfrac{(R_{2air})_{I}}{(R_{1a})_{I}} \right)} = \frac{d_2}{d_3} \frac{4Z_1 Z_a}{(Z_1 + Z_2 + Z_a)^2} \exp\left(-i2\bar{k}_1 t_s \right) \qquad (4\text{-}6)$$

$$\bar{k}_1 = \frac{-i}{2t_s} \ln\left(R_{3air\_2air} \frac{d_3}{d_2} \frac{(Z_1 + Z_2 + Z_a)^2}{4Z_1 Z_a} \right). \qquad (4\text{-}7)$$

Because the natural logarithm of a complex number is the logarithm of the absolute value plus i times the angle of the complex number, and the wave phase comes from the imaginary part of i times the wave number, the real part of the fast wave number is:

$$k_1 = \mathrm{Re}(\bar{k}_1) = \frac{1}{2t_s} \arg(R_{3air\_2air}), \qquad (4\text{-}8)$$

where the thickness is $t_s = 1.008$ in or 0.02560 m. Using MatLAB, k_1 (as a function of frequency) is "unwrapped" and adjusted so that its intercept is zero. The fast wave speed is:

$$c_1 = \frac{2\pi f}{k_1}, \qquad (4\text{-}9)$$

which is shown in Fig. 4.3.

The modal mass (effective density) of the fast wave is:

$$\rho_1 = \frac{Z_1}{c_1}. \qquad (4\text{-}10)$$

The density of the water filled sand is:

$$\rho = \frac{m_s^{(w)}}{V} + \rho_w \qquad (4\text{-}11)$$

and is plotted in Fig. 4.2. In eq. (4-11), $m_s^{(w)}$ is the buoyant weight of the sand, V is the total volume of the water filled sand, and ρ_w is the density of water. The diameter and thickness values are averages at 100 different locations measured to the nearest 0.001 in.

$$m_s^{(w)} = 14.462 \pm 0.004 \text{ kg}$$

$$V = \pi \frac{D^2}{4} t_s, \quad D = \text{diameter}, \quad t_s = \text{thickness of sand}$$

$$D = 31.992 \pm 0.001 \text{ in} = 0.81260 \pm 0.00003 \text{ m}$$

$$t_s = 1.008 \pm 0.001 \text{ in} = 0.02560 \pm 0.00003 \text{ m}$$

$$V = 810.3 \pm 0.3 \text{ in}^3 = 0.013278 \pm 0.000005 \text{ m}^3$$

$$\rho_w = 998.016 \text{ kg}/\text{m}^3 \text{ at } 20.9^o \text{C}.$$

The density and speed of the slow wave are:

$$\rho_2 = \rho - \rho_1 \tag{4-12}$$

$$c_2 = \frac{Z_2}{\rho_2}. \tag{4-13}$$

The magnitudes of the modal densities computed from eqs. (4-10) and (4-12) and their standard deviations are shown in Fig. 4.2. The wave speeds, eqs. (4-9) and (4-13) and standard deviations are shown in Fig. 4.3. Porosity and sand density, which will be used later, are:

$$\beta = 1 - \frac{m_s - m_s^{(w)}}{V \rho_w}$$

$$m_s = \text{mass of sand} = 23.076 \pm 0.004 \text{ kg} \tag{4-17}$$

$$\beta = 0.3500 \pm 0.0002$$

$$\rho_s = \frac{\rho_w m_s}{m_s - m_s^{(w)}} = 2673 \pm 2 \frac{\text{kg}}{\text{m}^3}. \tag{4-18}$$

The sand density compares to 2650 kg/m^3 commonly used for silica.

Figure 4.2
Modal Masses (Effective Densities)
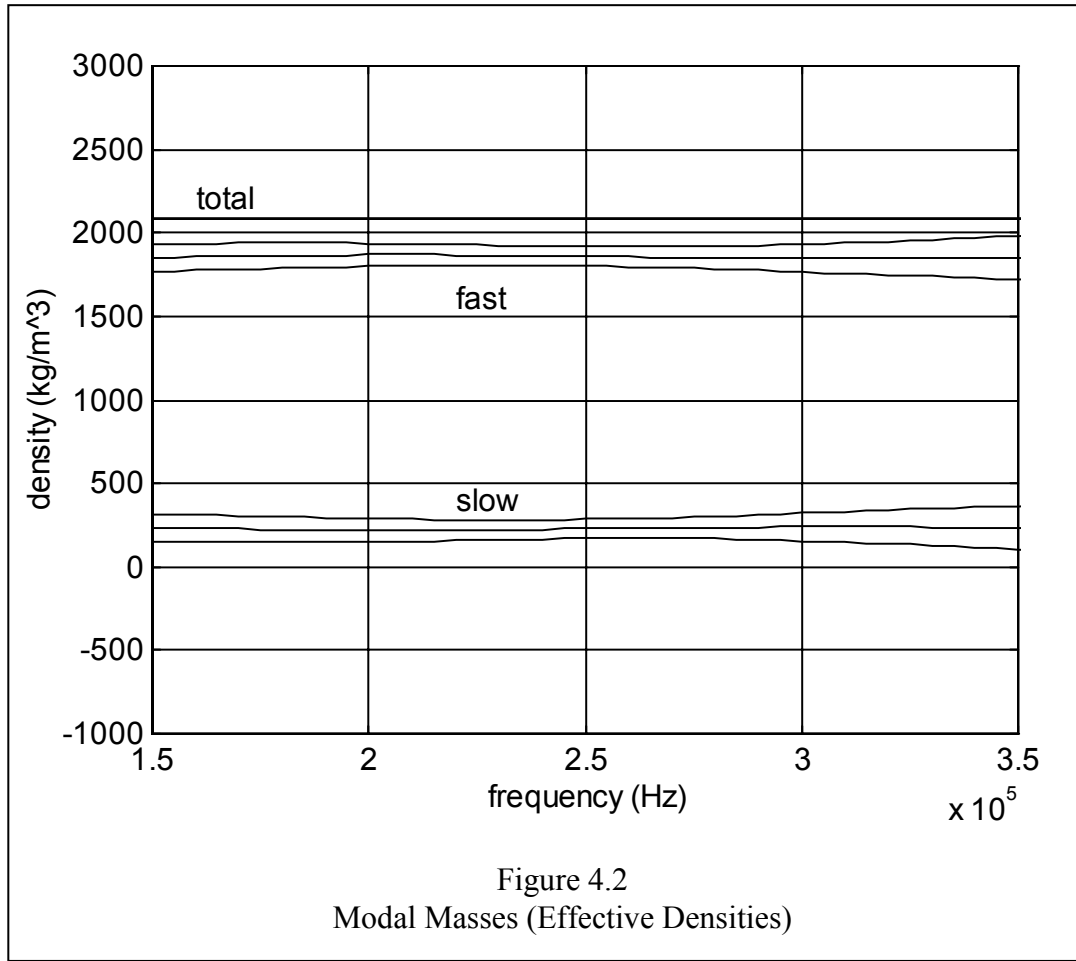
The densities are:

$$\rho = 2087.2 \pm 0.7 \quad \text{kg}\big/\text{m}^3$$

$$\rho_1 = 1860 \pm 58 \quad \text{kg}\big/\text{m}^3 \tag{4-14}$$

$$\rho_2 = 227 \pm 58 \quad \text{kg}\big/\text{m}^3 .$$

The fast and slow effective density numbers in eq. (4-14) are at 250 kHz. As can been seen, the density of the fast wave is 89% $\pm$ 3% of the total density. The difference between the total density and the fast effective density is 3.9 standard deviations. This fact indicates the existence of Biot waves in water-saturated sand. This compares favorably with Williams [42] who predicts a fast effective density that is 85% of total density (see Table 5.2).

Figure 4.3
Fast and Slow Wave
Speeds
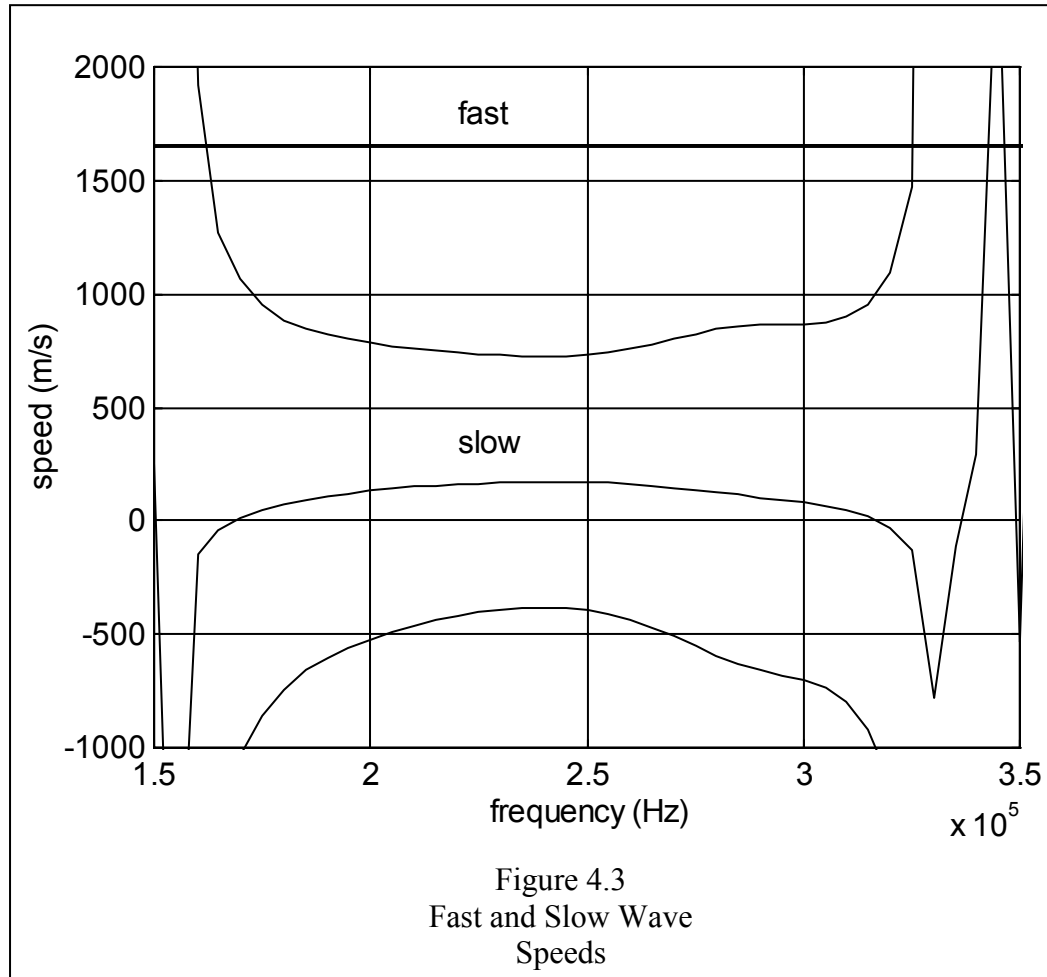
At 250 kHz the fast and slow wave speeds are:

$$c_1 = 1654 \pm 6 \; \text{m}/\text{s}$$
$$c_2 = 170 \pm 560 \; \text{m}/\text{s} .$$
(4-15)

This is the first time the speed of the slow wave has been bounded in sand. The speed of the slow wave is consistent with zero. But this is to be expected since Z_2 is consistent with zero.

The fast wave to water speed ratio is:

$$\frac{c_1}{c_w} = \frac{1654}{1485} = 1.11 .$$
(4-16)

4.3 EFFECTIVE PRESSURES

The effective pressures are calculated from the reflection ratio of the third surface consisting of sand-water and the third surface consisting of sand-air (combine eqs. (3-4), (3-1), and (3-6)):

$$R_{3w\_3air} = \frac{\left|\frac{(R_{3w})_{II}}{(R_{1a})_{II}}\right|}{\left|\frac{(R_{3air})_{I}}{(R_{1a})_{I}}\right|} = -\frac{P_1^2 Z_w Z_2 - Z_1 Z_2 - P_2^2 Z_w Z_1}{P_1^2 Z_w Z_2 + Z_1 Z_2 + P_2^2 Z_w Z_1},$$

(4-19)

with $Z_w = 1.48214e6$. Also:

$$P_1 + P_2 = 1.$$

(4-20)

Solve for P_1:

$$P_1 = \frac{(1 - R_{3w\_3air})Z_w Z_1 + \sqrt{\begin{array}{c}(1 - R_{3w\_3air})^2 Z_w^2 Z_1^2 \cdots \\ + (1 - R_{3w\_3air}^2)Z_w Z_2 Z_1 (Z_w + Z_2) \cdots \\ - (1 - R_{3w\_3air})^2 Z_w Z_1^2 (Z_w + Z_2)\end{array}}}{Z_w (1 + R_{3w\_3air})Z_2 + Z_w (1 - R_{3w\_3air})Z_1}.$$

(4-21)

The plus is used in front of the radical because the answer for a negative radical leads to an inconsistency in the mode shape calculation. In the next step, mode shapes are calculated and a negative radical produces a fast wave mode shape of one, i.e., $B_1/A_1 = 1.0 \pm 0.5$. Substitute $B_1/A_1 = 1$ back into eq. (2-46) the modal mass becomes 2087 rather than 1850. Effective pressures and their standard deviations are shown in Fig. 4.4.

Figure 4.4
Effective Pressures
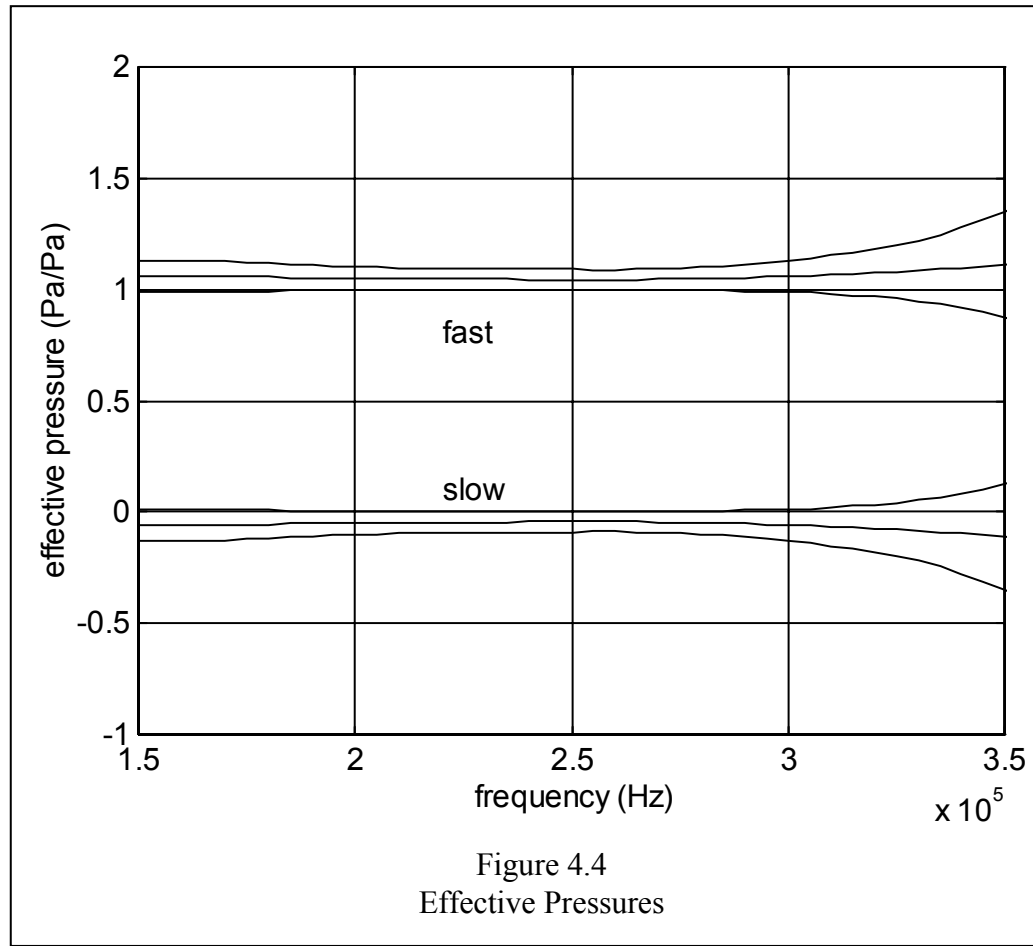
The effective pressures at 250 kHz are:

$$P_1 = 1.044 \pm 0.046 \; {}^{Pa}\!\!\big/\!{}_{Pa}$$

$$P_2 = -0.044 \pm 0.046 \; {}^{Pa}\!\!\big/\!{}_{Pa}.$$

(4-22)

The effective pressure of the slow wave is consistent with zero. The measurement of effective pressures neither supports nor denies the existence of Biot waves.

4.4 A SECOND LOOK AT THE PROPERTIES OF THE FAST WAVE

The effective density of the fast wave being smaller than the total density of the water-saturated sand is the only indication of the existence of Biot waves. The two other measured parameters that might confirm Biot waves, the slow wave impedance and slow

wave effective pressure, are zero within the standard deviation. The fast density is calculated from impedance and speed. The importance of these parameters (fast wave impedance and fast wave speed) justifies another look.

Fig. 3.4 shows the reflection from the second surface, which is acrylic-air (r_{2air}), at $0.92 \cdot 10^{-4}$ sec. But the reflection from the second surface in Fig. 3.2, acrylic-sand (r_{2s}), at the same time is practically non-existent. This implies the total impedance of the sand is equal to the impedance of the acrylic. In a closed pore situation, the total impedance of the sand is equal to the impedance of the fast wave plus the impedance of the slow wave. Therefore the impedance of the fast wave should be slightly less than the impedance of the acrylic. The measured impedance of the acrylic is $3.17 \cdot 10^{6}$ $\text{Pa} \cdot \text{s/m}$, see eq. (A-6). Ref [27] measures the speed of sound in cast acrylic at 2705 m/s and the density to be 1181 kg/m^{3}, which makes the impedance $3.19 \cdot 10^{6}$. The measured impedance of the fast wave in this report is smaller at $3.07 \cdot 10^{6}$ $\text{Pa} \cdot \text{s/m}$, which is consistent with expectations.

The speed of the fast wave in Fig. 4.3 was found to be c_1 = 1654 m/s by phase measurements in the frequency domain. In the time domain the reflection from the third surface in Fig. 3.6, which is a sand-Ethafoam interface (r_{3E}), arrives at a time of $1.23 \cdot 10^{-4}$ sec. This makes the time difference (r_{3E} minus r_{2air}, r_{2air} from above) of $0.31 \cdot 10^{-4}$ sec. The distance traveled is 2 times 0.02560 m, which gives a wave speed of 1650 m/s, consistent with the frequency domain result.

It can be concluded that the measured values for the fast wave impedance and speed of the fast wave are reasonable and consistent with expectations.

4.5 MODE SHAPES

Fig. 4.5 is a model of a closed pore-sediment interface for the first mode. If the incident and reflected waves on the interface have a combined amplitude of one (which makes the first mode displacement $u_1 = 1 \cdot \exp(i(\omega t - k_1 z))$), then from eqs. (2-26), (2-27), (2-48), and (2-49):

$$A_1(1 - \beta) + B_1\beta = \widetilde{P}_1 \ , \tag{4-23}$$

and likewise:

$$A_2(1 - \beta) + B_2\beta = \widetilde{P}_2 \ . \tag{4-24}$$

The participation factors, $\widetilde{P}_1$ and $\widetilde{P}_2$, are independent of boundary conditions but they just happen to be (luckily) numerically equal to the open pore effective forces, P_1 and P_2, eq. (4-22). Getting back to the closed pore interface, $A_1 + A_2 = B_1 + B_2$, which means there is no relative movement between sand and fluid in the sediment making viscous forces and tortuosity of the fast wave cancel viscous forces and tortuosity of the slow wave at the surface. Therefore the mass that moves is:

$$A_1(1 - \beta)\rho_s + B_1\beta\rho_f = \rho_1 \tag{4-25}$$

$$A_2(1 - \beta)\rho_s + B_2\beta\rho_f = \rho_2. \tag{4-26}$$

Figure 4.5
Sediment Displacement
Model
for Fast Wave
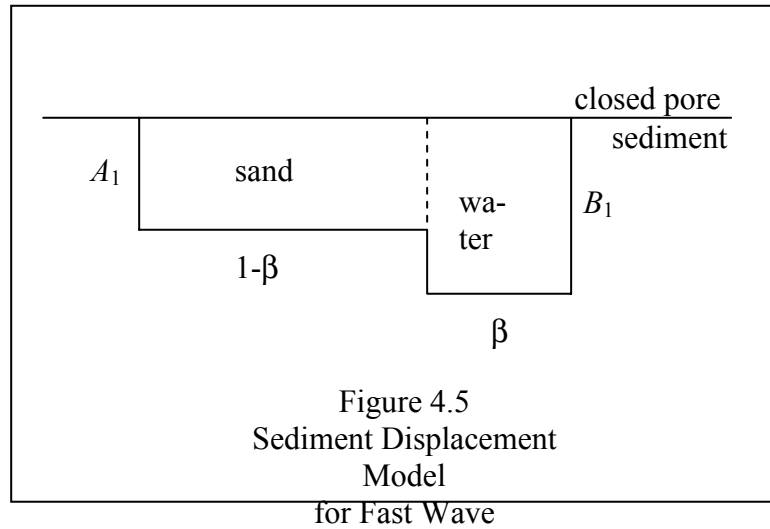
Solving for the mode shapes, i.e., the sediment fluid displacement divided by sand displacement:

$$\frac{B_1}{A_1} = \frac{\left(P_1\,\rho_s - \rho_1\right)\!\left(1 - \beta\right)}{\left(\rho_1 - P_1\,\rho_f\right)\!\beta} \tag{4-27}$$

$$\frac{B_2}{A_2} = \frac{\left(P_2\,\rho_s - \rho_2\right)\!\left(1 - \beta\right)}{\left(\rho_2 - P_2\,\rho_f\right)\!\beta}\,. \tag{4-28}$$

Figure 4.6
Mode Shapes
Fluid Amplitude divided by Sand Ampli-
tude
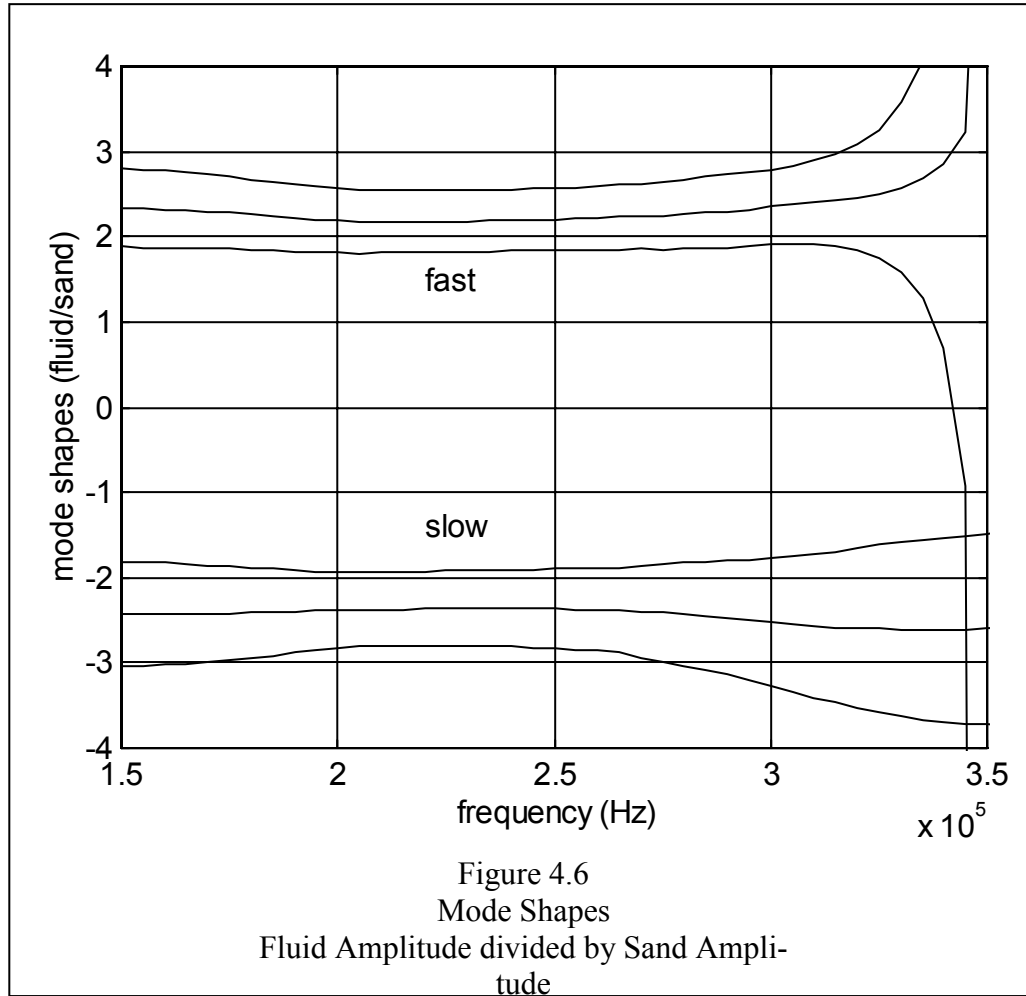
At 250 kHz the fast and slow mode shapes are:

$$\frac{B_1}{A_1} = 2.20 \pm 0.37 \quad \text{m}\!\!\bigg/\!\!\text{m} \tag{4-29}$$

$$\frac{B_2}{A_2} = -2.37 \pm 0.47 \quad \text{m}\!\!\bigg/\!\!\text{m}\,. \tag{4-30}$$

The fast wave mode shape is 3.2 standard deviations from one and helps support the existence of Biot waves.

The fast wave mode shape in Fig. 4.6 is an important measurement in this dissertation. This result means that the water in the sediment oscillates with an amplitude (and velocity and acceleration) 2.2 times the amplitude of the sand during the passing of a sound wave. A difference in vibration amplitudes between sand and fluid is one of the key properties of a Biot wave. This fact gives a clearer understanding of the physics of sound waves propagating through sandy sediment more than any other parameter measured in this dissertation.

4.6 TORTUOSITY AND VISCOSITY

The tortuosity and viscosity terms always appear together and cannot be solved for separately. Eq. (2-14) can be rewritten:

$$\begin{bmatrix} P & Q \\ Q & R \end{bmatrix} \begin{Bmatrix} A \\ B \end{Bmatrix} = c^2 \begin{bmatrix} (1-\beta)\rho_s - \beta\rho_f + \tilde{\alpha} & \beta\rho_f - \tilde{\alpha} \\ \beta\rho_f - \tilde{\alpha} & \tilde{\alpha} \end{bmatrix} \begin{Bmatrix} A \\ B \end{Bmatrix}. \tag{4-31}$$

Where the "mass factor" is (units of mass or density):

$$\tilde{\alpha} = \alpha\beta\rho_f - i\frac{F}{\omega} \tag{4-32}$$

and will be solved for in the next section.

4.7 MODULI

From eq. (4-31) P, Q, R, and $\tilde{\alpha}$ can be solved for:

$$\begin{Bmatrix} P \\ Q \\ R \\ \tilde{\alpha} \end{Bmatrix} = \begin{bmatrix} 1 & \dfrac{B_1}{A_1} & 0 & c_1^2\dfrac{B_1}{A_1} - c_1^2 \\ 0 & 1 & \dfrac{B_1}{A_1} & c_1^2 - c_1^2\dfrac{B_1}{A_1} \\ 1 & \dfrac{B_2}{A_2} & 0 & c_2^2\dfrac{B_2}{A_2} - c_2^2 \\ 0 & 1 & \dfrac{B_2}{A_2} & c_2^2 - c_2^2\dfrac{B_2}{A_2} \end{bmatrix}^{-1} \begin{Bmatrix} c_1^2\left[(1-\beta)\rho_s - \beta\rho_f + \beta\rho_f\dfrac{B_1}{A_1}\right] \\ c_1^2\beta\rho_f \\ c_2^2\left[(1-\beta)\rho_s - \beta\rho_f + \beta\rho_f\dfrac{B_2}{A_2}\right] \\ c_2^2\beta\rho_f \end{Bmatrix}. \tag{4-33}$$

The intermediate moduli are shown in Fig. 4.7. The mass factor is shown in Fig. 4.8.

Figure 4.7
Intermediate
Moduli
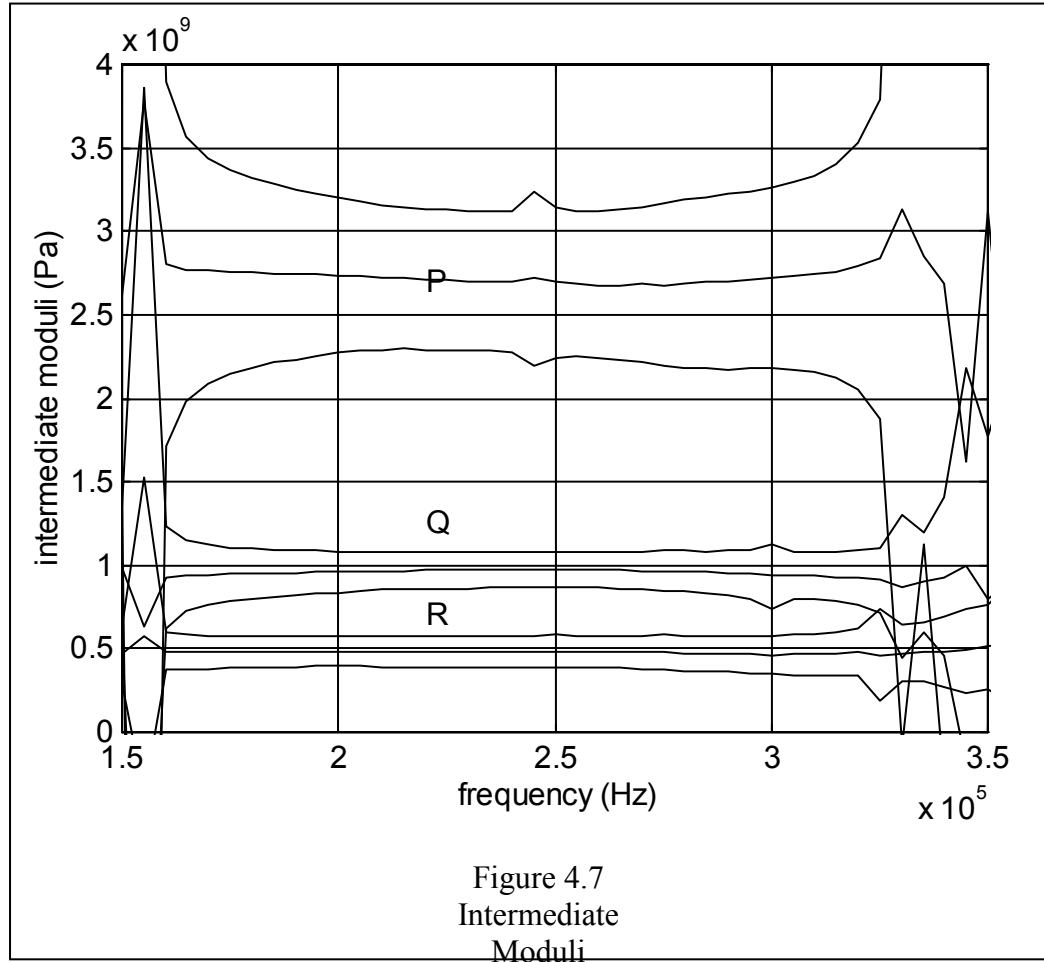
At 250 kHz values for the moduli are:

$$P = (2.69 \pm 0.45) \cdot 10^9 \quad \text{Pa} \tag{4-34}$$

$$Q = (9.7 \pm 1.1) \cdot 10^8 \quad \text{Pa} \tag{4-35}$$

$$R = (4.8 \pm 1.0) \cdot 10^8 \quad \text{Pa} . \tag{4-36}$$

The coupling modulus, Q, is 8.8 standard deviations from zero, which helps support the existence of Biot waves.

Figure 4.8
Mass Factor
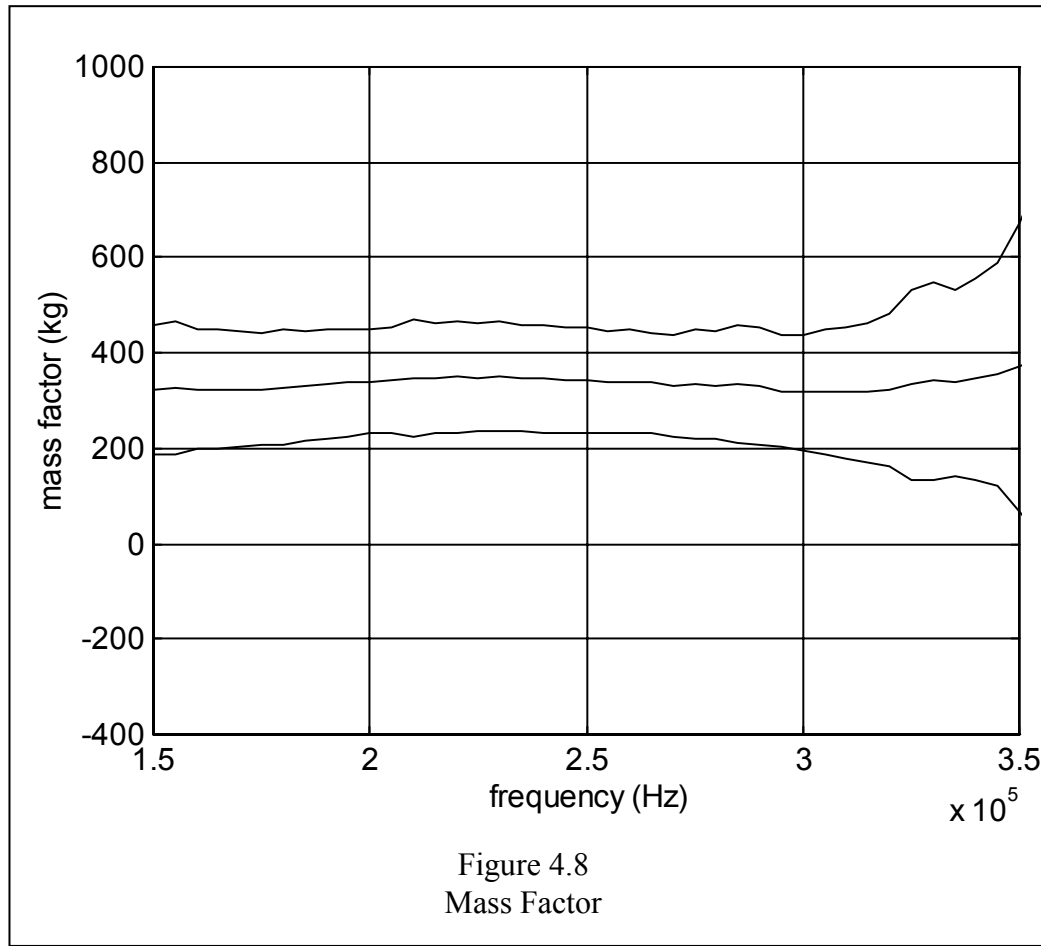
At 250 kHz the mass factor is:

$$\tilde{\alpha} = 340 \pm 110 \quad \text{kg} .$$
(4-37)

Using the known values of porosity and water density eq. (4-32) becomes:

$$\tilde{\alpha} \cong 349\alpha - i\frac{F}{\omega} .$$
(4-37a)

If $\alpha = 1$ and $F = 0$, i.e., no tortuosity or viscous effects, then $\tilde{\alpha}$ in eq. (4-37a) is 0.08 standard deviations from eq. (4-37). This agrees with an experiment previously referenced, [33], which concluded "attenuation shows no correlation with the viscosity" of the fluid in unconsolidated sand.

Note that up to now all graphed parameters are measured. Starting with the pressure reflection pulses and ending with the generalized moduli and mass factor, all math and theory (assuming the equations of motion and boundary conditions are true) are rigorous. But the following sand, frame, and shear moduli formulas are "semiphenomenological" [20] and not rigorous.

From eqs. (2-5) and (2-4) the sand and sand frame moduli are:

$$K_s = \frac{QK_w}{\beta K_w - R} \tag{4-38}$$

$$K_b = \left[(1 - \beta) - \frac{Q\beta}{R} \right] K_s . \tag{4-39}$$

The modulus of water, K_w, is $c_w^2 \rho_w = (1485.1)^2 (998.01) = 2.2012 \cdot 10^9$ Pa at $20.9°$ C.

From eq. (2-3) the shear modulus is:

$$N = \frac{3}{4} P - \frac{3(1-\beta)^2 K_s^2 K_w - 3(1-\beta) K_b K_s K_w + 3\beta K_s^2 K_b}{4(1-\beta) K_s K_w - 4 K_b K_w + 4\beta K_s^2} \tag{4-40}$$

Moduli at 250 kHz are:

$$K_s = (7.3 \pm 3.1) \cdot 10^9 \text{ Pa} \tag{4-41}$$

$$N = (9.0 \pm 7.5) \cdot 10^8 \text{ Pa} \tag{4-42}$$

$$K_b = (-5.6 \pm 7.3) \cdot 10^8 \text{ Pa} \tag{4-43}$$

These calculations do not appear correct. K_s is 9 standard deviations lower than the recognized value for sand modulus (about 36 GPa [32]). It is interesting that Chotiros [13] also calculated a sand modulus of $K_s = 7$ GPa using a numerical inversion technique from measured parameters (he concluded 7 GPa was low). The formulas for the generalized moduli, eqs. (2-3), (2-4), and (2-5), assume the bonding of the grains to be of the same material as the grains, ref. [20] p. 558. This assumption may not be correct for unconsolidated sand. The generalized moduli formulas appear correct when the grains are bonded [22], but the "bonding" of sand grains may include sliding friction and/or a fluid-reinforced frame [7, 11]. Finding good formulas for intermediate moduli of sandy sediments is a task for future work.

4.8 OPEN PORE PRESSURE REFLECTION COEFFICIENTS

The open pore pressure reflection coefficient, Table 2.1 is (Fig. 4.9):

$$R_{ww} = \frac{Z_1 Z_2 - Z_w Z_1 P_2{}^2 - Z_w Z_2 P_1{}^2}{Z_1 Z_2 + Z_w Z_1 P_2{}^2 + Z_w Z_2 P_1{}^2} \qquad (4\text{-}44)$$

Figure 4.9
Pressure Reflection Coefficient from
Sandy Sediment
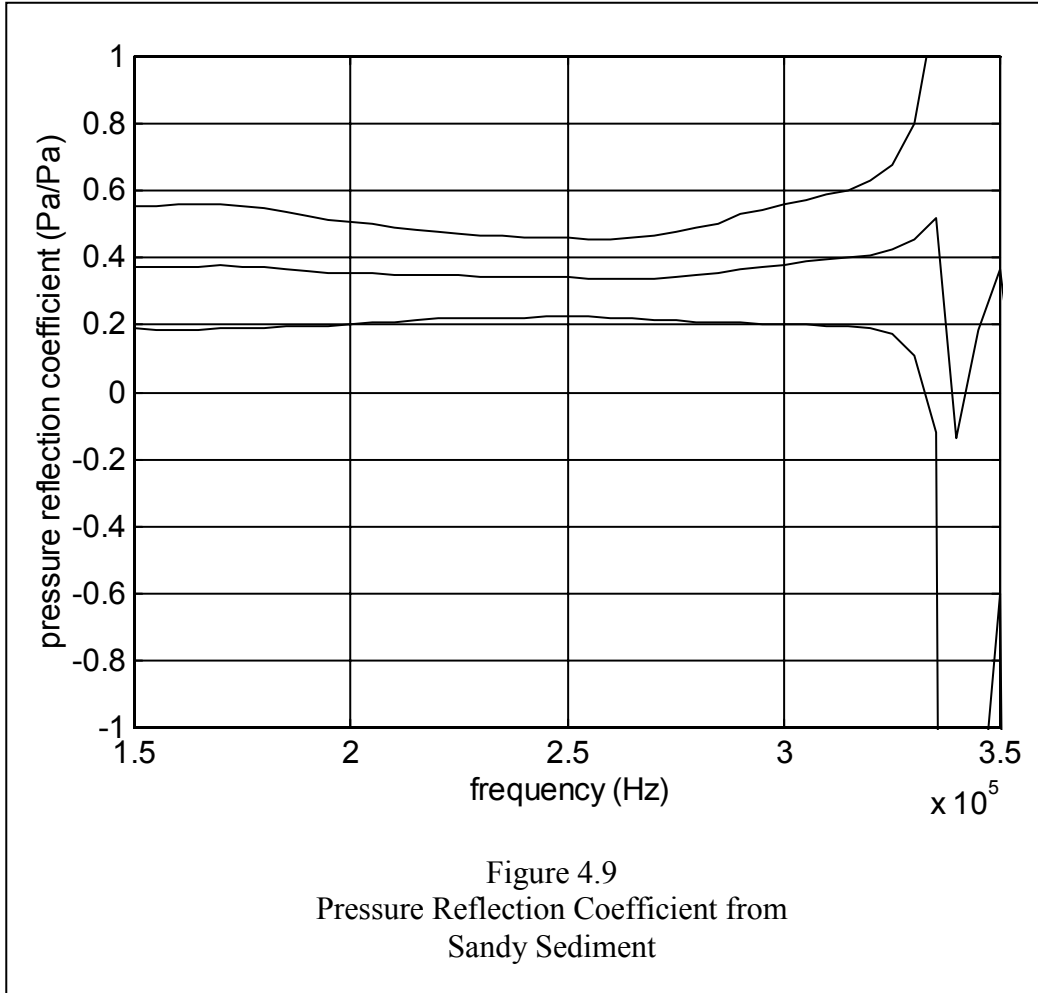
At 250 kHz:

$$R_{ww} = 0.34 \pm 0.11. \qquad (4\text{-}45)$$

An estimate of the reflection coefficient using the average Z_1, which is related to the effective density method [42], is:

$$R_1 = \frac{Z_1 - Z_w}{Z_1 + Z_w} = 0.35. \qquad (4\text{-}46)$$

The conventional reflection coefficient using the density of the water saturated sand and the speed of sound in sand:

$$R = \frac{\rho c_1 - Z_w}{\rho c_1 + Z_w} = 0.40 \,.$$ (4-47)

These reflection coefficients compare to a reflection experiment Chotiros et al. [12] did on sandy sediment. His reflection loss was 11 ± 2 dB ($R_{ww} = 0.28 \pm 0.08$), to be compared to a computed conventional reflection loss of 8 ± 1 dB ($R = 0.40 \pm 0.05$).

Chapter 5:
DISCUSSION

This was an experimental dissertation to help understand the physics of sound propagating through sandy sediments. The measurements, which were obtained through a reflection ratio technique, include acoustic impedances, effective densities, waves speeds, effective pressures, mode shapes, intermediate moduli, and pressure reflection coefficients. A lumped parameter model was developed to help aid in the interpretation of the measurements. The results show that the effective density of the fast wave is less than the total density of the water-saturated sand. This fact points to the existence of Biot waves in unconsolidated sand.

Three characteristics of a fast Biot wave are that it produces different water/sand oscillation amplitudes, that it does not use the full inertial energy in the sediment, and it has a different phase speed from its slower Biot wave even though both are compressional waves traveling through the same medium.

5.1 COMPARISONS

In the section that follows selected parameters are calculated from Biot theory at 250 kHz using published input parameters and compared to parameters measured from this experiment. Williams' parameters, ref. [42] in Table 5.1 are used to calculate selected parameters that are compared to parameters measured in this experiment. The comparisons are tabulated in Table 5.2. The deviations in Table 5.2 are the number of standard deviations the measured differs from theoretical. No deviations were listed for mechanically measured parameters. As previously mentioned the sand modulus is over 9 standard deviations lower than expected, presumably due to incorrect intermediate moduli formulas. The result of this is the large deviation of the fast wave speed.

The fast effective mass using Williams' parameters and lumped parameter model is (Table 5.2):

$$\rho_1 = 1692.2 - i6.5 \quad \text{kg}/\text{m}^3 \tag{5-1}$$

This compares with the effective mass using Williams' parameters and effective density method [42]:

$$\rho_{eff} = 1674.2 - i1.2 \quad \text{kg}/\text{m}^3 \qquad (5\text{-}2)$$

The sign on the imaginary part is negative because of the forms of the solutions assumed, eqs. (2-21) and (2-22). The difference between eqs. (5-1) and (5-2) is due to the approximations used in [42].

Table 5.1 Williams' Parameters ref. [42]			
Physical Constants	Symbols	Units	Values
Permeability, see note 1.	k	m^2	1e-10
Porosity	β	--	0.40
Density of fluid	ρ_f	kg/m^3	1000
Density of sand grains	ρ_r	kg/m^3	2650
Bulk modulus of grains	K_s	Pa	3.6e10
Bulk modulus of fluid	K_w	Pa	2.25e9
Bulk modulus of frame, see note 2.	K_b	Pa	4.4e7 + i2.0e6
Fluid viscosity	η	Ns/m^2	1e-3
Shear modulus, see note 2.	N	Pa	2.61e7 + i1.24e6
Virtual mass for liquid (tortuosity)	α	--	1.25
Pore size (radius)	a	m	$\sqrt{\dfrac{8\alpha k}{\beta}}$
Notes: 1. Wave number and permeability both use k. 2. The signs on the imaginary parts are positive because of the forms of the solutions assumed, eqs. (2-21) and (2-22).			

Table 5.2 Comparisons at 250 kHz			
Parameter (Symbols)	Measured	Williams' Parameters [42]	Deviation See note 1
Fast Impedance (Z_1)	$(3.072 \pm 0.097)e6$	$(2.967 - i0.005)e6$	-1.1
Slow Impedance (Z_2)	$(6.2 \pm 8.8)e4$	$(4.66 + i0.26)e4$	0.2
Total Density (ρ)	2087	1990	---
Fast Effective Density (ρ_1)	1860 ± 58 $89\%\pm3\%$ of total	$1692.2 - i6.5$ 85% of total	-1.3 dev. of %
Slow Effective Density (ρ_2)	227 ± 58 $11\%\pm3\%$ of total	$297.5 + i6.5$ 15% of total	1.3 dev. of %
Fast Wave Speed (c_1)	1654 ± 6	$1753.4 + i3.8$	see note 2
Slow Wave Speed (c_2)	170 ± 560	$156.7 + i5.4$	-0.02
Fast Effective Force (P_1)	1.044 ± 0.046	$1.0029 + i0.0002$	-0.9
Slow Effective Force (P_2)	-0.044 ± 0.046	$-0.0029 - i0.0002$	0.9
Fast Mode Shape (B_1/A_1)	2.20 ± 0.37	$2.100 + i0.036$	-0.3
Slow Mode Shape (B_2/A_2)	-2.37 ± 0.47	$-1.5235 - i0.0008$	1.8
Intermediate Modulus (P)	$(2.69 \pm 0.45)e9$	$(1.923 + i0.003)e9$	-1.7
Intermediate Modulus (Q)	$(9.7 \pm 1.1)e8$	$(1.2320 - i0.0001)e9$	2.4
Intermediate Modulus (R)	$(4.8 \pm 1.0)e8$	$8.2300e8 + i7e3$	3.4
Mass Factor $(\tilde{\alpha})$	340 ± 110	$511 - i12$	1.6
Sand Modulus (K_s)	$(7.3 \pm 3.1)e9$	$3.6e10$	9.3
Frame Modulus (K_b)	$(-5.6 \pm 7.3)e8$	$(4.4 + i0.2)e7$	0.8
Shear Modulus (N)	$(9.0 \pm 7.5)e8$	$(2.61 + i0.12)e7$	-1.2
Porosity (β)	0.35	0.40	---
Sand Density (ρ_s)	2673	2650	---
Water Speed (c_w)	1485	1500	---
Note 1: deviation = (Williams' minus measured)/standard deviation			
Note 2: A better comparison might be the fast speed to water speed ratios. For Measured this is 1.11. From Williams' parameters it is 1.17. A difference of 5%.			

Table 5.3 shows the units of the parameters.

Table 5.3 Parameter Units			
Parameter	Symbol	Continuous Units	Lumped Units
Fast Impedance	Z_1	Pa·s/m	Ns/m
Slow Impedance	Z_2	Pa·s/m	Ns/m
Total Mass	ρ	kg/m^3	kg
Fast Effective Mass	ρ_1	kg/m^3	kg
Slow Effective Mass	ρ_2	kg/m^3	kg
Fast Wave Speed	c_1	m/s	m/s
Slow Wave Speed	c_2	m/s	m/s
Fast Effective Force	P_1	Pa/Pa	N/N
Slow Effective Force	P_2	Pa/Pa	N/N
Fast Mode Shape	B_1/A_1	m/m	m/m
Slow Mode Shape	B_2/A_2	m/m	m/m
Intermediate Modulus	P	Pa	N/m
Intermediate Modulus	Q	Pa	N/m
Intermediate Modulus	R	Pa	N/m
Mass Factor	$\tilde{\alpha}$	kg/m^3	kg
Sand Modulus	K_s	Pa	N/m
Frame Modulus	K_b	Pa	N/m
Shear Modulus	N	Pa	N/m
Porosity	β	m^3/m^3	m/m
Sand Density	ρ_s	kg/m^3	kg

5.2 SIMPLIFIED EQUATIONS OF MOTION

At higher frequencies (250 kHz) for water-saturated sand at normal incidence the equations of motion, eqs. (2-1) and (2-2) reduce to (no viscous or tortuosity effects):

$$P\frac{\partial^2 u_s}{\partial z^2} + Q\frac{\partial^2 u_f}{\partial z^2} - (1-\beta)\rho_s \ddot{u}_s = 0 \qquad (5\text{-}3)$$

$$Q\frac{\partial^2 u_s}{\partial z^2} + R\frac{\partial^2 u_f}{\partial z^2} - \beta\rho_f \ddot{u}_f = 0 . \qquad (5\text{-}4)$$

These simplified equations only use seven of the 13 Biot parameters listed in Table 5.1: β, ρ_f, ρ_r, K_s, K_w, and K_b (complex counts as two).

5.3 FUTURE WORK

Future work should include (1) adding shear displacements to the lumped parameter model (allowing for angle of incidence), (2) deriving good intermediate moduli formulas, (3) using the reflection ratio technique on a different unconsolidated medium like glass beads. This may help to derive good moduli formulas. (4) The development of a "calibrated" piece of material, e.g., cast acrylic, that can be taken into the field and put on top of the sand. With a transducer and receiver mounted a fixed distance from the acrylic, coherently averaged fast wave impedances can be measured (may have to assume slow wave impedances are small). That way, together with the speed of sound, effective densities of the sediment can be measured in the field.

5.4 CONCLUSIONS

This dissertation is a data point in favor of Biot waves existing in sandy sediments because (1) the fast wave effective density is less than the total density, (2) the fast wave mode shape is not one, and (3) the coupling modulus, Q, is not zero. However, other measured parameters, e.g., slow wave impedance and speed, slow wave effective pressure, tortuosity and viscous effects, are consistent with zero and do not support the existence of Biot waves. Even the Biot open pore pressure reflection coefficient is consistent with the conventional pressure reflection coefficient.

The largest contribution toward understanding the physics of sound waves in sandy sediments is the measurement of mode shapes, which give relative oscillation amplitudes between the saturating fluid and solid particles. The knowledge that the sand and fluid vibrate with different amplitudes helps explain how a sound wave propagates without using the full mass of the medium. But the largest practical contribution is the measurement of the effective density of the fast wave. Effective densities can be used for more accurate predictions of scattering [44].

This experiment supports the conclusions that subcritical penetration in sandy sediment is from scattering and not from the Biot slow waves [17, 26, 34]. This is true for two reasons. The speed of the slow wave is essentially zero and the incident pressure wave does not excite the slow wave (participation factor is essentially zero). In other words, no energy goes into a slow wave and if it did it would not propagate.

REFERENCES

[1]   K. Attenborough. Acoustical Characteristics of Porous Materials. *Physics Reports*, 82:181-224, 1982.

[2]   R. O. Belsheim and G. J. O'Hara. "Shock Design of Shipboard Equipment. Dynamic Design-Analysis Method." NAVSHIPS 250-423-30. Naval Ship Systems Command, May 1961. (Selected parts copied in Appendix E).

[3]   M. A. Biot. Theory of propagation of elastic waves in a fluid-saturated porous solid. I. Low-frequency range. *J. Acoust. Soc. Am.*, 28:168-178, 1956.

[4]   M. A. Biot. Theory of propagation of elastic waves in a fluid-saturated porous solid. II. High-frequency range. *J. Acoust. Soc. Am.*, 28:179-191, 1956.

[5]   M. A. Biot. Generalized Theory of Acoustic Propagation in Porous Dissipative Media. *J. Acoust. Soc. Am.*, 34:1254-1264, 1962.

[6]   F. A. Boyle and N. P. Chotiros. Experimental detection of a slow acoustic wave in sediment at shallow grazing angles. *J. Acoust. Soc. Am.*, 91:2615-2619, 1992.

[7]   M. J. Buckingham. Wave propagation, stress relaxation, and grain-to-grain shearing in saturated, unconsolidated marine sediments. *J. Acoust. Soc. Am.*, 108:2796-2815, 2000.

[8]   R. N. Chandler. Transient streaming potential measurements on fluid-saturated porous structures: An experimental verification of Biot's slow wave in the quasi-static limit. *J. Acoust. Soc. Am.*, 70, 116 (1981).

[9]   N. P. Chotiros. Biot model of sound propagation in water-saturated sand. *J. Acoust. Soc. Am.,* 97:199-214, 1995.

[10]   N. P. Chotiros. Inversion of sandy ocean sediments. *Full Field Inversion Methods in Ocean and Seismo-Acoustic,* edited by Diachok, Caiti, Gerstoft, and Schmidt. Kluwer Academic Publishers, Norwell MA, pages 353-358, 1995.

[11]   N. P. Chotiros. Response to: "Comments on 'Biot model of sound propagation in water-saturated sand'" [J. Acoust. Soc. Am. 103, 2723-2725 (1998)]. *J. Acoust. Soc. Am.*, 103:2726-2729, 1998.

[12]   N. P. Chotiros, A. P. Lyons, J. Osler, and N. G. Pace. Normal incidence reflection loss from a sandy sediment. *J. Acoust. Soc. Am.*, 112:1831-1841, 2002.

[13] N. P. Chotiros. An inversion for Biot parameters in water-saturated sand. *J. Acoust. Soc. Am.*, 112:1853-1868, 2002.

[14] R. W. Clough and J. Penzien. Dynamics of Structures. McGraw-Hill Inc., New York NY. 1975.

[15] T. Geertsma and D. C. Smit. Some aspects of elastic waves propagation in fluid saturated porous solids. *Geophysics* 26, 169-181, 1961.

[16] K. V. Horoshenkov and M. J. Swift. The acoustic properties of granular materials with pore size distribution close to log-normal. *J. Acoust. Soc. Am.*, 110 (5), 2371-2378, 2001.

[17] D. R. Jackson, K. L. Williams, E. I. Thorsos, and S. G. Kargl. High-frequency subcritical acoustic penetration into a sandy sediment. *IEEE J. Ocean Eng.*, vol. 27, pp. 346-361, July 2002.

[18] D. L. Johnson. Equivalence between fourth sound in liquid He II at low temperatures and the Biot slow wave in consolidated porous media. *Appl. Phys. Lett.*, 37, 1065 (1980).

[19] D. L. Johnson, T. J. Plona, C. Scala, F. Pasierb, and H. Kojima. Tortuosity and Acoustic Slow Waves. *Physical Review Letters,* 49:1840-1844, 1982.

[20] D. L. Johnson and T. J. Plona. Acoustic slow waves and the consolidation transition. *J. Acoust. Soc. Am.*, 72:556-565, 1982.

[21]   D. L. Johnson. Elastodynamics of gels. *J. Chem. Phys.*, 77, 1531-1539, 1982.

[22] D. L. Johnson, T. J. Plona, and H. Kojima. Probing porous media with first and second sound. II. Acoustic properties of water-saturated porous media. *J. Appl. Phys.*, 76:115-125, 1994.

[23] D. H. Johnston, M. N. Toksöz, and A. Timur. Attenuation of seismic waves in dry and saturated rocks: II. Mechanisms. *Geophysics* 44, 691-711, 1979.

[24] C. D. Jones. High-frequency acoustic volume scattering from biologically active marine sediments. Technical Report APL-UW TR 9903, Applied Physics Laboratory, University of Washington, 1999.

[25] R. Lakes, H. S. Yoon, and J. L. Katz. Slow compressional wave propagation in wet human and bovine cortical bone. *Science* 220, 513-515, 1983.

[26]   A. Maguer, W. L. J. Fox, H. Schmidt, E. Pouliquen, and E. Bovio. Mechanisms for subcritical penetration into a sandy bottom: Experimental and modeling results. *J. Acoust. Soc. Amer.*, 107:1215-1225, 2000.

[27]   G. R. Mellema. Subcritical acoustic scattering across a rough fluid-solid interface. Dissertation for a Doctor of Philosophy degree, University of Washington, 1999.

[28]   J. E. Moe. Near and far-field acoustic scattering through and from two-dimensional fluid-fluid rough interfaces. Technical Report APL-UW TR 9606, Applied Physics Laboratory, University of Washington, 1996.

[29]   T. J. Plona. Observation of a second bulk compressional wave in a porous medium at ultrasonic frequencies. *Appl. Phys. Lett.*, 36:259-261, 1980.

[30]   T. J. Plona, R. D'Angelo, and D. L. Johnson. Velocity and attenuation of fast, shear and slow waves in porous media. *IEEE 1990 Ultrasonics Symposium*, edited by B. R. McAvoy, pages 1233-1239, 1990.

[31]   J.W.S. Rayleigh. The Theory of Sound, Volume Two. Dover Publications, Inc., New York NY. 1945.

[32]   M. D. Richardson, K. L. Williams, K. B. Briggs, and E. I. Thorsos. Dynamic measurement of sediment grain compressibility at atmospheric pressure: Acoustic applications. *IEEE J. Oceanic Eng.*, vol. 27, pp. 593-601, July 2002.

[33]   P. K. Seifert, B. Kaelin, and L. R. Johnson. Effect on ultrasonic signals of viscous pore fluids in unconsolidated sand. *J. Acoust. Soc. Am.*, 106:3089-3094, 1999.

[34]   H. J. Simpson and B. H. Houston. Synthetic array measurements of acoustical waves propagating into a water-saturated sandy bottom for a smoothed and a roughened interface. *J. Acoust. Soc. Am.*, 107:2329-2337, 2000.

[35]   R. D. Stoll and B. M. Bryan. Wave attenuation in saturated sediments. *J. Acoust. Soc. Am.*, 47, 1440-1447, 1969.

[36]   R. D. Stoll. Acoustic waves in saturated sediment. *Physics of Sound in Marine Sediments,* edited by Hampton. Plenum NY, pages 19-39, 1974.

[37]   R. D. Stoll. Theoretical aspects of sound transmission in sediments. *J. Acoust. Soc. Am.*, 68 (5):1341-1350, 1980.

[38] R. D. Stoll and T. K. Kan. Reflection of acoustic waves at a water-sediment interface. *J. Acoust. Soc. Am.*, 70:149-156, 1981.

[39] R. D. Stoll. Comments on "Biot model of sound propagation in water saturated sand" [J. Acoust. Soc. Am. 97, 199-214 (1995)]. *J. Acoust. Soc. Am.*, 103:2723-2725, 1998.

[40] E. I. Thorsos, D. R. Jackson, K. L. Williams. Modeling of subcritical penetration into sediments due to interface roughness. *J. Acoust. Soc. Am.*, 107:263-277, 2000.

[41] A. Turgut and T. Yamamoto. Measurements of acoustic wave velocities and attenuation in marine sediments. *J. Acoust. Soc. Am.*, 87 (6):2376-2383, 1990.

[42] K. L. Williams. An effective density fluid model for acoustic propagation in sediments derived from Biot theory. *J. Acoust. Soc. Am.*, 110 (5):2276-2281, 2001.

[43] K. L. Williams, D. R. Jackson, E. I. Thorsos, D. Tang, and S. G. Schock. Comparison of sound speed and attenuation measured in a sandy sediment to predictions based on the Biot theory of porous media. *IEEE J. Oceanic Eng.*, vol. 27, pp. 413-428, July 2002.

[44] K. L. Williams, D. R. Jackson, E. I. Thorsos, D. Tang, and K. B. Briggs. Acoustic backscattering experiments in a well characterized sand sediment: Data/model comparisons using sediment fluid and Biot models. *IEEE J. Oceanic Eng.,* vol. 27, pp. 376-387, July 2002.

[45] T. Yamamoto. Acoustic propagation in the ocean with a poro-elastic bottom. *J. Acoust. Soc. Am.*, 73 (5):1587-1596, 1983.

Appendix A:
IMPEDANCES OF ACRYLIC AND ETHAFOAM

A.1 IMPEDANCE OF ACRYLIC

The measurements and calculations for the impedance of the acrylic were accomplished using ratios of transfer functions. The acrylic was purchased from Port Plastics, Tukwila WA under the product name of "Clear Acrylic." The transfer functions were the ratios of reflections shown in Figs. A.1 and A.2. In these figures the transducer and receiver are in the water below the acrylic.

Figure A.1
Schematic for Acrylic-Air Transfer Function

Figure A.2
Schematic for Acrylic-Water Transfer Function
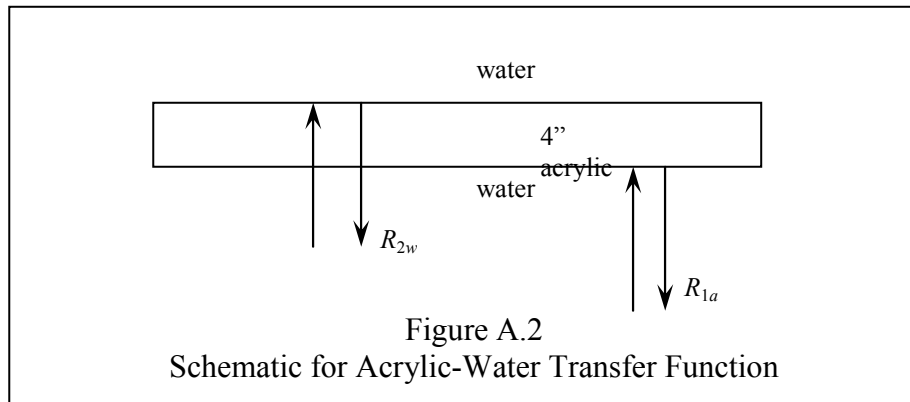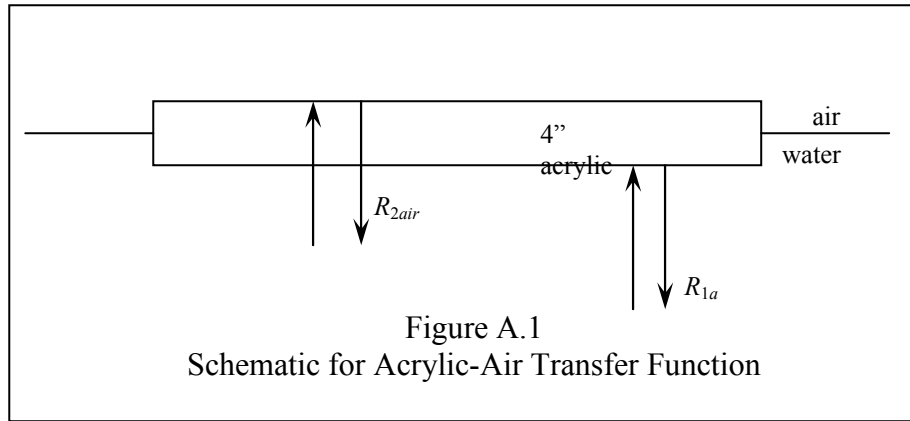
The received pressure from the transmitter, reflected off the water-acrylic interface, and back to the receiver is:

$$R_{1a} = \frac{A}{d_1} \frac{Z_a - Z_w}{Z_a + Z_w} \exp(-ik_w d_w).$$

(A-1)

A is the complex pressure amplitude a unit distance from the acoustic center, d_1 is the distance from the acoustic center, Z_a is the impedance of the acrylic, Z_w is the impedance of water, k_w is the wave number of water, and d_w is the distance the sound travels through water to the acrylic surface and back. Due to the mechanics of the transducers d_1 may not equal d_w. R_{2air} is:

$$R_{2air} = \frac{A}{d_2} \frac{2Z_a}{Z_a + Z_w} (-1) \frac{2Z_w}{Z_a + Z_w} \exp(-ik_w d_w) \exp(-i2k_a t_a). \tag{A-2}$$

Where d_2 is the spreading loss factor, k_a is the wave number of the acrylic, and t_a is the thickness of the acrylic. The reflection coefficient R_{2w} is:

$$R_{2w} = \frac{A}{d_2} \frac{2Z_a}{Z_a + Z_w} \frac{Z_w - Z_a}{Z_w + Z_a} \frac{2Z_w}{Z_a + Z_w} \exp(-ik_w d_w) \exp(-i2k_a t_a). \tag{A-3}$$

The ratio of transfer functions for the acrylic-air surface is:

$$T = \frac{\left|\frac{(R_{2w})_2}{(R_{1a})_2}\right|}{\left|\frac{(R_{2air})_1}{(R_{1a})_1}\right|} = -\left(\frac{Z_w - Z_a}{Z_w + Z_a}\right). \tag{A-4}$$

The subscripts 1 and 2 represent acoustic pulses, in which the transducer-generated amplitude, A, and the distance through the water, d_w, may be slightly different from one setup to the next. Also R_{2w} and R_{2air} are divided by R_{1a} to make the reflection from the acrylic surface the $t = 0$ trigger. Solving eq. (A-4) for Z_a:

$$Z_a = \frac{(1 + T)Z_w}{1 - T}. \tag{A-5}$$

The impedance and standard deviation at 100 locations of the 4" acrylic, Z_a, are shown in Fig. A.3.

Figure A.3
Impedance of
Acrylic

For the acrylic, at 250 kHz, the impedance is:

$$Z_a = (3.17 \pm 0.05) \cdot 10^6 \quad \text{Pa} \cdot \text{s/m}. \tag{A-6}$$

As a comparison, ref. [27] measures the speed of sound in cast acrylic at 2705 m/s and the density to be 1181 kg/m^3, which makes the impedance $3.19 \cdot 10^6$.

A.2 IMPEDANCE OF ETHAFOAM

Ethafoam is similar to Styrofoam. Ethafoam is a little denser but is easier to work with and glue. The transfer functions (ratios of reflections) are shown in Figs. A.1 and A.4.
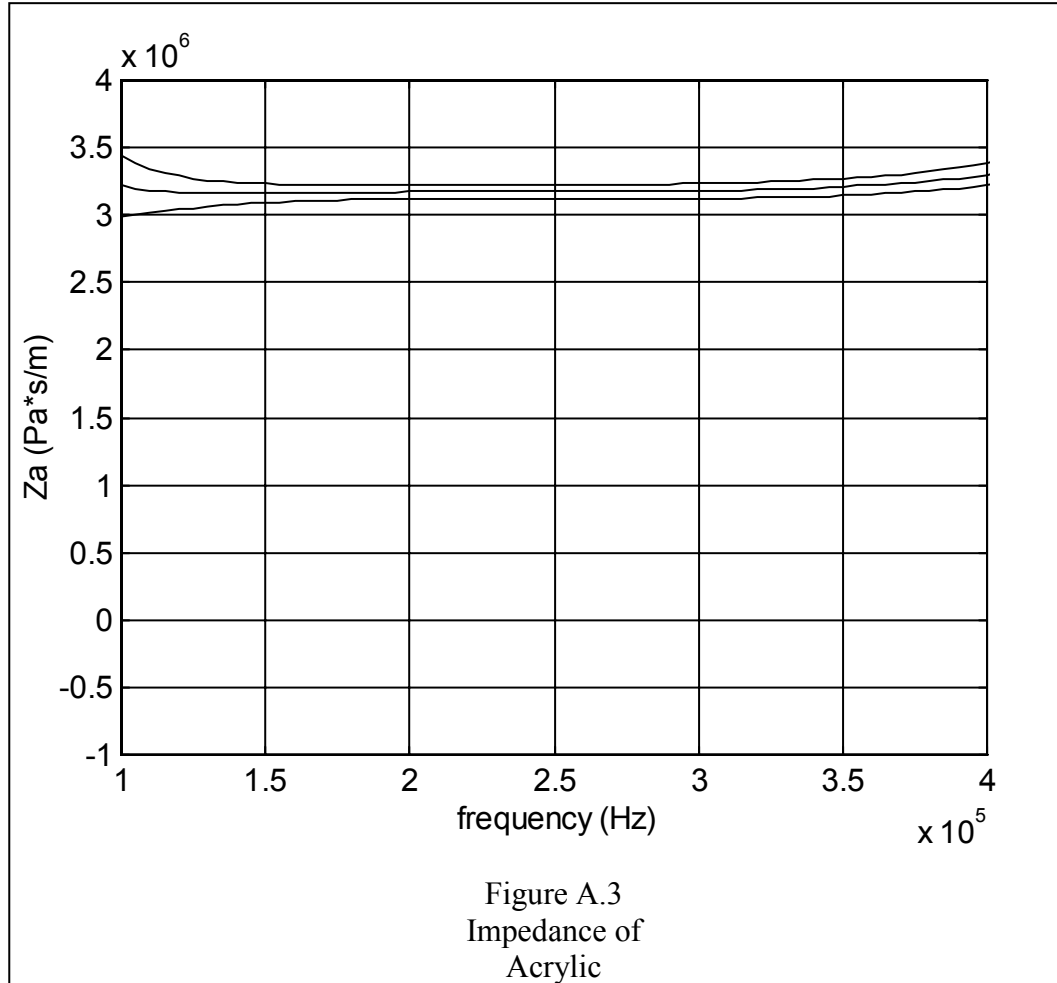

Figure A.4
Schematic for Acrylic-Ethafoam Transfer Function
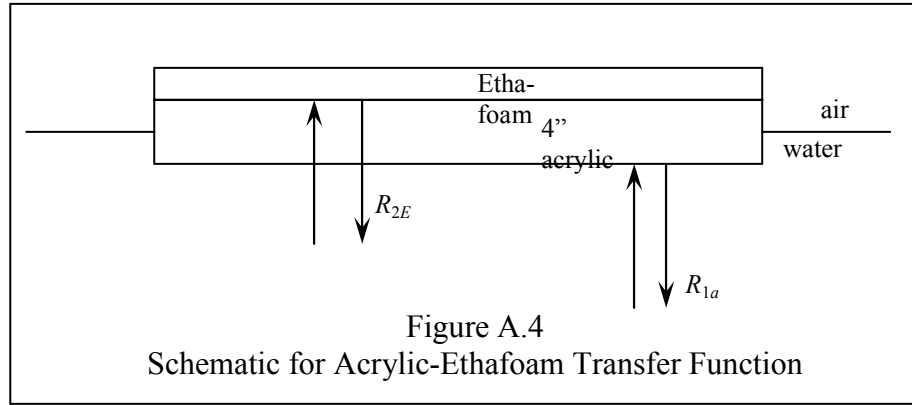
The ratio of transfer functions for the acrylic-Ethafoam surface is:

$$T = \frac{\left|\dfrac{R_{2E}}{R_{1a}}\right|}{\left|\dfrac{R_{2air}}{R_{1a}}\right|} = -\left(\frac{Z_E - Z_a}{Z_E + Z_a}\right) \tag{A-7}$$

Where Z_E is the impedance of the Ethafoam and Z_a is the impedance of the 4" acrylic. Solving eq. (A-7) for Z_E:

$$Z_E = \frac{(1 - T)Z_a}{1 + T} \tag{A-8}$$

The impedance of the Ethafoam, Z_E, and its standard deviation are shown with in Fig. A.5.

Figure A.5
Impedance of Ethafoam
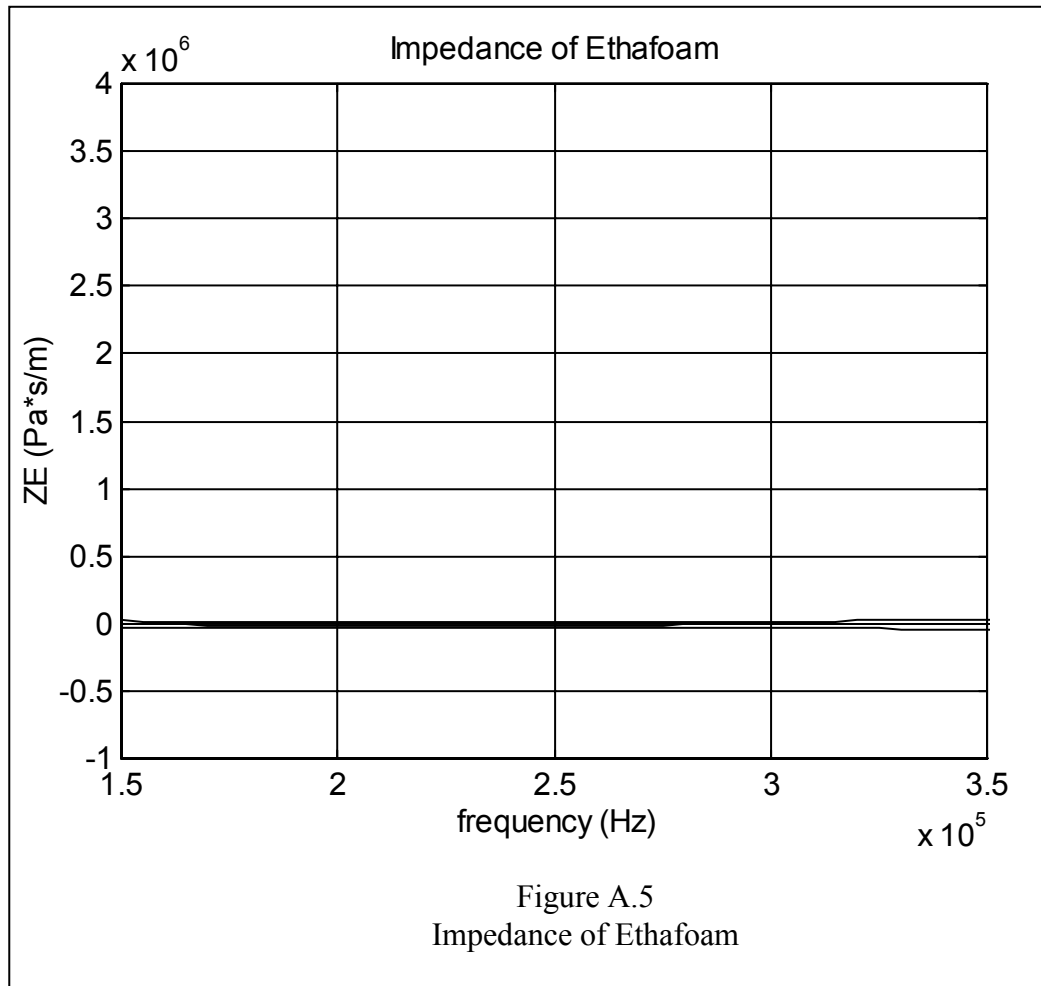
For the Ethafoam, at 250 kHz, the measured impedance was:

$$Z_E = (-1.1 \pm 2.2) \cdot 10^4 \quad \mathrm{Pa \cdot s/m} \tag{A-9}$$

Z_E is 0.5 standard deviations from zero. A Z_E of zero is used in the body of this report.

Appendix B:
NUMERICAL CHECKS

The lumped parameter method has two areas of new theory, where the final products are pressure coefficients and mode shapes; these two parameters are calculated from continuous and lumped parameter theory using Williams' parameters. Even though this is not a sufficient proof that the lumped and continuous parameter theories are equivalent, it shows the two methods are equivalent in the range of values measured in this experiment.

Pressure coefficients computed using Johnson and Plona's method [20] are calculated below and compared to pressure coefficients from the lumped parameter method, Table 2.1. Also modes shapes from Biot theory, eqs. (2-18) and (2-19), are calculated and compared to modes shapes from the lumped parameter method, eqs. (4-27) and (4-28). All pressure coefficients and mode shapes are calculated using the input parameters of Table 5.1.

As the incident pressure from the water acts upon the sediment, the force in the sand per unit area of sediment equals the force on the sand from the incident and reflected wave per unit area of sediment:

$$P\frac{\partial u_s}{\partial z} + Q\frac{\partial u_f}{\partial z} = (1-\beta)\left(K_w\frac{\partial u_i}{\partial z} + K_w\frac{\partial u_r}{\partial z}\right). \qquad \text{(B-1)}$$

And likewise, the force in the fluid (the fluid in the sediment) per unit area of sediment equals the force on the fluid from the incident and reflected wave per unit area of sediment:

$$R\frac{\partial u_f}{\partial z} + Q\frac{\partial u_s}{\partial z} = \beta\left(K_w\frac{\partial u_i}{\partial z} + K_w\frac{\partial u_r}{\partial z}\right). \qquad \text{(B-2)}$$

Another boundary condition is particle displacement below equals particle displacement above:

$$(1-\beta)u_s + \beta u_f = u_i + u_r. \qquad \text{(B-3)}$$

The forms of the solutions are:

$$u_s = A_1 \exp(i(\omega t - k_1 z)) + A_2 \exp(i(\omega t - k_2 z))$$
$$u_f = B_1 \exp(i(\omega t - k_1 z)) + B_2 \exp(i(\omega t - k_2 z))$$
$$u_i = A_i \exp(i(\omega t - k_w z))$$
$$u_r = A_r \exp(i(\omega t + k_w z)).$$

(B-4)

The five unknowns, A_1, A_2, B_1, B_2, and A_r, are solved in matrix form, assuming $A_i = 1$. The five equations are (B-1), (B-2), (B-3), (2-18), and (2-19), yielding

$$\begin{Bmatrix} A_1 \\ A_2 \\ B_1 \\ B_2 \\ A_r \end{Bmatrix} = \begin{bmatrix} Pk_1 & Pk_2 & Qk_1 & Qk_2 & (1-\beta)K_w k_w \\ Qk_1 & Qk_2 & Rk_1 & Rk_2 & \beta K_w k_w \\ 1-\beta & 1-\beta & \beta & \beta & -1 \\ M_{41} & 0 & M_{43} & 0 & 0 \\ 0 & M_{52} & 0 & M_{54} & 0 \end{bmatrix}^{-1} \begin{Bmatrix} (1-\beta)k_w K_w \\ \beta k_w K_w \\ 1 \\ 0 \\ 0 \end{Bmatrix},$$

(B-5)

where

$$M_{41} = k_1^2 P - \omega^2 \rho_{11} - i\omega F$$
$$M_{43} = k_1^2 Q - \omega^2 \rho_{12} + i\omega F$$
$$M_{52} = k_2^2 P - \omega^2 \rho_{11} - i\omega F$$
$$M_{54} = k_2^2 Q - \omega^2 \rho_{12} + i\omega F.$$

(B-6)

The equation (B-3) was multiplied by 10e5 to keep the inversion in eq. (B-5) from becoming singular.

The pressure reflection coefficient is

$$\frac{P_r}{P_i} = -A_r.$$

(B-7)

The transmitted pressures coefficients of the fast and slow waves are:

$$\frac{\sigma_1}{P_i} = \frac{k_1}{k_w K_w}[(P+Q)A_1 + (Q+R)B_1]$$

(B-8)

$$\frac{\sigma_2}{P_i} = \frac{k_2}{k_w K_w}[(P+Q)A_2 + (Q+R)B_2].$$

(B-9)

Pressure coefficient comparisons are in Table B.1.

Table B.1 Comparisons of Calculated Pressure Coefficients		
P_r/P_i	eq. (B-7)	$0.32564926491560 - i0.00091523022991$
R_{ww}	eq. (2-57)	$0.32564926491560 - i0.00091523022991$
σ_1/P_i	eq. (B-8)	$1.32943502471988 - i0.00069866204680$
T_{w1}	eq. (2-59)	$1.32943502471988 - i0.00069866204680$
σ_2/P_i	eq. (B-9)	$-0.00378575980428 - i0.00021656818311$
T_{w2}	eq. (2-60)	$-0.00378575980428 - i0.00021656818311$

Mode shape comparisons (continuous eqs. (2-18), (2-19) and lumped eqs. (4-27), (4-28)) using input parameters in Table 5.1 are in Table B.2.

Once again, even though these agreements in Tables B.1 and B.2 are necessary, they are not a sufficient proof that the lumped parameter method is equal to the continuous parameter method. It does show the two methods are numerically equivalent in the parameter range of interest.

Table B.2 Comparisons of Calculated Mode Shapes		
B_1/A_1	eq. (2-18)	$2.10033988149722 + i0.03549735086698$
B_1/A_1	eq. (4-27)	$2.10033988149741 + i0.03549735086701$
B_2/A_2	eq. (2-19)	$-1.52352553508303 - i0.00083813014479$
B_2/A_2	eq. (4-28)	$-1.52352553508303 - i0.00083813014479$

Appendix C:
ERROR ANALYSIS

All acoustically measured parameters were measured in 100 different locations. The bands or tolerances used in the plots in the body of this report are standard deviations. The following calculates the errors at the center-band frequency (250 kHz) and compares them to the standard deviations.

Three types of error are calculated, random, bias, and "absolute," on Z_1 and Z_2. Random error of a random quantity is the standard deviation divided by the square root of the number of measurements. So from eq. (4-5), the random error on the fast and slow wave impedances are 9700 and 8800 Pa·s/m respectively.

The residual ringing of the transmitting transducer caused a bias error, see Appendix G. Fig. C.1 is the pulse reflected from the water-air interface along with the envelope of the pulse for acrylic-air, r_{2air}, see Fig. 3.4. The envelope is placed at the same time the second pulse from the top acrylic surface would return. The value under the envelope of interest is used for the bias errors for R_{3E_3air} and R_{2s_2air} in eqs. (4-3) and (4-4). The bias errors of Z_1 and Z_2 are calculated using the partial derivatives of eqs. (4-3) and (4-4) with respect to R_{3E_3air} and R_{2s_2air} and the bias errors of R_{3E_3air} and R_{2s_2air}. The bias errors of Z_1 and Z_2 are 17,000 and 7500 Pa·s/m respectively.

The "absolute" error arises from the absolute values used instead of the complex on the reflections in eqs. (4-1) and (4-2). To obtain absolute errors, William's parameters are used to calculate complex Z_1 and Z_2, as in Table 5.2. The complex reflections are calculated from eqs. (4-1) and (4-2), made into absolutes, and absolute Z_1 and Z_2's are calculated with eqs. (4-3) and (4-4). The "absolute" errors are found to be 16,000 and 21,500 Pa·s/m respectively.

Assuming these errors are not correlated and can be added in quadrature, the total errors of Z_1 and Z_2 are 25,000 and 24,000 Pa·s/m respectively (relative error 0.008 and 0.39), compared to standard deviations of 97,000 and 88,000 Pa·s/m respectively (relative deviation 0.03 and 1.4).

The total errors are about one-third the standard deviations. Therefore the standard deviations are mostly a measure of spatial variability of the sand sample.

Figure C.1
Pulse Reflection from Water-Air Interface
with Envelope Used for Bias Error
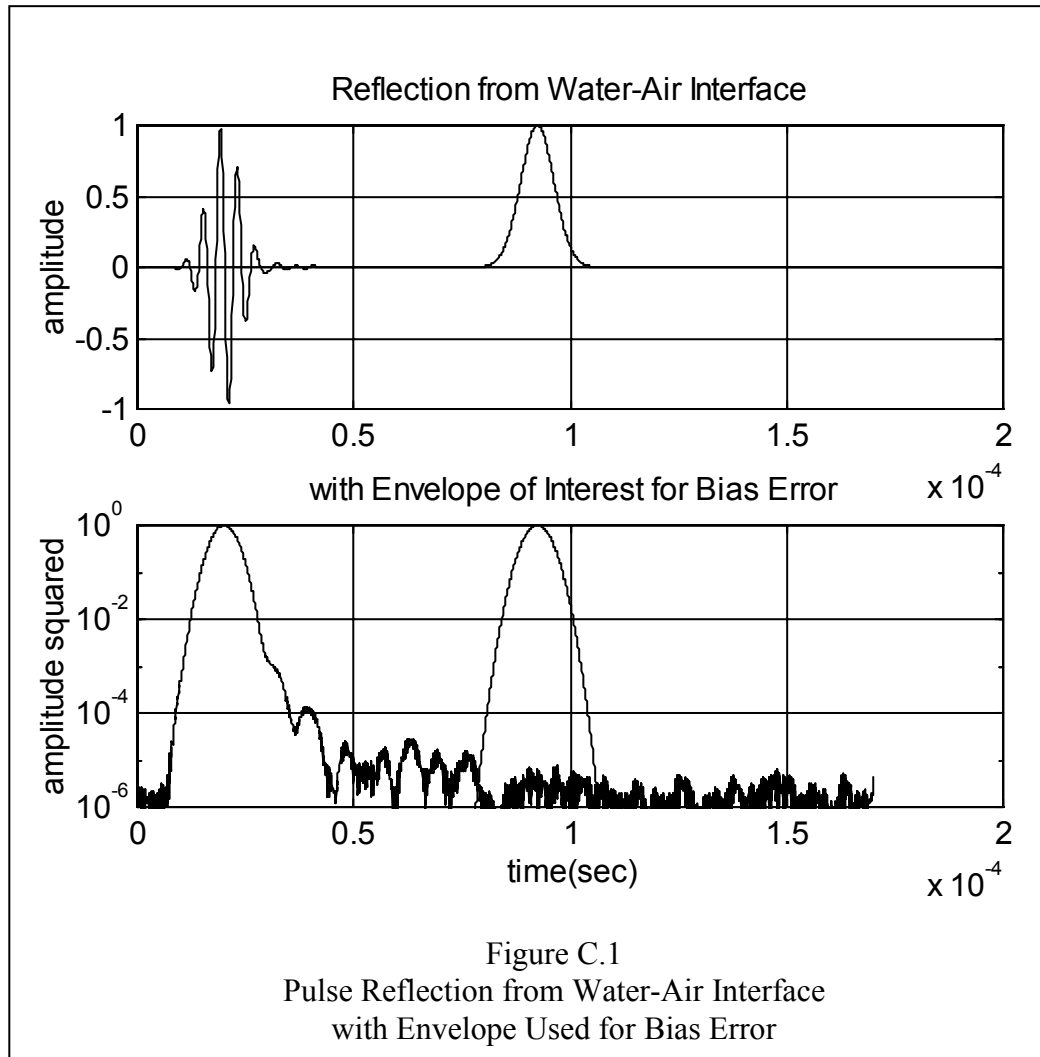
Appendix D:
SINGLE DEGREE-OF-FREEDOM LUMPED PARAMETER MODEL

The first part of this section shows that the motion from a lumped mass, linear spring model is identical to the motion of a particle in a continuous medium where there are no boundary effects. The second part does the same for the boundary.

D.1 HOMOGENEOUS (NO BOUNDARY EFFECTS)

Start by taking a single degree-of-freedom system, i.e., only one wave traveling through the medium, and find the homogeneous solution, see Fig. D.1 below.

Figure D.1
Mass-Spring Model
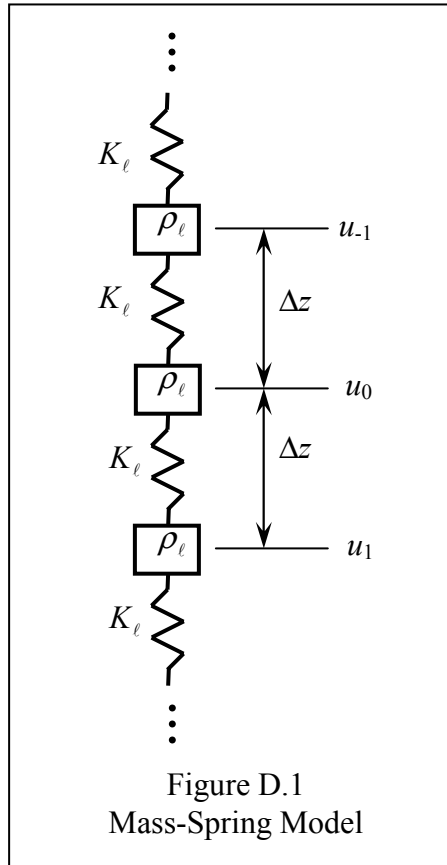
Where K_ℓ is the linear stiffness, ρ_ℓ is the lumped mass. The conversions of continuous parameters to lumped parameters are:

$$K_\ell \left(\text{N/m} \right) = \frac{K\left(\text{N/m}^2 \right) \times 1\left(\text{m}^2 \right)}{\Delta z\left(\text{m} \right)} \tag{D-1}$$

$$\rho_\ell \left(\text{kg} \right) = \rho\left(\text{kg/m}^3 \right) \times 1\left(\text{m}^2 \right) \times \Delta z(m). \tag{D-2}$$

Assume

$$\begin{aligned}
u_{-1} &= A\exp\left(i\omega\left(t + \tau \right) \right) \\
u_0 &= A\exp\left(i\omega\tau \right) \\
u_1 &= A\exp\left(i\omega\left(t - \tau \right) \right).
\end{aligned} \tag{D-3}$$

Where τ is a time delay.

The motions of the masses u_{-1} and u_0 and their differences are shown in Fig. D.2 as a function of time.

Figure D.2
Movements of Two Masses (u_{-1} and u_0)
and the Difference of Their Movements
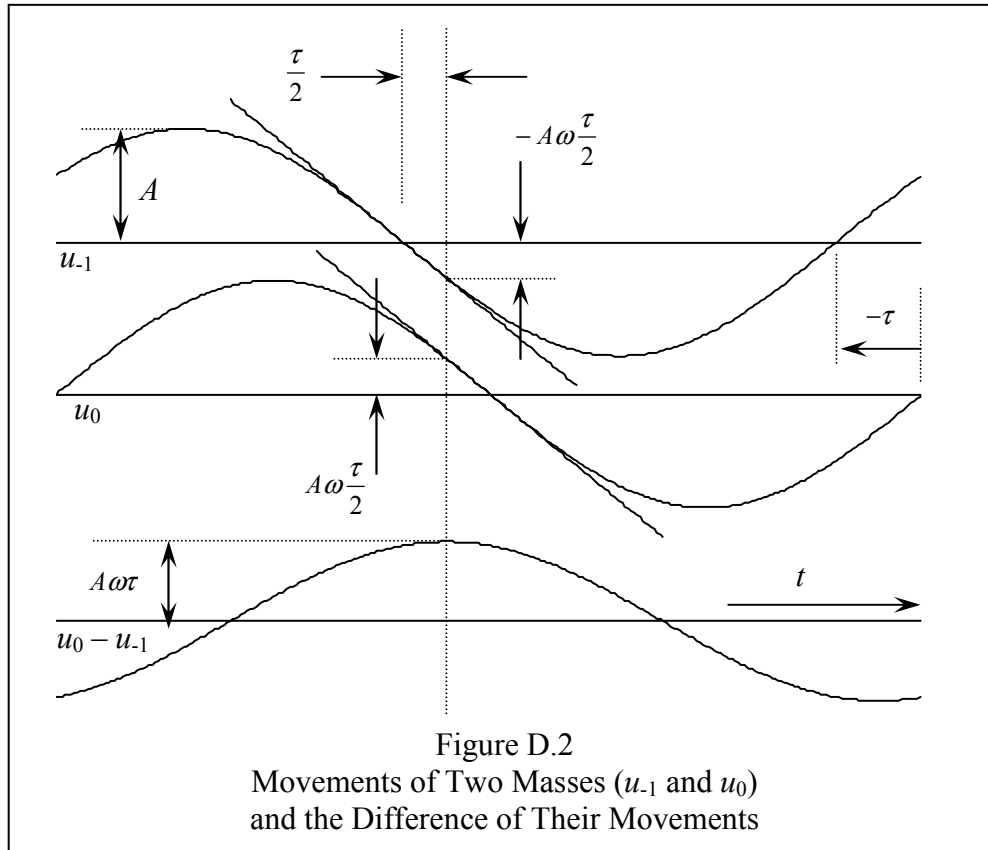
The slope at the zero crossing for u_{-1} and u_0 is $A\omega$. The amplitude at a time $\tau/2$ from the zero crossing is $A\omega\tau/2$ when τ is small. The difference between u_0 and u_{-1} is:

$$u_0 - u_{-1} = -iA\omega\tau \exp\left(i\omega\left(t+\frac{\tau}{2}\right)\right). \tag{D-4}$$

Likewise:
$$u_1 - u_0 = -iA\omega\tau \exp\left(i\omega\left(t-\frac{\tau}{2}\right)\right). \tag{D-5}$$

And:
$$(u_1 - u_0) - (u_0 - u_{-1}) = -A\omega^2\tau^2 \exp(i\omega t). \tag{D-6}$$

The equation of force on the mass at u_0 is ($\exp(i\omega t)$ suppressed):

$$[(u_1 - u_0) - (u_0 - u_{-1})]K_\ell = -A\rho_\ell\omega^2. \tag{D-7}$$

Substitute in eqs. (D-1), (D-2), and (D-5):

$$\frac{\Delta z^2}{\tau^2} = \frac{K}{\rho}. \tag{D-8}$$

The speed of the wave (c) is $\Delta z/\tau$, therefore:

$$c = \sqrt{\frac{K}{\rho}}. \tag{D-9}$$

This is the speed of a wave in a continuous medium. The speed of the wave is the same for a continuous medium as it is for a lumped medium given Δz is much smaller than the wavelength.

D.2 BOUNDARY

The pressure on the boundary ($z = 0$) for a continuous medium is the modulus times the first spatial derivative (strain).

$$p = K\frac{\partial u}{\partial z}$$
$$p = K(-iAk\exp(i\omega t)) \tag{D-10}$$

This is assuming the movement of a particle in the continuous medium is of the form:

$$u = A\exp(i(\omega t - kz)). \tag{D-11}$$

The force on the boundary for a lumped medium system is the stiffness times the difference in displacement of two points Δz apart.

$$f = K_\ell (u_1 - u_0)$$

$$f = -iAkK \exp\left(i\omega\left(t - \frac{\tau}{2} \right) \right) \cdot \qquad \text{(D-12)}$$

Where:

$$\frac{\omega\tau}{\Delta z} = \frac{\omega}{c} = k . \qquad \text{(D-13)}$$

As $\Delta z \to 0$, and therefore as $\tau \to 0$, the pressure and the force on the boundary are the same. As pointed out earlier stiffness (N/m) and modulus (N/m^2), mass (kg) and density (kg/m^3), force (N) and pressure (N/m^2), viscous damping (Ns/m) and body viscous damping (Ns/m^4), difference in displacement of two points (m) and strain (m/m), are used interchangeably. Hopefully this does not cause too much confusion.

This appendix shows that the continuous medium and lumped medium are equivalent for a single degree-of-freedom system. This dissertation assumes this equivalency holds for multiple degree-of-freedom systems.

Appendix E:
DYNAMIC DESIGN ANALYSIS METHOD

Figs. E.1, E.2, E.3, and E.4 are copies of selected pages of Belsheim and O'Hara's NAVSHIPS 250-423-30, *Shock Design of Shipboard Equipment, Dynamic Design Analysis Method* (DDAM), ref. [2]. DDAM analyzes shock on Naval ships from non-contact explosions. Belsheim and O'Hara were the first to derive expressions for effective mass and participation factors. Modal mass is also referenced in Clough and Penzien [14] for earthquake analysis of structures.

Rewriting the effective mass from DDAM ([2] eq. (7)) and Clough and Penzien, p. 559 [14] to include mass coupling (for the first mode only, second mode similar):

$$\rho_1 = \frac{\left[\begin{Bmatrix} 1 \\ 1 \end{Bmatrix}^T \begin{bmatrix} m_{11} & m_{12} \\ m_{21} & m_{22} \end{bmatrix} \begin{Bmatrix} 1 \\ B_1 \\ A_1 \end{Bmatrix} \right]^2}{\begin{Bmatrix} 1 \\ B_1 \\ A_1 \end{Bmatrix}^T \begin{bmatrix} m_{11} & m_{12} \\ m_{21} & m_{22} \end{bmatrix} \begin{Bmatrix} 1 \\ B_1 \\ A_1 \end{Bmatrix}} \tag{E-1}$$

Which is the same as eq. (2-46) if the mass matrix is:

$$\begin{bmatrix} m_{11} & m_{12} \\ m_{21} & m_{22} \end{bmatrix} = \begin{bmatrix} \rho_{11} - \dfrac{iF}{\omega} & \rho_{12} + \dfrac{iF}{\omega} \\ \rho_{21} + \dfrac{iF}{\omega} & \rho_{22} - \dfrac{iF}{\omega} \end{bmatrix} \tag{E-2}$$

The DDAM participation factor ([2] eq. (6)) is:

$$\overline{P}_1 = \frac{\begin{Bmatrix} 1 \\ 1 \end{Bmatrix}^T \begin{bmatrix} m_{11} & m_{12} \\ m_{21} & m_{22} \end{bmatrix} \begin{Bmatrix} 1 \\ B_1 \\ A_1 \end{Bmatrix}}{\begin{Bmatrix} 1 \\ B_1 \\ A_1 \end{Bmatrix}^T \begin{bmatrix} m_{11} & m_{12} \\ m_{21} & m_{22} \end{bmatrix} \begin{Bmatrix} 1 \\ B_1 \\ A_1 \end{Bmatrix}} \tag{E-3}$$

This is different than this dissertation's participation factor. To find the relationship between the two find the displacement of the sand, mass 1, and fluid, mass 2, from a first mode displacement of one:

$$X_{11} = 1 \times \overline{P_1}$$

$$X_{21} = \frac{B_1}{A_1} \overline{P_1} \tag{E-4}$$

The displacement of the fast wave from a unit displacement of the first mode is:

$$\widetilde{P_1} = (1 - \beta)X_{11} + \beta X_{21} \tag{E-5}$$

Which is this dissertation's participation factor eq. (2-48).

The last column of the Modal Computation Table in Fig. E.4 contains what this dissertation calls effective forces (V_a is the input velocity).

One of the biggest differences in the mathematics between DDAM and Biot Theory is that the eigenvalues for DDAM are the natural frequencies squared, whereas in the Biot Theory the eigenvalues are the wave numbers squared.
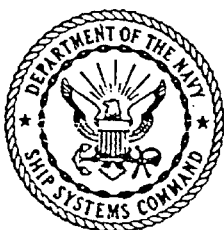
As mentioned earlier, DDAM had a big influence in developing the lumped parameter model.

NAVSHIPS 250-423-30

SHOCK DESIGN

OF

SHIPBOARD EQUIPMENT

DYNAMIC

DESIGN-ANALYSIS METHOD

MAY 1961

NAVAL SHIP SYSTEMS COMMAND

DEPARTMENT OF THE NAVY
WASHINGTON, D.C. 20360

Figure E.1
Cover Page of NAVSHIPS 250-423-30

DEPARTMENT OF THE NAVY
BUREAU OF SHIPS
WASHINGTON 25, D. C.

IN REPLY REFER TO
Code 423
May 1961

From: Chief, Bureau of Ships
To: All Activities concerned with Shock Design of Shipboard Equipment

Subj: Dynamic Design-Analysis Method of Shock Design

1. This publication presents a method for the shock design of shipboard equipment by dynamic analysis and is promulgated to aid in the design, development and production of shock-resistant equipment.

2. Extracts from this document may be made to facilitate the preparation of other Department of Defense publications.

3. Errors found in this manual (other than obvious typographical errors), which have not been corrected by means of Temporary Corrections or Permanent Changes, should be reported. Such report should include the complete title of the publication and the publication number (short title); identify the page and line or figure and location of the error; describe the error or indicate what change should be made; and be forwarded to the Ship Protection Section of the Bureau of Ships, Code 423.

J. H. McQUILKIN
Captain, U. S. Navy
Director, Ship Design Division

RETURN TO
TECH. PUB LIBRARY CODE 244.82
PUGET SOUND NAVAL SHPYD
FILE NUMBER
NAVSHIPS............COPY 2

Figure E.2
Authorization of NAVSHIPS 250-423-30

SHOCK DESIGN OF SHIPBOARD EQUIPMENT
PART I - DYNAMIC DESIGN-ANALYSIS METHOD

R. O. Belsheim and G. J. O'Hara

INTRODUCTION

During recent years the Bureau of Ships, through its laboratories and contractors, has carried out an extensive program to decrease vulnerability of submarines and ships to underwater-explosion attack. This vulnerability has been considered in terms of hull and equipment* shock damage, each of which may cause ultimate loss of the ship (1). Perhaps because shock damage is not as definite a concept as hull damage, or because the war damage reports did not show it to be as damaging (2), the experimental research effort has been directed more toward the understanding of hull damage. A strong exception to this trend has been the design of nuclear power plant components, which today are stronger on the average than other equipment as a result of extensive tests and resultant design procedures (3-9). Another notable exception is the Polaris missile installation, which is designed to protect against relatively severe shock motions, even though the missile itself is very fragile (10). Overall, however, recent predictions of damaging radii for pressure hull damage (11) and equipment shock damage (12) suggest that equipment is relatively more prone to damage in modern submarines. A similar conclusion in the case of some surface ships, i.e., destroyers, is found from study of results of recent tests in the Pacific (13). Only full-scale tests on operational ships and submarines can give a definite evaluation of vulnerability.

Even though many problems remain, a considerable amount of research has been done and the authors believe information is available so that better design analyses can be made. The purpose of this report is to review this material and to propose a dynamic design-analysis method for evaluating shock resistance of shipboard equipment which is essentially linear and elastic and which does not rest on noise or vibration mounts which often are non-linear and/or will bottom. All of the required information is not yet available, since only realistic underwater explosion tests can give correct inputs, but the missing information can be obtained. It is not intended that this design analysis-method supersede present laboratory shock-test and evaluation procedures, which will always be desirable, but it should help

---

*Equipment, as used here, includes machinery, electronic equipment, and other items which are attached internally to the ship by some intervening structure; it does not include items subjected directly to the shock wave in the water.

4

Figure E.3
Author's Page of NAVSHIPS 250-423-30

Step 2 - Calculate the set of influence coefficients for these points and form the influence coefficient matrix.

Step 3 - Using the method of matrix iteration, find the mode shapes and natural frequencies of the first few modes, say two or three. (There is a numerical example worked out in Appendix A for the first three modes of a uniform cantilever beam.) Of course the design analyst may use other procedures he is more familiar with. For example, formulas for the computation of the mode shapes and natural frequencies of a two degree of freedom system are given in Appendix B.

Step 4 - For each separate mode "a" complete the following table:

Modal Computation Table (Mode a)

Mass Number	Mass = M_i	Mode Shape = $\overline{X}_{ia}$	$M_i\overline{X}_{ia}$	$M_i\overline{X}_{ia}^2$	$M_i\overline{X}_{ia}\overline{P}_a V_a \omega_a$ *
1	M_1	$\overline{X}_{1a}$	$M_1\overline{X}_{1a}$	$M_1\overline{X}_{1a}^2$	$M_1\overline{X}_{1a}\overline{P}_a V_a \omega_a$
2	M_2	$\overline{X}_{2a}$	$M_2\overline{X}_{2a}$	$M_2\overline{X}_{2a}^2$	$M_2\overline{X}_{2a}\overline{P}_a V_a \omega_a$
-	-	-	-	-	-
n	M_n	$\overline{X}_{na}$	$M_n\overline{X}_{na}$	$M_n\overline{X}_{na}^2$	$M_n\overline{X}_{na}\overline{P}_a V_a \omega_a$
$\sum$			$M_i\overline{X}_{ia}$	$M_i\overline{X}_{ia}^2$	$M_i\overline{X}_{ia}\overline{P}_a V_a \omega_a$

Step 5 - Calculate the participation factors for each mode "a"

$$\overline{P}_a = \frac{\sum\limits_i M_i\overline{X}_{ia}}{\sum\limits_i M_i\overline{X}_{ia}^2}. \tag{6}$$

Step 6 - Calculate the "effective mass" in each mode by means of the formula

$$\overline{M}_a = \overline{P}_a \sum_i M_i\overline{X}_{ia} = \frac{\left[\sum\limits_i M_i\overline{X}_{ia}\right]^2}{\sum\limits_i M_i\overline{X}_{ia}^2}. \tag{7}$$

*See Steps 5, 6, 7, 8, 9, and 13.

24

Figure E.4
Modal Analysis of NAVSHIPS 250-423-30

Appendix F:
PLANS OF TRAY AND LID

The following AUTOCAD plans show the construction of the foundation, tray, and lid used in the reflection ratio method. Fig. F.1 shows the assembly with the receiver and transmitter under the sand. Fig. F.2 is the tray that holds the sand. Fig. F.3 is the lid used when the Ethafoam is on the top surface of the sand. And Figs. F.4 and F.5 show the profile and plan view of the aluminum foundation. These items were constructed in the machine shop at the University of Washington's Applied Physics Laboratory.
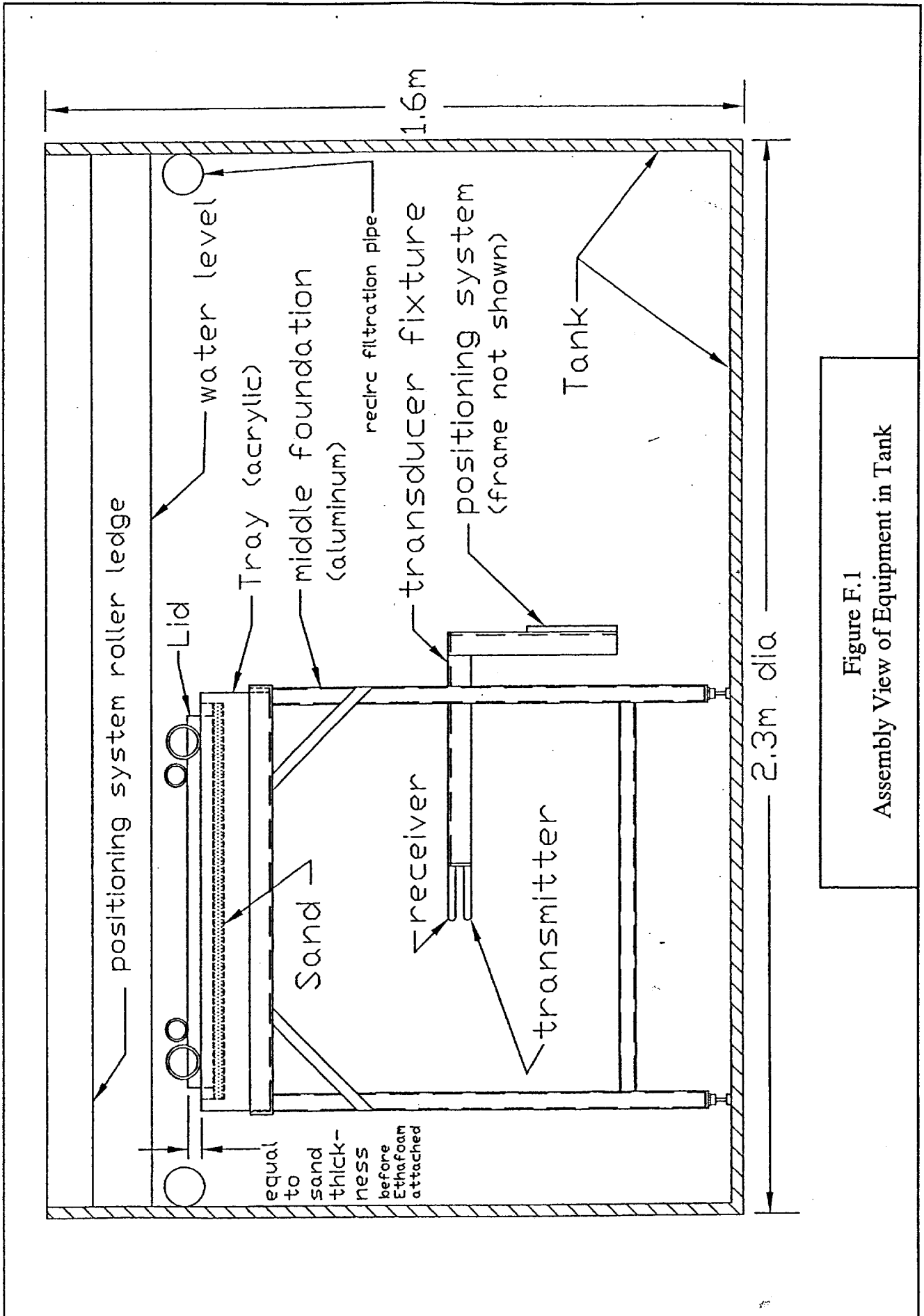
Figure F.1
Assembly View of Equipment in Tank

tap 1"+ for 1-8 thd

$\frac{9}{16}$" ∅ thru 2"

∅ for 1" thd

1x1-8 thd brass rod w/ 1/2-13 thd thru center

weld ring to nut and stud

2x$\frac{3}{8}$ ring CRES ⟨4⟩

2" acrylic

4" acrylic

7×$\frac{1}{2}$-13 thd stud ⟨4⟩
$\frac{1}{2}$" nuts ⟨8⟩
$\frac{1}{2}$" washers ⟨8⟩

⟨0,0⟩   ⟨5,5⟩   ⟨33,8⟩   ⟨31,5⟩

$\frac{9}{16}$" thru
4 PLCS
drill press OK

⟨31,31⟩   ⟨5,31⟩

A

18"

36" ref

18"

36' ref

A-A

Measure finished I.D. to within .001" and record actual I.D. here

32 ± .005

glue $\frac{1}{2}$"

2" ref   4" ref

Figure F.2
Plan of Tray

For 1-8
Thd brass rod (4)

26" BC (4)
drill press OK

LID

Thd Brass Rod (4)
2x1-8 thd

For 1x3-16 thd
2" OD eye (4)
or plastic cap (4)

2"

Ethafoam

Acrylic

¼" ref

30" dia
band saw OK

2" ref

Figure F.3
Plan of Lid

Brass Plug

$1\frac{1}{2}''$ square

snug
fit

$1''$

$1\frac{1}{4}''$

drill and tap
For $3 \times \frac{1}{2}-13$ bolt,
nut, and washer
4 each

2x2x0.25
angle

Brass Plug (4)

38"

1.5 box
tube

1x0.25 bar
8 PLCS

36.5"

6"

$\frac{1}{4}''$ air holes
top and bottom
on all 4 braces

$\frac{1}{4}''$ air hole
on all 4 legs

6"

1.5 box tube
4 PLCS

$\frac{3}{8} \times \frac{1}{4}-20$ bolt
and nut
(4 ea)

tack weld nut

6"

1.5 box
tube

$\frac{5}{16}''$ hole

MIDDLE FOUNDATION
Profile View

Figure F.4
Profile View of Foundation
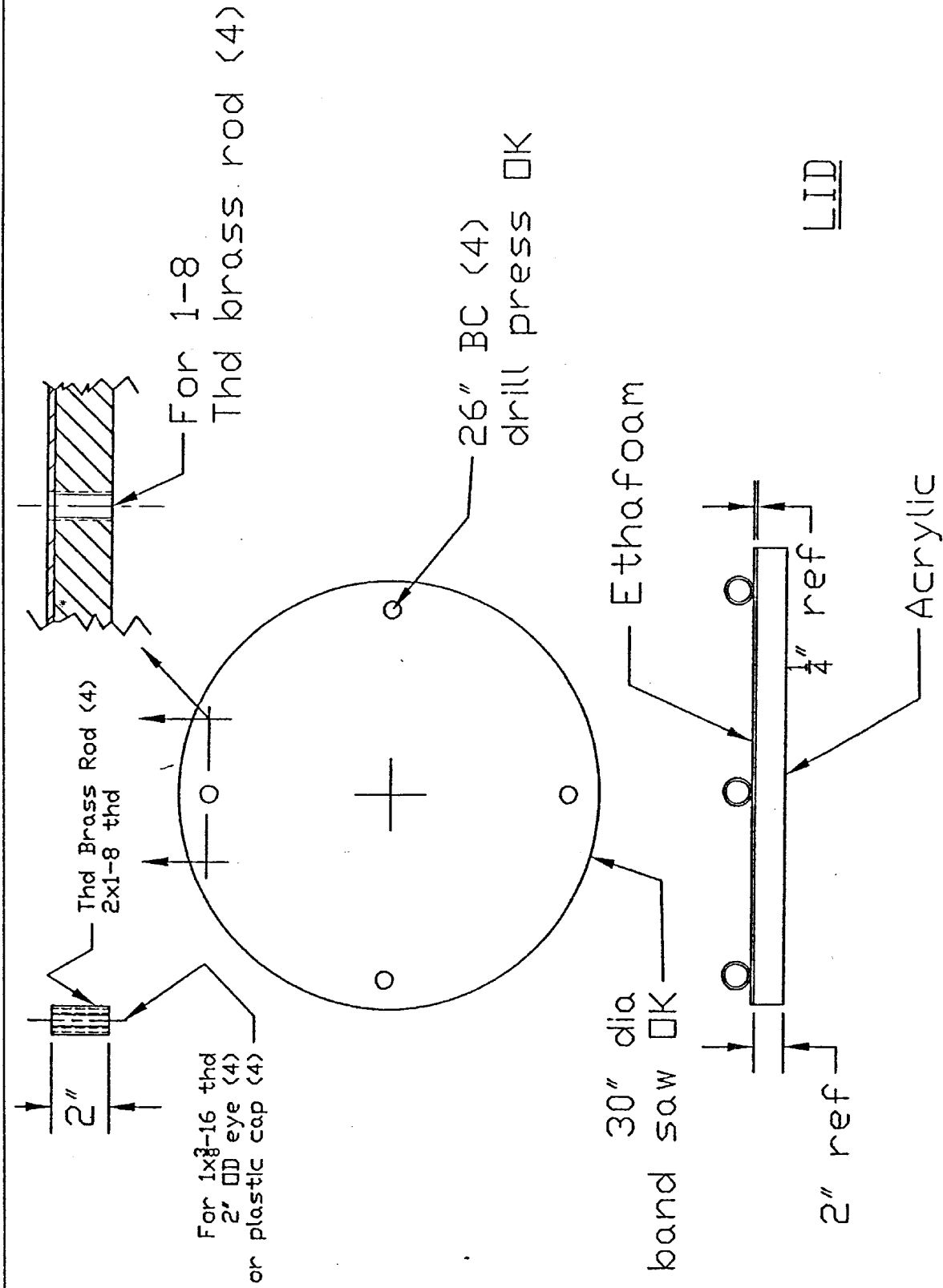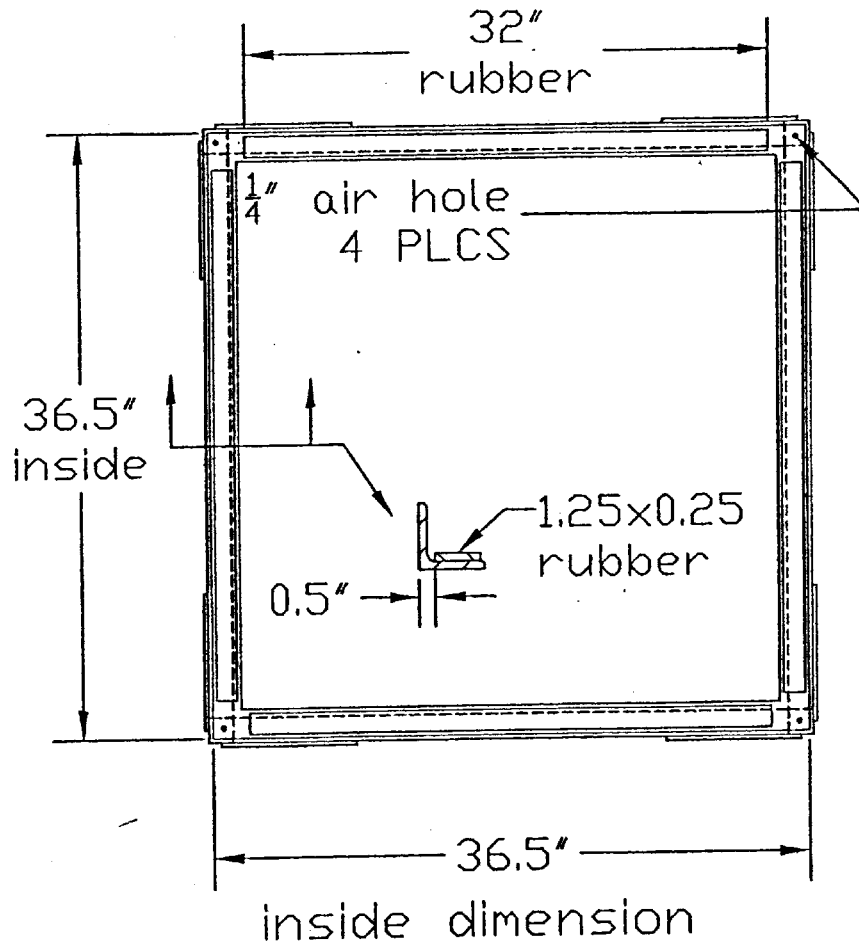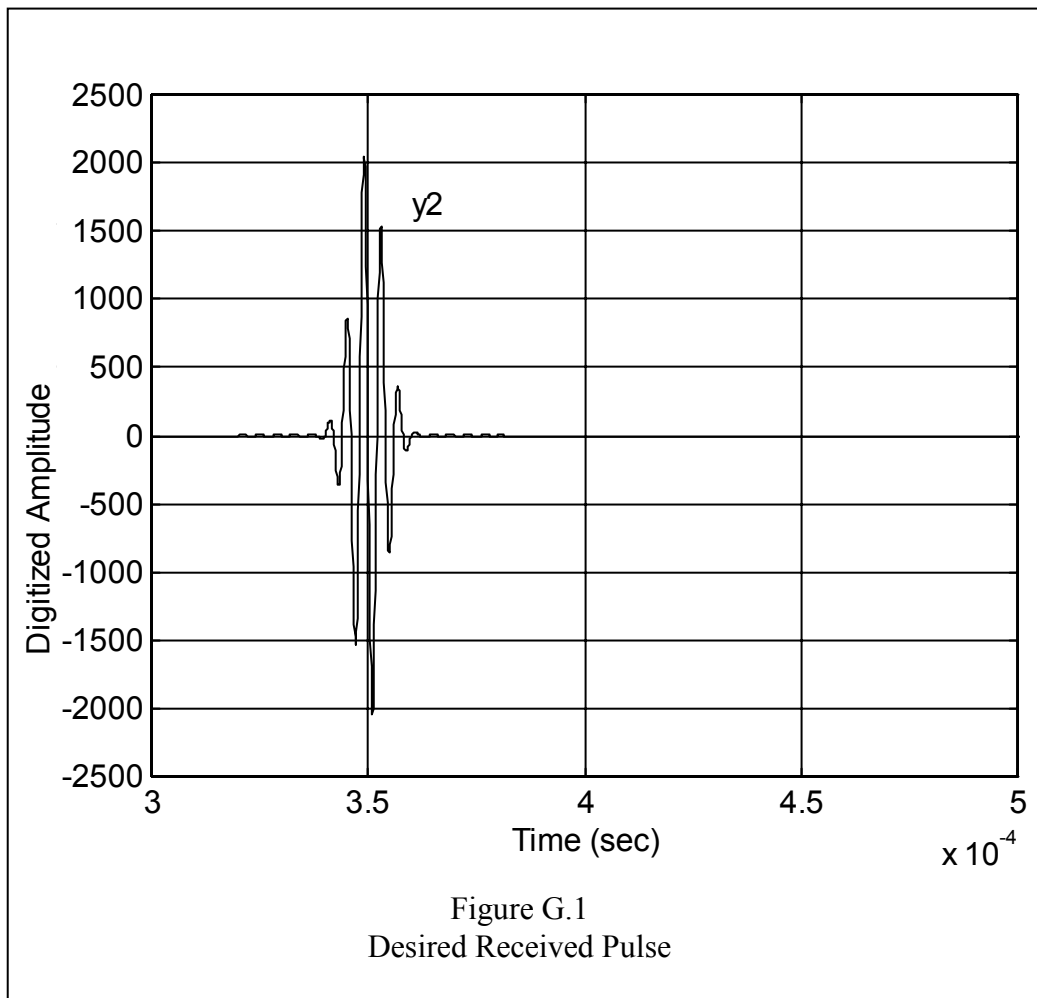
MIDDLE FOUNDATION

Plan View

Figure F.5
Plan View of Foundation

Appendix G:
PULSE FORMATION

A pulse was needed that had no side lobes after 0.03 ms. This is the time for sound to go through 4" of acrylic. The desired received pulse, y_2, eq. (G-1), is shown in Fig. G.1. The desired pulse is comprised of a sine wave at 250,000 Hz with a Gaussian envelope.

Figure G.1
Desired Received Pulse

The equation for the desired received pulse centered at 0.35 ms is:

$$y_2 = \exp\left[\left(t - 0.35 \cdot 10^{-3}\right)^2 \left(-3.6968\mathrm{e}10\right)\right] \sin\left(2\pi \cdot 2.5\mathrm{e}5 \cdot t\right) \qquad \text{(G-1)}$$

To find the transfer function of the system the transducers were excited with a pulse x_1, centered at 0.05 ms, shorter in time than y_2, hence with more frequency content.

$$x_1 = \exp\left[4\left(t - 0.05 \cdot 10^{-3}\right)^2 \left(-3.6968e10\right)\right] \sin(2\pi \cdot 2.5e5 \cdot t) \qquad \text{(G-2)}$$

The received signal from an excitation of x_1 is y_1. The signal y_1 is a signal reflected from a water-air interface with a travel distance selected so that the pulse returns at 0.35 ms. The goal is to manufacture an excitation signal for the transfer function $\frac{y_1}{x_1}$ that will produce the desired received signal y_2. This was done by converting x_1, y_1, and y_2 into the frequency domain and finding the frequency content of x_2.

$$X_2 = \frac{X_1}{Y_1} Y_2 \qquad \text{(G-3)}$$

Where X_2 is the Fourier transform of x_2, etc. The frequency contents of x_1 and y_1 are shown in Fig. G.2.

The forcing function fed into the transmitting hydrophone, x_2, to produce the desired received pulse, y_2, is the inverse Fourier transform of X_2. See Fig. G.3.

Using the excitation signal x_2 the received pulse, y_{2rec}, is close to the desired received pulse, y_1. See Fig. G.4. The received pulse is the coherent average of 100 samples reflected off a water-air interface.
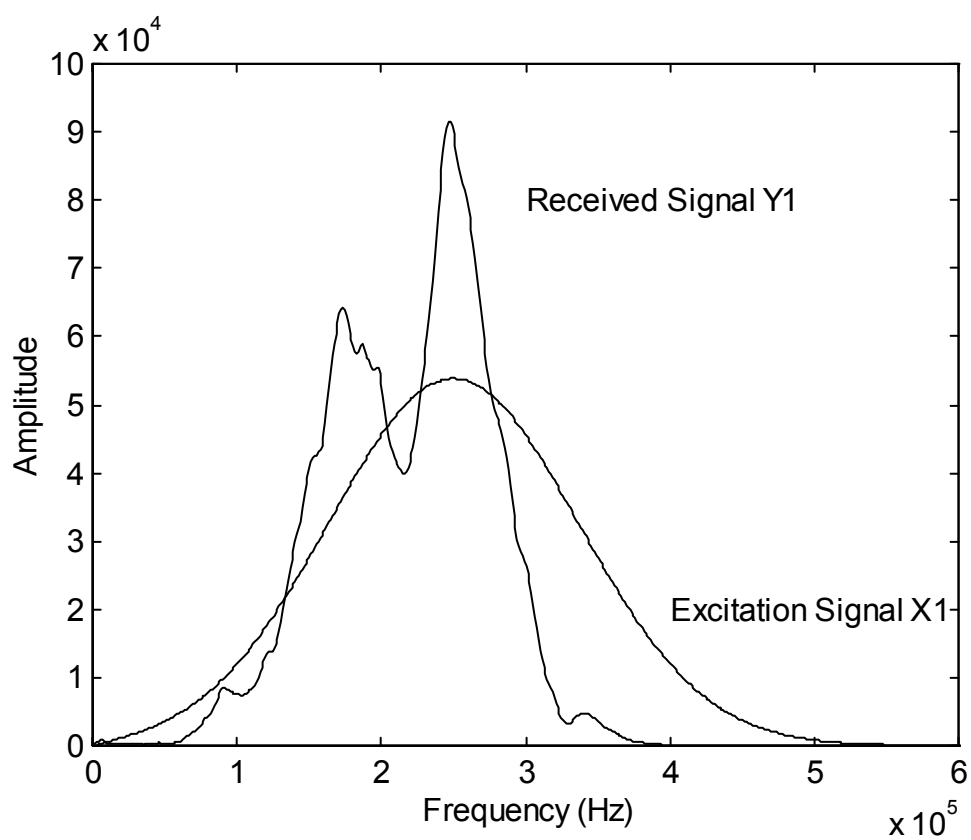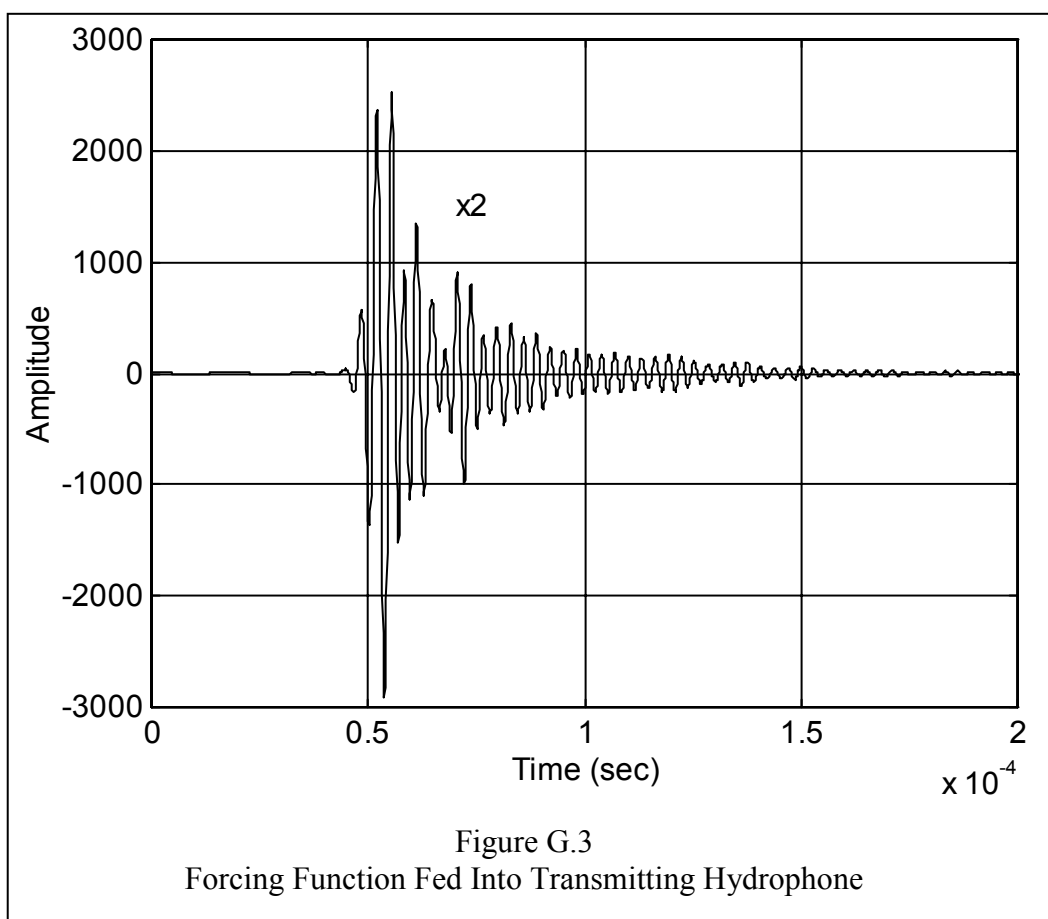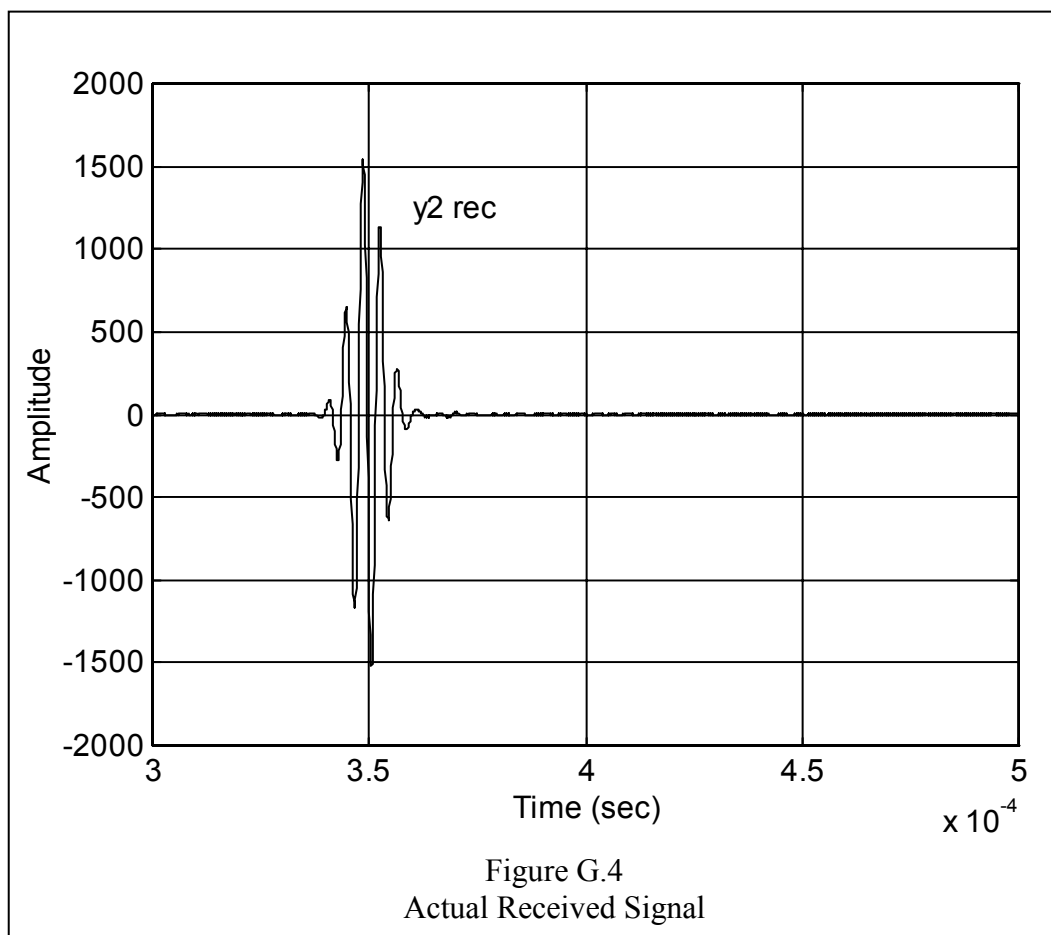
Figure G.2
Frequency Contents of Received and Excitation Signals

Figure G.3
Forcing Function Fed Into Transmitting Hydrophone

Figure G.4
Actual Received Signal

Appendix H:
SAND SIZE

Sand size and other properties are listed below. A thanks is given to Kevin Briggs of the Naval Research Laboratory (NRL) for providing the sand and the following properties. The sand was obtained from Ward's Natural Science Establishment, Inc., Rochester, NY, and has a product name of "Sand; Ottawa, Sea." The sand properties measured at NRL (from sand with the same product name) are:

<u>Phi size at percentage levels</u>:

5	16	25	50	75	84	95
1.60	1.82	1.92	2.14	2.43	2.62	3.02

<u>Percentages of</u>:

Gravel	Sand	Silt	Clay.
0.00	99.68	0.25	0.08

<u>Moment measures</u>:

Mean	S.Dev.	Skew	KG
1.84	0.53	2.91	93.83

Post-analytical weight: 129.66

Note that phi units are logarithmic such that the grain size in mm, d, is related to the size, ϕ, in phi units through the expression:

$$d = 2^{-\phi} \tag{H-1}$$

Table H.1 Sand Size Distribution								
phi Size	Frac. Wgt.	Frac. %	Cum. %		phi Size	Frac. Wgt.	Frac. %	Cum. %
-4.00	0.000	0.00	0.00		1.75	10.939	8.44	10.01
-3.75	0.000	0.00	0.00		2.00	29.125	22.46	32.48
-3.50	0.000	0.00	0.00		2.25	40.853	31.51	63.99
-3.25	0.000	0.00	0.00		2.50	20.163	15.55	79.54
-3.00	0.000	0.00	0.00		2.75	12.474	9.62	89.16
-2.75	0.000	0.00	0.00		3.00	7.290	5.62	94.78
-2.50	0.000	0.00	0.00		3.25	3.887	3.00	97.78
-2.25	0.000	0.00	0.00		3.50	1.713	1.32	99.10
-2.00	0.000	0.00	0.00		3.75	0.472	0.36	99.46
-1.75	0.000	0.00	0.00		4.00	0.277	0.21	99.68
-1.50	0.000	0.00	0.00		4.50	0.101	0.08	99.75
-1.25	0.000	0.00	0.00		5.00	0.031	0.02	99.78
-1.00	0.000	0.00	0.00		5.50	0.031	0.02	99.80
-0.75	0.000	0.00	0.00		6.00	0.031	0.02	99.83
-0.50	0.007	0.01	0.01		6.50	0.031	0.02	99.85
-0.25	0.000	0.00	0.01		7.00	0.031	0.02	99.87
0.00	0.001	0.00	0.01		7.50	0.031	0.02	99.90
0.25	0.030	0.02	0.03		8.00	0.031	0.02	99.92
0.50	0.010	0.01	0.04		9.00	0.017	0.01	99.94
0.75	0.197	0.15	0.19		10.00	0.017	0.01	99.95
1.00	0.116	0.09	0.28		11.00	0.017	0.01	99.96
1.25	0.142	0.11	0.39		12.00	0.017	0.01	99.97
1.50	1.543	1.19	1.58		13.00	0.017	0.01	99.99
1.75	10.939	8.44	10.01		14.00	0.017	0.01	100.00
2.00	29.125	22.46	32.48					

REPORT DOCUMENTATION PAGE

1. AGENCY USE ONLY *(Leave blank)*	2. REPORT DATE May 2003	3. REPORT TYPE AND DATES COVERED Technical Report

4. TITLE AND SUBTITLE
Experimental Study of Sound Waves in Sandy Sediment

5. FUNDING NUMBERS
N00014-98-1-0040

6. AUTHOR(S)
Michael W. Yargus

7. PERFORMING ORGANIZATION NAME(S) AND ADDRESS(ES)
Applied Physics Laboratory
University of Washington
1013 NE 40th Street
Seattle, WA 98105-6698

8. PERFORMING ORGANIZATION REPORT NUMBER
APL-UW TR 0301

9. SPONSORING / MONITORING AGENCY NAME(S) AND ADDRESS(ES)
Office of Naval Research
800 N. Quincy Street
Arlington, VA 22217-5660

10. SPONSORING / MONITORING AGENCY REPORT NUMBER

11. SUPPLEMENTARY NOTES

12a. DISTRIBUTION / AVAILABILITY STATEMENT
Approved for public reslease; distribution is unlimited.

12b. DISTRIBUTION CODE

13. ABSTRACT *(Maximum 200 words)*

This dissertation describes experiments intended to help understand the physics of sound (compressional waves) propagating through sandy sediments (unconsolidated porous media). The theory (using a lumped parameter model) and measurements (using a reflection ratio technique) includes derivations and measurements of acoustic impedances, effective densities, wave speeds (phase velocities), effective pressures, mode shapes, pressure reflection coefficients, and material moduli. The results show the acoustic impedance divided by the phase velocity, rendering an "effective density," is less than the total density of the sediment (effective density = $89\% \pm 3\%$ of total). The results also show the fluid in the sediment oscillates back-and-forth 2.2 ± 0.4 times farther than the sand in the sediment (mode shape) during the passing of a sound wave. These facts suggest the existence of Biot waves (two compressional waves) in water-saturated sand.

14. SUBJECT TERMS
Underwater acoustics, Biot theory, poroelastic media, sediment acoustics

15. NUMBER OF PAGES
115

16. PRICE CODE

17. SECURITY CLASSIFICATION OF REPORT	18. SECURITY CLASSIFICATION OF THIS PAGE	19. SECURITY CLASSIFICATION OF ABSTRACT	20. LIMITATION OF ABSTRACT
Unclassified	Unclassified	Unclassified	SAR